CHALMERS

Modelling and Simulation of a Hybrid Electric Vehicle for Shell Eco-marathon and an Electric Go-kart

EMMA GRUNDITZ
EMMA JANSSON

Master of Science Thesis in Electric Power Engineering
Department of Energy and Environment
CHALMERS UNIVERSITY OF TECHNOLOGY
Performed at Division of Electric Power Engineering and QRTECH AB
Göteborg 2009, Sweden

Abstract

The first part of this master thesis describes the MATLAB/Simulink modelling and simulation of the series hybrid car, Smarter, that was built by master students in electrical and mechanical engineering and competing for Chalmers in Shell Eco-marathon in May 2009. This simulation tool is meant as a help in the design and evaluation of the Smarter vehicle. Components in the driveline can be varied and the effect on the Smarter fuel efficiency can be investigated.

The second part of this thesis describes the work of modelling and simulating an electric go-kart, that was carried out at QRTECH. There is no original for the modeled go-kart, but the model is a mixture of a real electrical go-kart built at Chalmers and a partly designed go-kart intended to be built at QRTECH. Through the simulations lessons can be learned regarding the dimensioning of the QRTECH go-kart components.

Both simulation tools are based on CAPSim and consist of a Simulink vehicle model, where the driveline components are represented as interconnected blocks that are communicating physical signals between each other in the level of seconds. Component parameters are set in an accompanying MATLAB m-file. The simulation input is a vector containing the vehicle reference speed as a function of time. The output can be any desired simulated signal, and in the Smarter simulator it is also the coverable distance per liter of fuel.

None of the models have been verified against measurements on the real objects. However, simulations show that with the driveline setup that was used in Shell Eco-marathon 2009, Smarter would have a fuel efficiency of about 255 km per liter of fuel and would place as number 10 in the overall Urban concept competition. Furthermore, it seams that adjustments of parameters of the current driveline only have moderate effects on the fuel efficiency. Therefore it is suggested that the Smarter body is modified in order to increase the fuel efficiency, or perhaps a parallel driveline is designed to be simulated and evaluated.

Sammanfattning

Den första delen av examensarbetet beskriver MATLAB/Simulink modelleringen och simuleringen av seriehybridbilen, Smarter, som byggts av masterstudenter i elkraft och mekanik vid Chalmers Tekniska Högskola och som representerade Chalmers i Shell Eco-marathon i maj 2009. Modellens syfte är att fungera som en hjälp vid design och utvärdering av Smarter. Smarters bränsleförbrukning kan undersökas genom att variera komponenterna i drivlinan.

Den andra delen beskriver modelleringen och simuleringen av en elgokart, som utfördes på QRTECH. Modellen är en blandning av den elgokart som byggdes av studenter på Chalmers och den gokart som är planerad att byggas på QRTECH. Med hjälp av simulatorn kan man få en uppfattning om hur komponenterna i gokarten skall dimensioneras.

Båda simulatorerna bygger på CAPSim och består av en Simulink modell av ett fordon, där drivlinans komponenter är representerade som ihopkopplade block med fysiska signaler emellan. Komponenternas parametrar anges i den tillhörande MATLAB m-filen, där anges även simuleringsvektorn som består av fordonets referenshastighet som funktion av tiden. Utsignaler kan varieras beroende på önskemål men i Smarter-simulatorn fås även möjlig körsträcka per liter bränsle.

Ingen av modellerna har verifierats med mätningar på de verkliga komponenterna, men simuleringar visar att med den drivlina som Smarter hade vid Eco-marathon 2009 så skulle den komma 255 km på en liter bränsle och därmed placera sig på en tionde plats i UrbanConcept-delen. Det verkar dessutom som att justeringar av komponenterna i den aktuella drivlinan inte har någon större påverkan på Smarters bränsleförbrukning, utan man kanske skall överväga att modifiera Smarters utförande eller kanske designa om drivlinan till en parallellhybrid som kan simuleras och utvärderas.

Acknowledgements

Our special thanks goes to our supervisor at Chalmers, Anders Lindskog, for offering us the opportunity to do this thesis work, and for his commitment and the many encouraging discussions. We would also like to thank our examiner at Chalmers, Torbjörn Thiringer, and Lars-Åke Johansson at QRTECH, as well as our supervisor at QRTECH, Nikola Vorkapić for his technical support and involvement. Finally we would like to thank the employees at QRTECH, particularly Andreas Magnusson and Mikael Åkerman-Kolmodin for their technical support, as well as the people at the Electric Power Engineering division at Chalmers, especially Stefan Lundberg for his patience and insightful recommendations.

Contents

Part I

Prologue

Chapter 1

Introduction

This report describes the two parted master thesis work completing our studies at the Electric Power Engineering master programme at Chalmers University of Technology. The first part, performed at Chalmers concerned modelling and simulating a hybrid electric vehicle for Shell Eco-marathon. The second part, performed at QRTECH involved modelling and simulating an electric gokart.

Next follows a description of the purpose of this master thesis work along with its extent and limitations.

1.1 Purpose and scope of the thesis

The purpose of the first part of the master thesis, performed at Chalmers, was to build a Simulink model representing the hybrid electric vehicle *Smarter*, and to simulate its performance in Shell Eco-marathon 2009.

Smarter is a series hybrid electric vehicle constructed and built by master students in one of the Chalmers Automotive Projects, Chalmers EcoMarathon. Chalmers was competing with Smarter in the Urban Concept category in Shell Eco-marathon Europe 2009.

The purpose with the model was to, if possible already before the 2009 competition, provide the project with some guidelines regarding choice of components and settings predicted to increase the fuel efficiency of Smarter. Interesting information could be how the fuel efficiency was affected by; size of internal combustion engine, choice of gear ratio, vehicle weight, rolling resistance coefficient, having a separate starter motor or using the generator as starter motor.

As a starting point a Simulink model of an electric vehicle based on work done by CAP-Sim (Center for Automotive Propulsion Simulation) was used, CAPSim is a cooperation between Chalmers and Linköpings University and is supervised by the Swedish automotive industry, Energimyndigheten (the Swedish energy agency) and Vinnova.

The Simulink model was not to contain any special blocks/components that are only available in additional toolboxes, such as SimPowerSystems, in order to make the model usable for everyone with a general MATLAB/Simulink license. To make the simulator more user friendly all vehicle and component parameters such as; battery, motor, converter, chassis specifications etc. are supposed to be set in a m-file.

The second part of the master thesis, performed at QRTECH, was to create a Simulink model representing an electric go-kart intended to be built by QRTECH. Since the go-kart was not yet built, the model is a mixture between an electric go-kart built by undergraduate students at Chalmers and the intended QRTECH go-kart.

The purpose with the model was not only to be able to simulate the performance of the go-kart, but also to create a Simulink block controlling the torque reference sent to the go-kart motor. This block is intended to be used to generate C-code, which will be implemented in the motor control of the physical go-kart.

QRTECH is currently mainly working with embedded systems for the automotive industry, but are hoping to expand their business activities to also include controlling, modelling and simulation of hybrid electric vehicles for the same industry. As a way for QRTECH to increase their knowledge in the area, they are planning to build an electric go-kart in cooperation with the Swedish Automobile Sport Federation.

1.1.1 Delimitations of the thesis work

This work has been completely theoretical, that is no measurements or testing have been conducted in the frame of this thesis work. All the data and parameter values spring from information from the manufacturers or measurements and testing done by fellow master students at Chalmers.

Chapter 2

Electric and hybrid electric vehicles and their components

This chapter deals with basic concepts and what is considered to be necessary information for taking part of the rest of the report.

2.1 Series hybrid

The series hybrid electric vehicle was initially developed from the electric vehicle in order to extend the drive range. By adding an engine to an electric vehicle, on board charging of the energy storage device is enabled.

The propulsion of the vehicle is carried out by an electric motor which is powered by an energy storage device and/or an engine-generator unit. When the load power demand is large, the engine-generator unit helps the buffer system to power the electric motor and when the load power demand is small the engine-generator unit charges the buffer system. The performance of the vehicle, such as acceleration, gradeability, and maximum speed, is totally determined by the size and the characteristics of the electric motor.

The series hybrid topology can be seen in Figure 2.1. There is no mechanical connection between the engine-generator system and the wheels in a series hybrid electric vehicle. The advantage with this topology is that the ICE can be turned off and another one is that the engine-generator unit can be mounted separately from the traction motor. Since the engine is mechanically decoupled from the wheels it is possible to always run the engine in its optimal operation region. This drivetrain topology also eliminates the need for clutches and conventional transmissions.

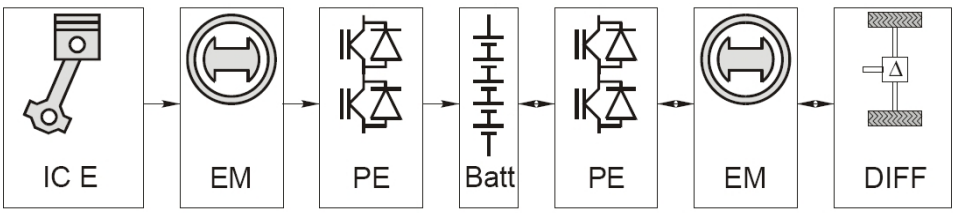

Figure 2.1: Series Hybrid Electric Vehicle, [4].

Depending on the driving condition and the wish of the driver, the series hybrid electric

drivetrain has five operating modes to switch between. The operating modes are:

- Hybrid traction mode: When there is a high amount of demanded power, both the engine-generator and the energy storage device, also called peaking power source (PPS), supply power to the electric motor drive. For efficiency and emission reasons the ICE should be operated in its optimal region.

- Peak power source - alone traction mode: The peak power source alone supplies the demanded power.

- Engine-generator - alone traction mode: The engine-generator alone supplies the demanded power.

- PPS charging from the engine-generator: The PPS needs to be charged when its energy has decreased to a bottom line. The PPS can be charged by regenerative braking or by the engine-generator. Regenerative braking charging is often insufficient and hence engine-generator charging is usually needed.

- Regenerative braking mode: The electric traction motor can be used as a generator when the vehicle is braking. Consequently, converting part of the kinetic energy of the vehicle mass into electric energy to charge the PPS.

If the ICE is used as the primary power source there will be a creation of inefficiencies since the power output from the ICE needs to be converted into electricity before driving the electric motor. Therefore, the series hybrid topology usually is set up with a small ICE to extend the drive range of an energy storage device. During stop-and-go driving the series topology has very low emissions and very good efficiency since it minimizes inefficient operation of the ICE and maximizes resumed energy from regenerative braking. One drawback with this topology is that it requires a large, heavy, energy storage system which drastically increases cost and reduces vehicle performance and another one is reduced efficiency during highway driving due to conversion of mechanical power to electricity and then back to mechanical motion in the electric motor.

2.2 Parallel hybrid

The propulsion of the parallel hybrid electric vehicle can be carried out both by the internal combustion engine and the electric motor since both are, in parallel, directly connected to the drivetrain. The ICE is mechanically connected to the wheels via a gearbox. Figure 2.2 shows the parallel hybrid topology.

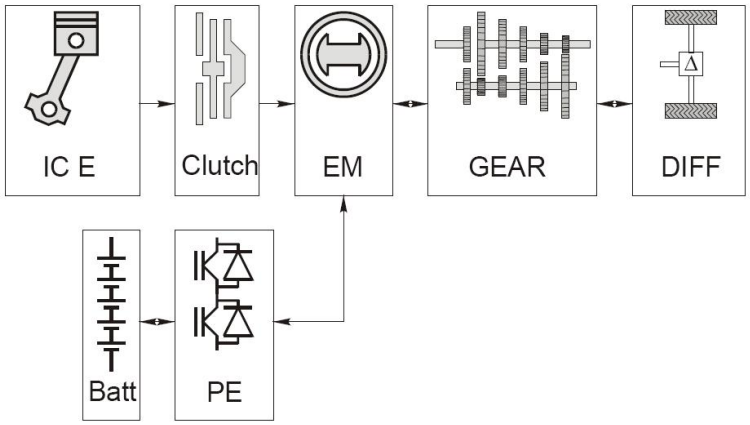

Figure 2.2: Parallel Hybrid Electric Vehicle, [4].

In a parallel hybrid electric vehicle the performance of the vehicle does not only rely on the size and the characteristics of the electric motor. The parallel topology also has some other advantages, such as; no demand for a generator and elimination of inefficiency due to multiconversion since the engine is connected directly to the wheels, i.e. no need to convert mechanical power from the engine into electricity in order to then convert it back to mechanical power.

Some drawbacks are enclosed due to the mechanical coupling of the ICE to the wheels; partly the operating point cannot be chosen freely and partly the parallel hybrid drivetrain has a more complex control than the series hybrid drivetrain.

The parallel electric drivetrain mainly has the five following operation modes:

- Engine-alone traction: When the demanded power is less than the power the ICE can produce when operating in its optimal region and the PPS has reached its upper SOC limit, only the engine is operated.
- Electric-alone traction: When the speed of the vehicle is less than the minimum vehicle speed where the engine still operates steadily, only the electric motor supplies the demanded power.
- Hybrid traction: When the load power is greater than what the ICE can produce, both the engine and the electric motor need to provide their power to the driven wheels.
- Regenerative braking: In this operation mode the demanded braking power is less than the maximum regenerative braking power possible to be provided from the electric system. Now the electric motor is operating as a generator.
- Peaking power source (PPS) charging from the engine: The power demand is less than what the ICE can provide when operating in its optimal region and the SOC of the PPS is below the SOC's upper limit, then the PPS will be charged.

2.3 Components in the driveline

This section deals with some of the components that are common in hybrid electric and electric vehicles, namely internal combustion engines, electrical machines, electrical energy

buffers and power electronic converters. For each component necessary background information is given, as well as suggestions regarding how the the components can be modeled.

2.3.1 The internal combustion engine

The most common primary energy source in automobiles is the piston-type *Internal Combustion Engine*, ICE, also called the *reciprocating engine*. The engine converts the electrochemical energy from the fuel into heat, which then produces a mechanical work. This is achieved through a cyclic process, where a piston is moving up and down (reciprocating) inside a cylinder driving a crank shaft via a rod, see Figure 2.3.

The engine can have one or more cylinders depending on the required power. The fuel is being combusted inside the cylinder, hence the name *internal* combustion engine.

2.3.1.1 General working principle of the four stroke ICE

In most engines the power process type is the *four stroke cycle*, or the Otto cycle (invented 1876, by Nicolaus Otto). As the name implies, the piston moves four times during one engine power cycle.

The first stroke, intake stroke, starts with the piston in the up position and ends with the piston in the down position, while an air/fuel mixture is being drawn in to the cylinder through the inlet valve.

The inlet vault is then closed, and the piston is moving to the up position, compressing the mixture, the second/compression stroke. At the up position the mixture is ignited, initiated by a spark plug if the fuel is gasoline.

That is the start of the third stroke, the power or expansion stroke, where the heat and pressure increases so that the piston is pushed to the down position and the crank shaft is forced to rotate. This is where the major work of the engine is being done, in fact about five times more than in the compression stroke.

Now the exhaust vault is opening and in the fourth and last stroke, the exhaust stroke, the piston moves to the up position as the cylinder is cleared from the exhausts of the combustion.

After this the first stroke follows and the process starts all over again. [1], [2], [3]

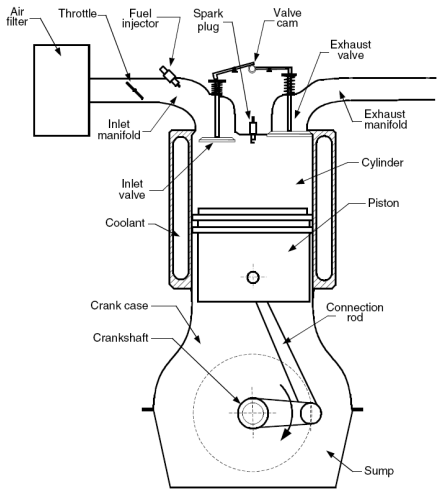

Figure 2.3: Schematic figure of one cylinder, piston and fuel-exhaust manifolds in a four stroke ICE, [3].

There is an optimal ratio of the mass flow of air to the mass flow of fuel, called *stoichiometric* fuel/air ratio, with which the combustion can be fully completed. For a gasoline engine this ratio is typically about 14.6, i.e. for each kg mass of fuel, $14.6\,kg$ of air is needed. For a reliable combustion, it is best to keep the air/fuel ratio close to this value.

The $\lambda - value$ (*lambda-value*) is the ratio of the actual air/fuel relation to the stoichiometric air fuel relation. For maximum power output (at full load and wide open throttle), λ should be about $0.85 - 0.95$, since less air is needed. At part load (part-throttle) a reduced power output and reduced fuel consumption is achieved with $\lambda > 1$.

It is thus important to be able to control both the air and the fuel flow into the inlet manifold where the two are mixed. This is usually done using a *carburetor* or a *fuel injection system*, in which the fuel flow is depending on the momentary flow of air. The air flow or the flow of fuel/air mixture into the cylinder is then controlled via a *throttle* whose angle of position is depending on the position of the gas pedal. Historically the carburetor has been dominating in the Otto engines, but since the injection systems, especially the electronically controlled, gives improved engine performance (ease the air flow, which gives increased power and torque as well as faster engine response to changes in throttle position, to mention a few), they are becoming more and more common.

To achieve a better engine performance, a large part of the details concerning the operation of the engines, can today be controlled electronically, using different types of *Engine Management Systems*, EMS's.

2.3.1.2 Engine performance parameters

One of the engine parameters is the *compression ratio*, which is the ratio of the cylinder volume when the piston is in the down position, to the volume when the piston is in the up position. A higher compression ratio gives higher engine efficiency at part load. However it also increases the risk of premature ignition of the air/fuel mixture. This is called *knocking* due to the arising metallic noise. It causes a power loss and it can damage the piston and cylinder.

The torque produced by the engine is directly proportional to the engine size or *displacement volume*, which is defined as the piston swept volume from the down to the up position. The power is proportional to the area of the piston head as well as to the mean piston speed. That is, the larger the engine size, the higher the produced torque and power. Other factors that influence the torque and power production are; the fuel conversion efficiency, the so called volumetric efficiency, the heat released from the fuel at combustion, the density of the inlet air and the fuel air mixture. Most of these factors are not usually given in the data sheet from the manufacturer, but they must be measured or estimated by the user.

The mechanical efficiency, i.e. the ratio of the power produced in the cylinder to the power available on the crank shaft, depends on the throttle position as well as the engine speed and design. The main mechanical losses are due to friction of the bearings and the piston.

Another interesting parameter, which can be found through engine testing, is the *brake Specific Fuel Consumption*, bSFC, usually measured in g/kWh. The bSFC is defined as the mass flow of fuel per unit time, per net crank shaft power output, and it is a measure of how efficiently the engine can utilize the supplied fuel to produce work. The lower the SFC the better, where a typical good value for an ICE is about $250 - 270\,g/kWh$ [3].

2.3.1.3 Engine operating characteristics

As can be seen in Figure 2.4 and Figure 2.5, the SFC for a typical ICE varies significantly over the engine speed range and loading (throttle position). The engine has its *optimal operating region* in about the middle of the engine speed range, that is close to the maximum output torque, and at about half of the maximum output power, but close to full load operation (wide open throttle). It is here that the losses during the first and last of the engine strokes are the smallest. For the most fuel efficient operation, it is thus desirable to operate the engine close to or rather in its optimal operating range.

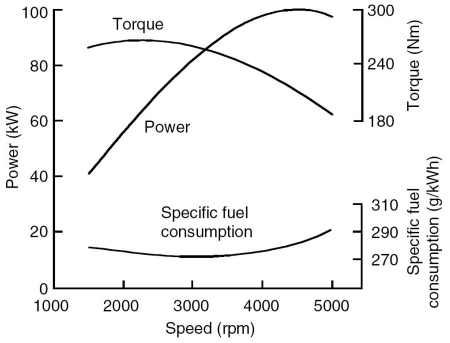

Figure 2.4: Typical output torque, power and SFC for an ICE at wide open throttle, [3].

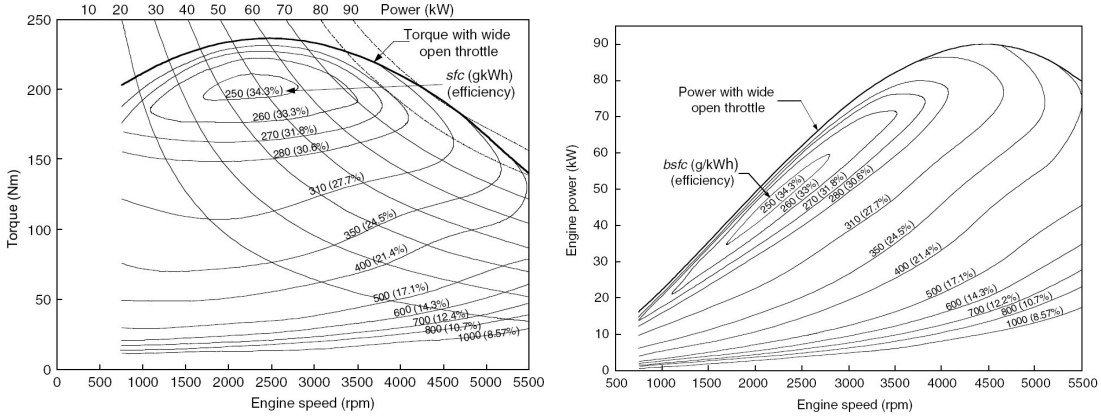

(a) Crank shaft torque vs. engine speed

(b) Output power vs. engine speed

Figure 2.5: Fuel consumption and efficiency for a typical ICE at different load conditions, [3]

2.3.2 The electric machine

The electric machine(s) used in HEVs or EVs convert electric energy into mechanical energy to propel the vehicle or to brake the vehicle regeneratively. They can also be used to generate electricity when charging the onboard buffer system. Differing from electric motors used in industrial applications these motors typically require frequent starts and stops, need high rates of acceleration/deceleration, high torque and need a very wide speed range.

All electric motors mainly have the same limitations depending on the materials (copper and iron) from which they are made. Firstly, the possible output power of a motor is dependent on the allowable temperature rise of the windings, and possible permanent magnets, if used. Higher insulation level and better cooling system allow higher currents.

Secondly, motors of roughly the same volume can be expected to produce almost the same torque. Thirdly, the output power per unit volume is directly proportional to the speed. Therefore it is typically better to use a high-speed motor and then mechanically reduce the speed. Fourthly, larger motors are more efficient than small ones. E.g. a very small motor can have an efficiency as low as about 1% whereas larger motors can have efficiencies above 95%. Fifthly, the efficiency of a motor improves with speed.

The electric motor types that will be treated are; the DC motor, the induction motor and the permanent magnet synchronous motor. The two latter ones are commutatorless motors, resulting in higher efficiency, higher power density, lower operating cost, higher reliability and maintenance-free operation.

The efficiency of an electric motor varies depending on at which point in the torque-speed plane the motor is operating, see Figure 2.6.

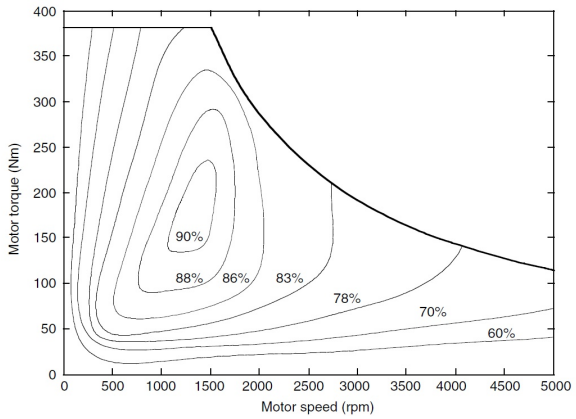

Figure 2.6: General electric motor efficiency characteristics, [3].

The electric motors all have the possibility of regenerative operation. Then the motors are controlled to operate as generators to convert the vehicle's kinetic or potential energy into electric energy which can be stored in the buffer system and reused. Usually the electric motor can not produce enough torque to meet the required braking torque, consequently the mechanically frictional braking must coexist with the electrically regenerative braking.

2.3.2.1 The DC machine

The brushed DC machine was until the 1980s the automatic choice where speed or torque control was desired. After that a transition towards inverter-fed induction machines has been taken place. The DC machines range from a few watts to several megawatts output power. Figure 2.7 shows a two pole field winded DC machine.

Torque is created when the axial current-carrying conductors on the rotor interacts with the radial magnetic flux produced by the stator. However, the magnetic flux does not contribute to the mechanical output power, it only makes the energy conversion possible. The total developed torque in Nm is

$$T = k_t I, \tag{2.1}$$

where k_t (Nm/A) is the motor torque constant and I (A) is the armature current.

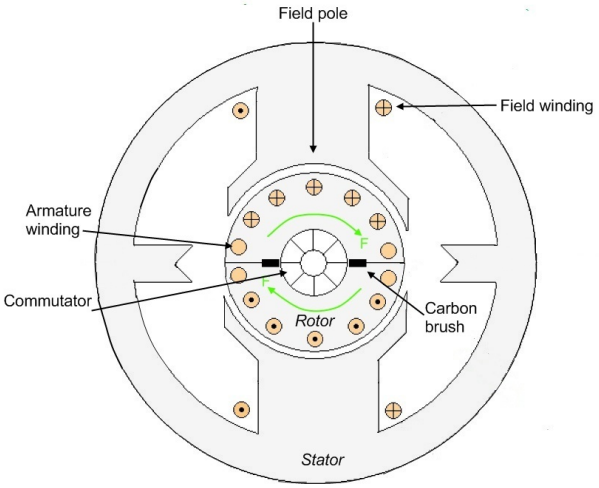

Figure 2.7: A field winded DC machine with two poles.

When the rotor turns, the armature winding will cut the radial magnetic flux and an EMF will be induced in the conductors. The resultant EMF in V developed at the brushes is

$$E = k_e \omega, \tag{2.2}$$

where k_e (Vs/rad) is the EMF constant and ω (rad/s) is the angular speed.

k_t and k_e are essentially the same number, the difference between them is only a matter of which units are used.

The stator consists of either permanent magnets or DC windings to produce the magnetic flux, see Figure 2.8. Machines with permanent magnets are usually available for smaller motors, ranging from a few watts up to a few kilowatts, whereas machines with field windings range from about 100 W up to megawatt output levels.

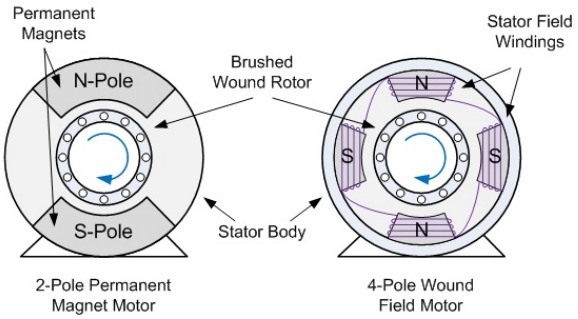

Figure 2.8: Permanent magnet DC motor and field winding DC motor, [33].

The DC motor's equivalent circuit can be seen in Figure 2.9 and it can be described by the following equation,

$$U = E + IR + L\frac{dI}{dt}, \tag{2.3}$$

where U (V) is the armature voltage, I (A) the current through the armature winding, R (Ω) the armature resistance and L (H) is the armature inductance. The last term in equation (2.3) can be ignored during steady-state.

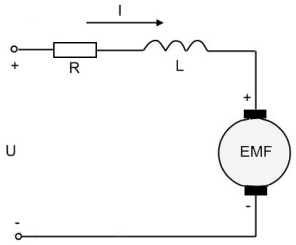

Figure 2.9: Equivalent circuit for a DC motor, [10].

Figure 2.10 shows the steady-state characteristics of a DC motor. In the full field area the motor is capable of producing its full rated torque at any speed up to base speed. To operate the motor at a speed above base speed the flux must be reduced, called field weakening. As can be seen in Figure 2.10 field weakening is only applicable where full torque at high speeds are not demanded. The field weakening range varies a lot between different motors, but maximum speed seldom exceeds three or four times the base speed.

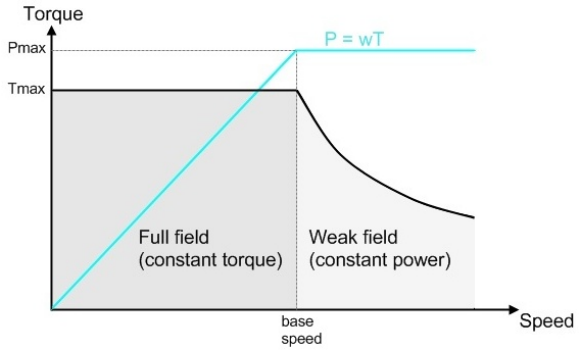

Figure 2.10: Steady-state characteristics of a DC motor.

The DC machine can operate in all four quadrants, see Figure 2.11. In quadrants number one and number three the DC machine is operating as a motor, but in the first quadrant the machine is running in forward direction and in the third quadrant it is running in the opposite direction. In quadrants number two and number four the DC machine is operating as a generator. Here the back EMF is larger than the applied armature voltage in contrast to when the DC machine is operating as a motor where the applied armature voltage is larger than the back EMF.

2.3.2.2 The induction machine

Until the early 1970s the induction machine was operating uncontrollable with constant frequency and voltage. The appearance of reliable variable-frequency inverters, due to the advent of controlled semiconductor power switches in the 1960s, made it possible to use the induction machine in variable-speed applications. It became now feasible to convert direct voltage from a battery to alternating voltage of variable frequency and amplitude. However, it was not until the 1990s that the variable-speed drives became more frequently used and it was then only in industrial and traction applications.

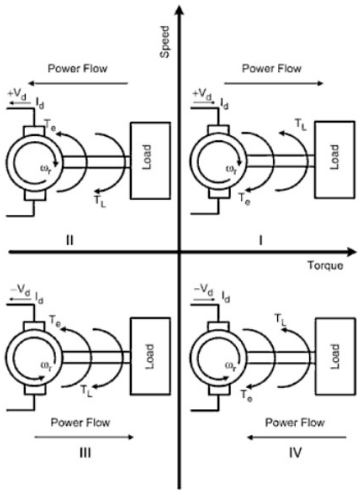

Figure 2.11: Four-quadrant operation of a DC motor, [34].

The torque in an induction machine is produced in the same way as in a DC machine, axial currents in the rotor interact with a magnetic field produced by the stator. However, in the induction machine there is no need for neither brushes nor commutator to feed the torque-producing currents into the rotor, as it is in the DC machine. Instead, the rotor currents will be induced by the air-gap field as long as the rotor and the magnetic flux wave are not rotating at the same speed, i.e. the slip is not 0. If the slip would be 0 the rotor would rotate at synchronous speed with no induced electromagnetic force and thus no induced rotor currents, i.e. the machine will operate in idle.

Figure 2.12 shows the torque-speed characteristic of an induction machine. When the slip is between zero and one the IM is operating as a motor, with a slip above one the machine is in braking mode and when the slip is negative the IM is operating as a generator.

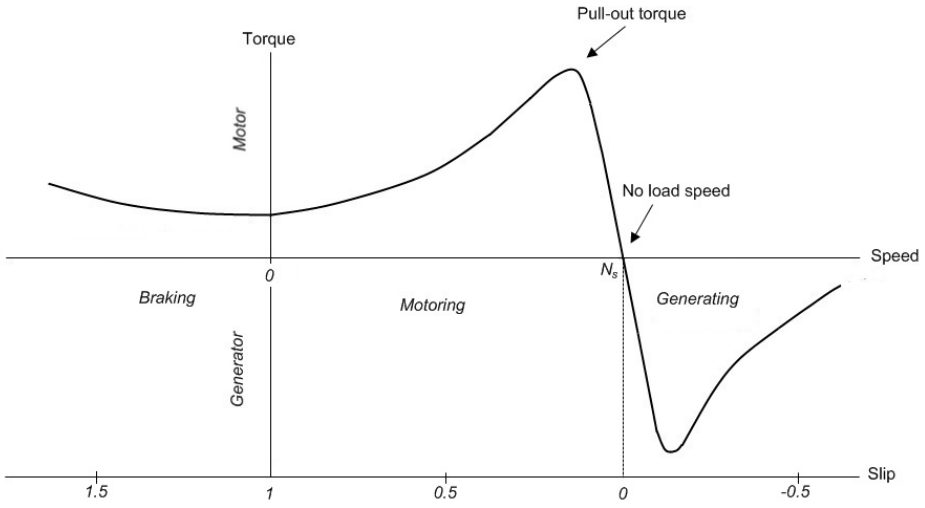

Figure 2.12: Torque-speed characteristic of an induction machine.

The induction machine has a series of advantages over the DC machine such as; less maintenance due to the absence of sliding mechanical contacts, size, weight and cost.

The dynamic model of the induction machine
The induction machine can be modeled as a dynamic T-equivalent circuit or as a dynamic inverse-Γ circuit. This thesis focus only on the dynamic T-equivalent circuit which can be seen in Figure 2.13. The magnetic hysteresis losses, the iron losses, are neglected. These could have been modeled as a resistance in parallel with the magnetizing inductance in the equivalent circuit.

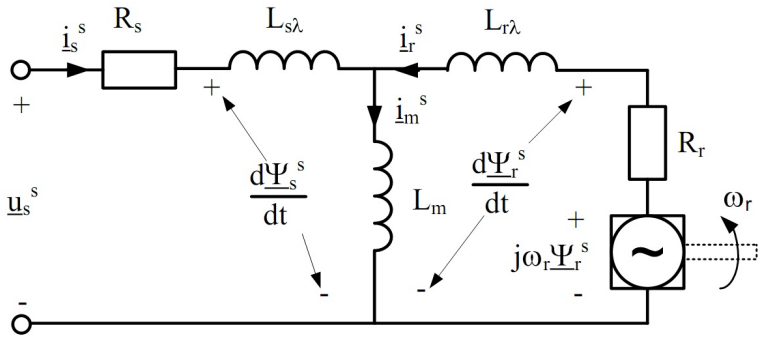

Figure 2.13: The dynamic T-equivalent circuit of the induction machine in $\alpha\beta$-coordinates, [**?**].

The following ten equations describe the induction machine in stationary coordinates ($\alpha\beta$-system),

$$\underline{u}_s^s = R_s \underline{i}_s^s + \frac{d\underline{\Psi}_s^s}{dt} \tag{2.4}$$

$$u_{s\alpha} = R_s i_{s\alpha} + \frac{d\Psi_{s\alpha}}{dt} \tag{2.4a}$$

$$u_{s\beta} = R_s i_{s\beta} + \frac{d\Psi_{s\beta}}{dt} \tag{2.4b}$$

$$0 = R_r \underline{i}_r^s + \frac{d\underline{\Psi}_r^s}{dt} - j\omega_r \underline{\Psi}_r^s \tag{2.5}$$

$$0 = R_r i_{r\alpha} + L_r \frac{di_r\alpha}{dt} + L_m \frac{di_s\alpha}{dt} + \omega_r L_r i_r\beta + \omega_r L_m i_s\beta \tag{2.5a}$$

$$0 = R_r i_{r\beta} + L_r \frac{di_r\beta}{dt} + L_m \frac{di_s\beta}{dt} + \omega_r L_r i_r\alpha + \omega_r L_m i_s\alpha \tag{2.5b}$$

$$\underline{\Psi}_s^s = L_s \underline{i}_s^s + L_m \underline{i}_r^s \tag{2.6}$$

$$\underline{\Psi}_r^s = L_r \underline{i}_r^s + L_m \underline{i}_s^s \tag{2.7}$$

$$\frac{J}{n_p}\frac{d\omega_r}{dt} = T_e - T_L \tag{2.8}$$

$$T_e = \frac{3n_p}{2}(\Psi_{s\alpha} i_{s\beta} - \Psi_{s\beta} i_{s\alpha}), \tag{2.9}$$

where

$\underline{u}_s^s$	:	complex stator voltage in stationary coord. (V)	L_s	:	stator inductance (H)
R_s	:	stator resistance (Ω)	L_m	:	mutual inductance (H)
$\underline{i}_s^s$	:	complex stator current in stationary coord. (A)	J	:	machine inertia (kgm^2)
$\underline{\Psi}_s^s$	:	complex stator flux linkage in stationary coord. (Vs)	n_p	:	pole pair number
R_r	:	rotor resistance (Ω)	ω_r	:	electrical rotor speed (rad/s)
$\underline{i}_r^s$	:	complex rotor current in stationary coord. (A)	T_e	:	electrodynamical torque (Nm)
$\underline{\Psi}_r^s$	:	complex rotor flux linkage in stationary coord. (Vs)	T_L	:	load torque (Nm).

Induction Motor Control

It is complicated to control an induction motor since the stator field is rotating. It is even more complicated in the case of a squirrel-cage induction motor as the rotor currents or rotor flux cannot be monitored.

Traditionally, the speed of the induction motor was controlled by Volt/Hz control. This type of control is a scalar control method, where the motor is controlled by, as the name indicates, linearly adjusting the stator frequency and the magnitude of the stator voltage. Scalar control is only suitable for steady-state operation of the motor. To achieve better dynamic performance vector control, which is also called Field Oriented Control (FOC), is desirable. Due to higher allowable speeds and shorter time constants of AC motors, vector controlled AC drives have the capability of better dynamic performance than DC drive systems.

Direct Torque Control is another, a bit younger, technique for instantaneously controlling the torque of high-performance variable speed drives, however this method will not be treated in this thesis.

Rotor flux estimation

In order to find the transformation angle, which is used when transforming between $\alpha\beta$- and the so called dq-system, flux measurements need to be done. This requires sensors being placed in the airgap, but these sensors are expensive and not very reliable and therefore the rotor flux should be estimated instead.

Basically, there exist two different vector control techniques; Direct Field Orientation (DFO) and Indirect Field Orientation (IFO). With DFO, the rotor flux position is estimated from quantities in the $\alpha\beta$-system. Whereas, with IFO, the rotor flux position is estimated from quantities in the dq-system.

There are two types of flux estimators; the current model (CM) and the voltage model (VM). The current model, which uses rotor equations, is suitable for lower rotor speeds. The voltage model, which uses stator equations, is better suited for higher rotor speeds.

2.3.2.3 The Permanent Magnet Synchronous Machine

A synchronous machine can be compared to a DC machine which has been turned inside out. A SM provides constant speed for a wide range of loads, see Figure 2.14. In a synchronous motor the rotor flux is produced by permanent magnets or by a field winding supplied from an external DC source inside the rotor.

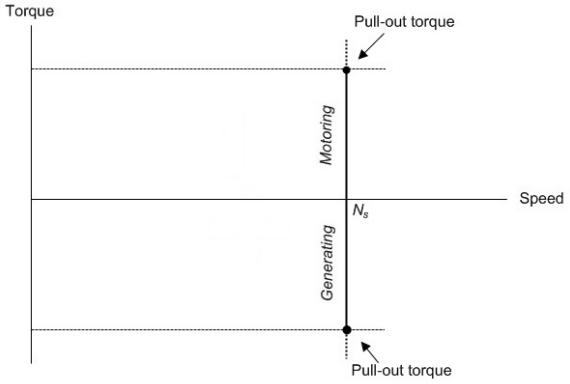

Figure 2.14: Torque-speed characteristic of a synchronous machine.

The inverter-fed synchronous motor has one apparent advantage over the induction motor. The speed is exactly determined by the frequency in a synchronous motor, whereas the motor speed in an induction machine always run with a slip relative to the synchronous speed.

As the name implies a PMSM uses permanent magnets to produce the rotor flux. The PMSM has advantages such as; no slip-rings and no RI^2 losses in the rotor since permanent magnets are used instead of a field winding. At the same time the use of permanent magnets involves a drawback due to fixed excitation.

The dynamic model of the PMSM
The dynamic model of the PMSM can be seen in Figure 2.15.

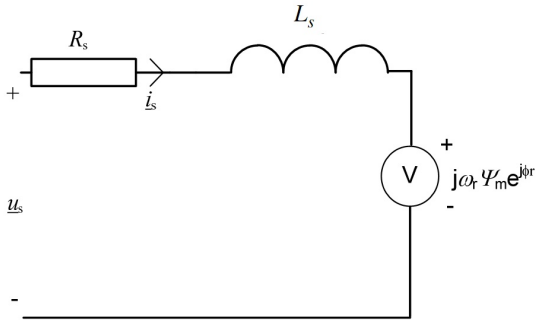

Figure 2.15: Dynamic model of the permanent magnet synchronous machine, [?].

The following four equations describe the PMSM in stationary coordinates,

$$u_{s\alpha} = R_s i_{s\alpha} + L_s \frac{di_{s\alpha}}{dt} - \omega_r \Psi_m sin(\Phi_r) \tag{2.10}$$

$$u_{s\beta} = R_s i_{s\beta} + L_s \frac{di_{s\beta}}{dt} - \omega_r \Psi_m cos(\Phi_r) \tag{2.11}$$

$$T_e = \frac{3n_p}{2} \Psi_m (i_{s\beta} cos(\Phi_r) - i_{s\alpha} sin(\Phi_r) \tag{2.12}$$

$$\frac{J}{n_p} \frac{d\omega_r}{dt} = T_e - T_L, \tag{2.13}$$

where

$u_{s\alpha}$	:	α-coord. of the stator voltage (V)	Ψ_m	:	flux linkage (Vs)
$u_{s\beta}$	:	β-coord. of the stator voltage (V)	Φ_r	:	rotor position [rad]
R_s	:	stator resistance (Ω)	n_p	:	pole pair number
$i_{s\alpha}$	:	α-coord. of the stator current (A)	J	:	machine inertia (kgm^2)
$i_{s\beta}$	:	β-coord. of the stator current (A)	T_e	:	electrodynamical torque (Nm)
L_s	:	stator inductance (H)	T_L	:	load torque (Nm).
ω_r	:	electrical rotor speed (rad/s)			

To be able to perform vector control of a PMSM, the rotor position needs to be known at all times,

$$\frac{d\Phi_r}{dt} = \omega_r. \tag{2.14}$$

This can be solved by using a mechanical sensor such as a resolver or an encoder, however a mechanical sensor will occupy a significant amount of space. There are mainly two different methods to obtain the rotor position without using a mechanical sensor; the signal injection method and the back EMF method.

2.3.3 Electric energy storages

In HEV's, an electric energy storage can be used as a buffer to absorb the temporary excess of energy, during braking, and deliver the momentary extra energy needed during acceleration, which is the characteristic of automotive driving. Apart from that, the storage device may also be used as an alternative energy source when the ICE is turned off and the electric machine is used as a tractive motor. This means that it is desired that the HEV electric energy storage device has a high energy capacity, and perhaps more importantly a high peak power capacity.

In EV's, on the other hand, the electric energy storage is the only source of energy. Then the feature of having a high energy density becomes even more important, in order to reach longer traveling distances for each charging.

Other desirable properties of energy storage devices are; high efficiency as well as long calendar and cycle life. Operational temperature range, initial and replacement costs, weight and volume, safe operation and reliability, are all important considerations when it comes to electrical energy storage devices.

Traditionally the main electric energy storage device in HEV's and EV's are batteries. However lately, thanks to its relatively high power density, the so called *Supercapacitors* or *Ultracapacitors*, are also becoming interesting for this matter, perhaps not to replace the battery, but to complement it. Then the power storage, i.e. the supercapacitor, could

be used during accelerations, later to be charged by the energy storage, i.e. the battery, during more undemanding driving.

This section gives a short introduction of the two and their properties. Additionally a relatively new capacitor technology, lithium ion capacitors is given a short review.

2.3.3.1 Batteries

Batteries store electrical energy as potential chemical energy in a battery cell, or many cells stacked together to form a battery pack. Every cell consist of two metal plates (electrodes), one electrically positive (cathode) and one negative (anode), with an electrolyte solution in between. Each charge and discharge is a conversion between the two energy forms, and is utilized by chemical reactions between the plates and the electrolyte.

Battery parameters

The amount of charge stored in a battery is expressed in Ampere-hours, (Ah), and is also referred to as the battery's *capacity*. In data sheets from the manufacturers, the capacity is often given for a discharge current rate of C/20. That is, during an iterative process the constant current magnitude has been found, such that the battery is fully discharged after 20 hours. The battery capacity is then, this current magnitude times 20, i.e. the capacity is the current magnitude that will discharge the battery in one hour.

When the battery is discharged the terminal voltage drops to the *cut-off voltage*. Below the cutoff voltage the cell voltage drops dramatically, and this should be avoided, see Figure 2.16(a).

Higher currents will naturally discharge the battery in shorter time. However it may also be that the cell voltage then will reach the cut-off voltage sooner, so that the delivered capacity is less than for smaller currents, see Figure 2.16(b). This tendency makes it rather difficult to say when the battery is actually fully discharged.

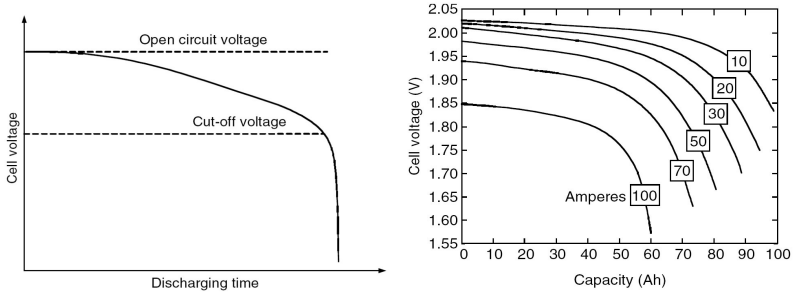

(a) Constant current discharge for a typical battery.

(b) Different levels of discharge currents for a typical lead-acid battery.

Figure 2.16: Battery cell voltage, [3]

The battery's remaining amount of charge is expressed as the *State Of Charge*, SOC. That is the remaining amount of charge relative to the initial capacity of the fully charged battery, i.e. a value between 0 to 1 or 0 to 100 %. The momentary SOC of a battery can be estimated as

$$SOC(t) = SOC_{init} - \frac{\int_0^t i(t)\,dt}{Q_{tot}} \tag{2.15}$$

where SOC_{init} is the initial value of SOC, $i(t)$ is the momentary battery current and Q_{tot} is the battery capacity. There is also a parameter called *Depth Of Discharge*, DOD, that

is simply the delivered amount of charge relative to the capacity, and this is also a value between 0 and 1.

When comparing different batteries the two terms *specific energy* and *specific power* (or energy and power density) are often used. The specific energy is the battery's energy capacity relative to its weight, (Wh/kg), or volume. Thus the specific power is the maximum short time deliverable power relative to the battery mass, (W/kg), or volume. This value is inversely proportional to the battery's inner resistance, i.e. higher resistance means lower specific power, [3].

The life expectancy of a battery is expressed in *cycle life*, where a cycle is a charge followed by a discharge. As the numbers of cycles for a battery is increasing, during use, the capacity starts to decrease and after a while the internal resistance and self discharge starts to increase at a higher paste. The deeper the cycles, the faster is the decay. When the capacity has gone down to a certain level (for example 70 or 80 % of the nominal value), the battery cycle life is said to be ended, [4].

Battery model

The charge separation that takes place in each battery cell give rise to a cell voltage, or *Open Circuit Voltage*, OCV. As soon as the terminal ends are closed in an electrical circuit, chemical reactions start to take place in the cell, causing the flow of a current. However, due to the charge transport in the electrolyte, and the chemical reactions at the surface of the plates and the current in the plates, there is a resistance to the current, which is called the battery's *internal resistance*, R. Thus the voltage over the battery terminals is affected by the voltage drop over the internal resistance. That means the terminal voltage also depend on the load current.

A simple circuit model of a battery is depicted in Figure 2.17(a), where the OCV is depending on the SOC, and the resistance is constant. There are, however, a number of factors that are not included in this simple model, such as the charge accumulation at the plates, which gives capacitive contributions to the resistance, SOC and temperature dependence of all parameters (OCV, R and C), and finally a self discharge of the battery, that can be modeled as a shunt resistance to the OCV. This gives the more complex model of Figure 2.17(b).

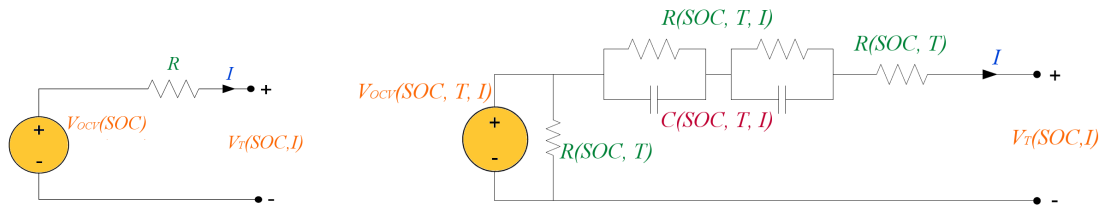

(a) Simple. (b) Complex.

Figure 2.17: Battery circuit model.

Battery types

Depending on the structure of the plate surface, the sort of metal/-s or alloy/-s of the plates, and the type of electrolyte used, the properties of different battery types differs. Not all types of batteries are suitable for electric vehicles. The most frequently used types, traditionally; Lead-acid (PbA) and Nickel-Cadmium (NiCd), are now being replaced by Nickel-Metal Hydride (NiMH) and Lithium ion (Li-ion), which is still under development.

The **lead acid** battery technology is about one and a half century old, and is among the cheapest and thus most common. The cell voltage is about $2\,V$. It has a good cycle life, is electrically and mechanically rugged, and has a relatively high power capability, but a low specific energy. It also preforms rather poor at low temperatures. The lead in the plates, is a toxic heavy metal and hydrogen gas and the sulfuric acid are potential safety hazards. [3]

The **nickel-cadmium** battery is an about 80 year old invention (since the early 1930s), [15], but the cost is about four times that of the lead acid, [4]. The advantages are many. It has a long cycle life, high specific power, electric and mechanical ruggedness, a wide temperature operating range ($-40 - 85$ ℃), a small voltage drop for many levels of currents and a low self discharge, [3]. It can also be charged rather quickly, [3]. During charging it is important to survey the battery temperature, since it rises steeply if the cell is overcharged. The main disadvantages apart from the cost, is the toxicity of the heavy metal cadmium, the relatively low cell voltage (typically $1.3V$) and that it suffers from the so called *memory effect*. This means that if the battery is cycled many times to a certain SOC, then changes in the plate structure (crystalline formation) will cause the cut-off voltage to shift to this value of SOC. Then the range of operation will be decreased. To prevent this, the user should occasionally let the battery be discharged to $1\,V$ per cell, [23]. Furthermore, the battery is polarity sensitive, and a polarity reversal is destructive.

The **nickel-metal hydride** battery and its characteristics is very similar to the Nickel-Cadmium battery, but it lacks the toxic cadmium, which makes it more environmental friendly. The technology is relatively young, from the middle of the 1970s, and is partly still under development. Other advantages over the NiCd is the much higher specific energy, a higher capacity per volume, and a somewhat smaller voltage drop. The disadvantages are that the self discharge is slightly larger than for the NiCd, and it charges a bit slower, [15]. The charging efficiency is best at about 0.5 to 0.7 SOC, [23]. Above 0.7 the heat losses increase. The temperature rise at the end of the charging is steeper than for the NiCd, thus demanding a more sensitive temperature surveillance. In addition this type of battery may have a memory effect, [3].

The **lithium-ion** battery is the youngest battery technology (since the early 1990s) of the ones mentioned, in fact it is still under world wide development, and is considered to be a very promising technology, [3]. The main advantage is the high specific energy and power, thanks to the lightness of lithium and the high cell voltage of about $4\,V$, [3]. The battery has a relatively low self discharge, and it does not suffer from memory effect. However, the battery preforms the best if it is only partly discharged, rather than frequently fully discharged, [23]. The battery capacity also decays over time if the battery is exposed to high temperature environments. At last the internal resistance is a bit higher in the Li-ion battery, compared to the Nickel-based batteries. This resistance will only increase during use, and will finally block the stored energy from being utilized. To limit the aging, the battery should be stored in a cool environment, at about 0.4 SOC, [23].

Some of the main battery parameters for the four different types are summarized i Table 2.1. These figures are constantly changing, especially for the NiMH and Li-ion types, and are to be considered as typical values for each type, since there is a variation within each type of category.

Table 2.1: Comparisons of different battery types for EV and HEV applications, [3], [4].

	Wh/kg	**W/kg**	**Cycle life**
Lead-acid	35-50	150-400	600-1000
Nickel-Cadmium	50-60	175-220	1500-2000
Nickel-Metal Hydride	70-95	200-300	1500
Lithium-ion	100-200	1000	1000 [1ex]

2.3.3.2 Supercapacitors (EDLC)

A capacitor is a passive component, consisting of two electrodes with an isolating medium in between, that can store electrical energy. As the electrodes are exposed to a potential difference, positive and negative charge is accumulated on the positive and negative electrodes respectively, and the isolating medium will uphold an electric field. The amount of energy, W_e (J), that a capacitor can store is directly proportional to its capacitance, C (F), and the square of the potential difference, U (V), over it, as in

$$W_e = \frac{CU^2}{2}, \tag{2.16}$$

The capacitance of the capacitor is in turn a physical property, that depends on the geometry of the electrodes and the permittivity, ϵ (F/m), of the insulator material. For a parallel plate capacitor, the capacitance is ideally found as

$$C = \frac{\epsilon A}{d}, \tag{2.17}$$

where A (m^2) is the surface area of the electrodes and d (m) is the separation distance between the electrodes or the positive and negative charge.

There are thus four factors to manipulate in order to increase the amount of energy that can be stored in the capacitor; large potential difference over the device, maximal surface area of the electrodes, minimal separation distance and use a suitable high permittivity insulator.

Supercapacitor structure

Depending on the type of insulator material used, there are three main categories of capacitors; electrostatic, electrolytic and Electrochemical Double Layer Capacitors, (EDLC), [24]. The EDLC, *supercapacitor* or *ultracapacitor*, has the largest capacitance value; on the cell level about a few kF, which is up to a thousand times larger than the electrolytic capacitance and even larger than the electrostatic types that are usually in the range pF to μF.

The extra high capacitance spring from the porosity of the activated carbon often used as electrodes, giving a very large surface area (up to $2000 m^2/g$), and the size of the carbon pours and ions of the electrolyte used, making the charge separation distance as short as hardly 10 $\AA$, see Figure 2.18, [24]. The negative electrolyte ions are attracted to the positive electrode, and the positive ions to the negative electrode, thus the charge separation is achieved without any chemical reactions, in contrast to batteries.

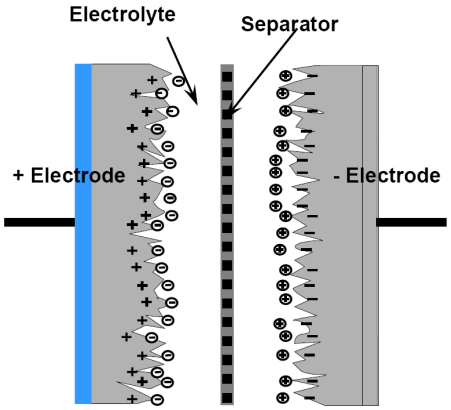

Figure 2.18: Principal description of a typical electrochemical double layer capacitor, or supercapacitor. The separator is ion-permeable. [16]

Supercapacitor circuit model

A simple circuit model of the supercapacitor can be seen in Figure 2.19, where C is the capacitance, V_C is voltage over the capacitance, R is the internal resistance, I is the load current and V_T is the terminal voltage. The internal resistance depend mostly on the contact resistance, electrode resistivity and the mobility of charges in the electrolyte. V_C is linearly dependent on the state of charge of the capacitance. V_T depend on V_C and the I dependent voltage drop over R.

There is also a self discharge in the capacitor, which is rather high compared to batteries. This resistance can modeled as a parallel resistor to the C.

The supercapacitor is quite independent of temperature, that is the capacitance is fairly constant over the whole temperature operating range. The resistance however increases with decreasing temperature, since the electrolyte mobility decreases.

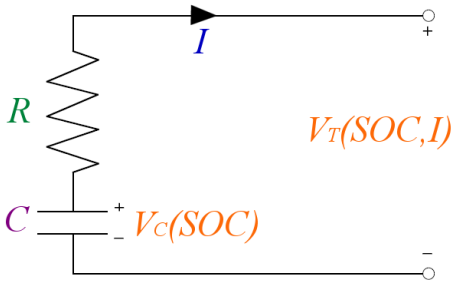

Figure 2.19: Simple circuit model of a typical supercapacitor.

Supercapacitor characteristics

Limited by the dielectric strength of the electrolyte, the maximum voltage per cell is only about $2 - 3\,V$. To reach higher voltage levels, a number of cells must be connected in series. Then the total capacitance of the device will naturally be lower than the per cell value, but it is still exceptionally high (a few hundred F).

Charging and discharging is fast, within about $10\,s$, since there is no chemical reactions, only limited by the heat development at the electrodes. For the same reason, the charging and discharging efficiency is the same, and rather high, at least 90%, [16].

The acceptable cell voltage is from maximum down to $0\,V$. Occasional over voltage spikes will not damage the cell, but contribute to the aging of the device. Along with over temperature, over voltage will cause a decrease in capacitance and an even larger increase

in internal resistance. The performance is decaying almost exponentially, initially being the most rapid, but later just level out. The end of the life for the component is said to be when it does not fulfill the application requirements anymore. Still a supercapacitor has a life cycle of some hundred thousand cycles, which is much higher than for a battery. [16]

The main advantage over the battery is the high specific power of the supercapacitor, which can go up to $20\,kWh/kg$, [24]. Unfortunately the specific energy is much lower than for a battery; only about $5\,Wh/kg$, [24].

The maximum power is delivered at maximum current, and thus it will depend on the remaining device voltage. At lower values of SOC, the voltage is lower as well, hence the maximum deliverable power is lower. For this reason, it is reasonable not to utilize too deep cycles for the supercapacitor. A lower voltage level will also limit the available energy output, $W_e = \frac{1}{2}C(Vmax^2 - Vmin^2)$.

2.3.3.3 Li-ion capacitors

In the lithium ion capacitor, the positive electrode is made of activated carbon, just like the EDLC. The negative electrode, on the other hand, is made of a lithium pre-doped carbon material, see Figure 2.20. This makes it possible for cell voltages of about $3.8\,V$. Another consequence is that the capacitance of the negative electrode is much higher than the one of the positive electrode, resulting in a higher per cell capacitance than for the EDLC.

Both a higher voltage and a higher capacitance is resulting in a higher energy density for the Li-ion capacitor compared to the EDLC. However the power density is more or less similar. A comparison of energy and power densities for different electrical buffers is presented in Figure 2.21.

The capacitor structure makes it polarity sensitive, and it has both a maximum and a minimum permissable voltage level. Exceeding these limits can cause pressure increase, heating, leaking or in the worst case possible explosion.

The technology is still very new and under development, currently by only a few manufacturers. For this reason, general information about the technology is scarce.

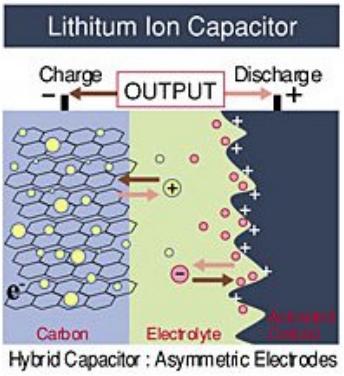

Figure 2.20: Structure of a Li-ion capacitor, [22]

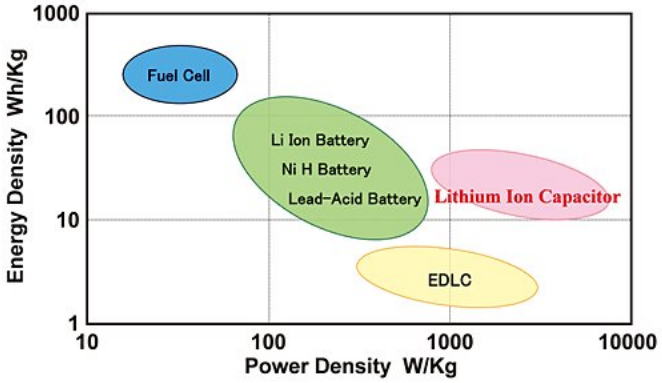

Figure 2.21: Energy and power densities for different electrical energy storage technologies, [22]

2.3.4 Power electronic converters

A power electronic converter between the electric buffer and the electric machine, is regularly used in hybrid electric and electric vehicles. This way the electric machines can be fed with the currently appropriate voltage magnitude, and DC voltages can be converted to AC voltages, by for example using PWM (Pulse Width Modulation), for the cases where three phase AC machines are used. Depending on the converter topology it can be designed to operate in either one, two or four quadrants (see previous section for information about quadrants).

In automotive applications switching converters (forced-commutated) can be used, in which one or more transistor switch/-es are controlled to operate either fully on or fully off at a certain switching frequency, f_s $(1/s)$.

When the switch is on, the current through it is relatively high, and the voltage drop over it is low, typically a few volts depending on the magnitude of the current and value of the transistors internal on-state resistance. When the switch is off, the voltage over it is often as large as the full system voltage, but the current through it is close to zero.

The commutation or switching between fully on and fully off is not immediate, but it takes some micro to nano seconds. This is mostly because the switches are realized by semiconductor devices, and they utilize charge transport, build up and sweep out when commutating, [6].

The converter losses are comprised of commutation losses and on-state losses, which are simply active power loss, i.e. the momentary voltage times the current, $P_{loss}(t) = i(t)v(t)$.

The commutation losses depend on the type of commutation/switching that is being utilized, *soft* or *hard switching*. In soft switching, either the voltage or the current is kept close to zero during the switching in order to minimize the switching losses. A more simple switching scheme to utilize is the hard switching, where the voltage and current is simultaneously nonzero during switching, see Figure 2.22.

As can be seen in Figure 2.22, the energy loss in each on-off or off-on switching, can be assumed to have a triangular shape in the time domain, making it rather simple to estimate the value of the average power loss. Apart from the voltage and current level, the switching loss also depend on the the turn-on , and turn-off times of the switch, $t_{c(on)}$ and $t_{c(off)}$ respectively. This is the time it takes for the current to rise and voltage to drop over the switch during turn on, and the voltage to rise and current to drop during turn off. Since the procedure is repeated in time, the *average switching power loss*, thus also

depend on the switching frequency, as in:

$$P_{sw} = \frac{1}{2} V_d I_o f_s (t_{c(on)} + t_{c(off)}) \tag{2.18}$$

The *average on-state losses*, depend on the on-state voltage, V_{on}, and current, I_o, but it also depend on the duty ratio, that is the on-time, t_{on}, relative to the total switching period, T_s (where $T_s = 1/f_s$), as in

$$P_{on} = V_{on} I_o \frac{t_{on}}{T_s} \tag{2.19}$$

For a MOSFET (Metal-Oxide-Semiconductor Field Effect Transistor), the on-state losses can also be represented by the resistive RI^2 losses, with the drain-source resistance, $R_{DS_{on}}$, and the drain current.

Thus, when investigating which type of transistor to use in the converter both the switching and the on-state characteristics may considered. MOSFET transistors have, for example, shorter switching times than BJT's (Bipolar Junction Transistor), however their on-state losses are slightly higher. The IGBT (Insulated Gate Transistor) is faster than a BJT, but not as fast as a MOSFET. The on-state losses for a IGBT is similar to those for the BJT, but much lower than those for the MOSFET. [6]

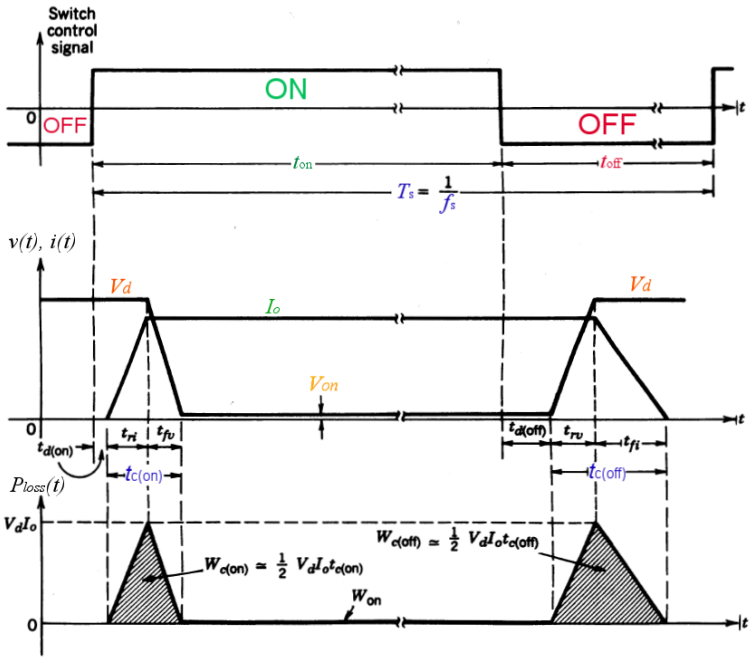

Figure 2.22: General converter losses at hard switching. For a more detailed explanation of this switching characteristics, see [6].

The efficiency of these converters are usually rather high, with peak values at $97-98\,\%$. Usually the efficiency does not vary dramatically with different points of operation, thus a modern well designed converter can be modeled having a constant efficiency. [4]

Finally there are certain limits for the range of operation of the converter, which are due to the limits of operation for the semiconductors used. The current should not exceed a certain value, or the component structure could be damaged. The temperature, and thus the power loss, should be kept within acceptable limits set by the components thermal

resistance (see section 2.4). It is possible to enhance the heat capability of the converter by using a heat sink or a fan. The last limit that should be taken into consideration is the maximum allowed voltage level, which is related to the amount of voltage the semiconductor can resist or block as the switch is off.

2.4 Thermal considerations and modelling

As have been stated in the previous sections of this chapter, the components in the driveline are not ideal, they are in fact producers of heat, whether it may be due to combustion, friction or electrical resistance. This heat will affect the material properties of the components, for instance the resistance of the the electric machine, and change the operating point of the component. Another consequence of high working temperature is that the component is aging or even worse, permanently damaged.

It is thus very important to, not only supervise the temperature development of the different components in the driveline, but also to try to keep the temperature within acceptable limits. For the later, one can in thermal design, utilize the fact that heat can be transported either through conduction, convection or radiation.

This section first deals with the thermal dependence of electrical resistance, and secondly it deals with stationary as well as transient thermal conduction and how these phenomena can be modeled.

2.4.1 Temperature dependence of electrical resistance

The electrical resistance of a conductive material is, around room temperature, linearly increasing with temperature, as in

$$R_T = R_{T_0}[1 + \alpha(T - T_0)], \tag{2.20}$$

where $R_T\,(\Omega)$ is the resistance at the arbitrary temperature $T\,(K)$, R_{T_0} is the resistance at temperature T_0 and $\alpha\,(1/K)$ is the material dependent temperature coefficient. For copper the temperature coefficient is $3.9 \cdot 10^{-3}\,K^{-1}$, [1]. This means that if the temperature of a conductor rises by 25 ℃, the resistance of a copper winding will increase by almost 10 %.

2.4.2 Steady state heat transfer by conduction

A temperature gradient inside a material will cause heat to be transferred by conduction, from the area of higher temperature to the area of lower temperature. Such a condition is illustrated by Figure 2.23, where a power source, $P\,(W)$, at one side of an isolated piece, causes the temperature T_2 to rise. This is leading to a net flow of energy per unit time, $P_{cond}\,(W/m^2)$, towards the side with lower temperature T_1. The relation between P_{cond} and the temperature difference is described by

$$P_{cond} = \frac{\lambda A\,(T_2 - T_1)}{d} = \frac{\Delta T}{R_\theta}, \tag{2.21}$$

where $T\,(K)$ is the temperature where $T_2 > T_1$, $\lambda\,(W/m\,K)$ is the thermal conductivity of the material, $A\,(m^2)$ is the parts cross section area, $d\,(m)$ is the parts length, [6]. Together the last three parameters comprise the parts *thermal resistance*, R_θ (℃/W).

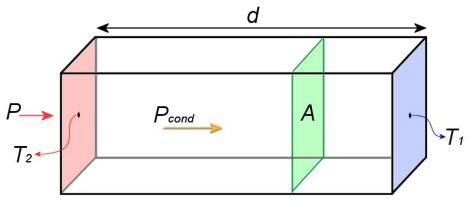

Figure 2.23: An isolated piece with a heat source, P, causing a temperature gradient, so that the power P_{cond} (W) is conducted from the higher towards the lower temperature side.

By assuming that all of the rate of heat energy, P, is also conducted through the piece, that is no heat is escaping along the sides of the piece, and by knowing the temperature, T_1 (which is often the ambient temperature and therefore assumed constant), the dimensions and material of the piece, one can calculate the value of the temperature at the heat source, T_2.

If the piece is comprised by two or more layers of different material and/or dimensions, the equivalent thermal resistance of the system is simply the sum of the individual contributions.

To keep the temperature down at the heat source it is then desired that the thermal resistance is as low as possible. This means a thin layer and a wide area, as well as a high thermal conductivity of the material/-s.

2.4.2.1 Modelling of steady state thermal behavior

The thermal behavior of a system can be modeled in the same manner as an electrical circuit, as in Figure 2.24, where the rate of heat energy resembles a constant current source, the temperatures of each layer is the potential relative to a ground point and the thermal resistance resembles the electrical resistance. The ambient temperature is assumed to be constant. It may also be assumed that the materials are homogenous, and that the temperature is the essentially same in the whole body of one layer.

By making these assumptions, the system is modeled as a so called *lumped parameter model*. The temperature at layer 1 can thus be calculated as in equation 2.22. Should there be parallel paths for the heat flow, it is simply modeled as parallel coupled resistors along with current division.

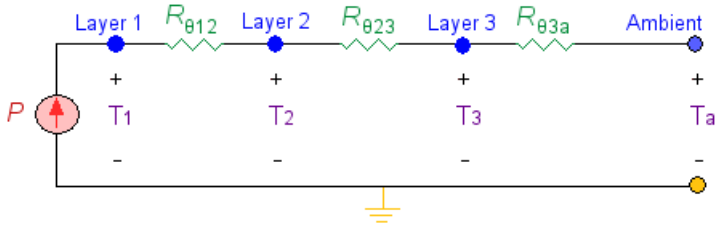

Figure 2.24: Equivalent thermal circuit of a three layer system.

$$T_1 = P(R_{\theta 12} + R_{\theta 23} + R_{\theta 3a}) + T_a. \tag{2.22}$$

2.4.3 Transient heat transfer by conduction

So far only steady state heat conduction has been described, where there is a constant heat source, and where the rise of temperature in a material, caused by the heat source, is immediate. However, in reality the rise of the temperature in a piece is not immediate, but it takes some time for the temperature to reach the steady state level. The time it takes depends on the materials specific heat, c_p $(J/kg\,K)$, and the mass, m (kg), of the piece, and is called the *thermal capacity*, C_θ (Ws/K) or (J/K), [7].

2.4.3.1 Modelling of transient thermal behavior

For systems where the magnitude of the heat source varies over time, as in automotive applications, it may be preferable to also consider the time it takes for the temperature to rise or fall, that is the systems *transient thermal response*. The transient thermal response of a component or physical system is characterized by its total equivalent *thermal impedance*, Z_θ, which is based on both its thermal resistance, R_θ and thermal capacity, C_θ.

The electrical analogy for the thermal capacity is the capacitance, meaning that it takes time for the temperature to rise inside a part, much like the voltage over a capacitive component.

The equivalent thermal impedance of a system represents its thermal step response to an input power pulse; $Z_\theta(t) = (T(t) - T_a)/P(t)$, [6], [9].

When it comes to making lumped parameter equivalent circuits of a component or system of layers, there are two ways of interpreting the given information from a manufacturer regarding the components thermal behavior. Either the component can be represented by the Foster-type thermal equivalent circuit, or by the Cauer type, see Figure 2.25.

However only the Cauer-type can represent real physical thermal behavior, since with the Foster-type model, the temperature rise would be immediate, but with the Cauer type, there is a time delay of temperature rise due to the grounded capacitors, which thus represent the material mass in the system, [8].

This also means that for the Foster-type model the nodes does not correspond to any specific layer or bound inside the system, [9]. The equivalent Foster-type circuit merely gives a much more simple mathematical expression (in the time domain) for the total equivalent thermal impedance of the system, i.e. a sum of exponential expressions like: $R(1 - e^{-t/RC})$ for each pair of parallel R and C in the circuit, [8]. This makes it much easier for manufacturers to fit measured data of thermal transient response to a Foster-type equivalent circuit.

In the exponential expression of the thermal impedance above, the RC parameter is called *time constant*, $\tau\,(s)$. When exposed to a power step, it will take one time constant for the temperature inside the part to rise to 63.2 % of its final value.

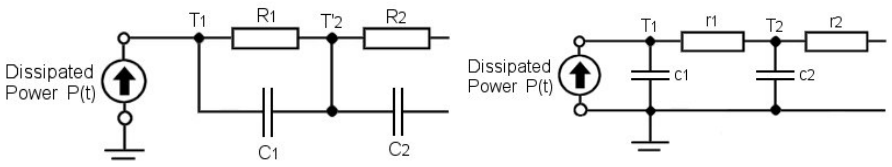

(a) Foster-type. (b) Cauer-type.

Figure 2.25: Thermal equivalent circuits for transient heat conduction, [8]

2.5 Vehicle Dynamics

There are four major forces acting on a moving vehicle. The acceleration force and the three forces opposing the motion of the vehicle due to; air drag, rolling resistance and climbing resistance. The forces due to air drag and rolling resistance is pure losses. The forces due to climbing resistance and acceleration are, on the other hand, conservative forces with possibility to, at least partly, recover.

2.5.1 Aerodynamic Drag

The force opposing the motion of the vehicle due to air drag consists mainly of two components; *shape drag* and *skin friction*. When a vehicle is moving there will be one zone in front of the vehicle where the air pressure is high and one zone behind the vehicle where the air pressure is low, these two zones will oppose the motion of the vehicle. The resulting force on the vehicle is the shape drag. The second component of aerodynamic drag, skin friction, is created due to the fact that two air molecules with different speed create friction. Since the speed of the air close to the vehicle moves almost with the same speed as the vehicle, in contrast to the air speed far away from the vehicle there will be a creation of friction

The aerodynamic forces are becoming more significant regarding vehicle power requirements at moderate and higher speeds,

$$F_a = \frac{1}{2} \cdot \delta \cdot C_d \cdot A \cdot v^2, \tag{2.23}$$

where δ (kg/m^3) is the air density, C_d aerodynamic drag coefficient characterizing the shape of the vehicle, A (m^2) cross-sectional area of the car where it is the widest, and v (m/s) is the speed of the vehicle. The aerodynamic drag coefficient can vary from 0.15 for an optimum streamlined car to 0.50 for an offroad car.

2.5.2 Rolling Resistance

Hysteresis in the tire materials is the major contribution to the rolling resistance of tires on hard surfaces. Hysteresis arises when the carcass of the tire is deformed, causing an asymmetric distribution of ground reaction forces. Hysteresis is minimized when having a high pressure of the tire and a hard road surface. There are also other factors affecting the rolling resistance such as; friction between tire and road, and circulating air in the tire. The rolling resistance force is given by

$$F_r = C_r \cdot m \cdot g, \tag{2.24}$$

where C_r is the friction constant, m (kg) the mass of the vehicle, and g (m/s^2) is the gravitational constant.

The rolling resistance coefficient, C_r, is influenced by parameters such as; tire material, tire structure, tire temperature, tire inflation pressure, tread geometry, road roughness, road material and the presence or absence of liquids on the road.

2.5.3 Climbing Resistance

The weight of a vehicle going up or down a hill will create a force directed downward. This force will either oppose the motion when traveling upwards or it will contribute to the motion when traveling downwards. The climbing resistance force is given by

$$F_c = m \cdot g \cdot sin(\alpha), \tag{2.25}$$

where m (kg) is the mass of the vehicle, g (m/s^2) the gravitational constant, and α (rad) is the road angle.

2.5.4 Acceleration force

The acceleration force is the total tractive effort of the vehicle minus the summation of forces opposing the motion of the vehicle. The net force results in an acceleration of the vehicle in the direction of the force. The acceleration force can be described as a linear motion,

$$F_{acc} = m \cdot a, \tag{2.26}$$

where m (kg) is the mass and a (m/s^2) is the acceleration of the vehicle or as a rotational movement,

$$\frac{d\omega}{dt} = \frac{\sum T}{J}, \tag{2.27}$$

where ω (rad/s) is the speed of the vehicle, $\sum T$ (Nm) the resultant torque acting on the wheels and J (kgm^2) is the total inertia of the vehicle.

Figure 2.26 shows the forces acting on a vehicle in motion, where F_t is the tractive force, F_a the aerodynamic resistance force, F_r the rolling resistance force and F_g is the climbing resistance force.

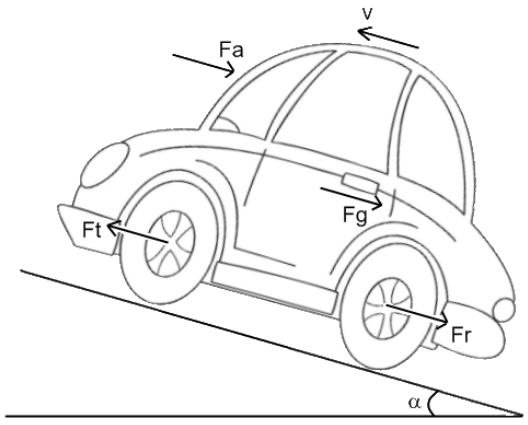

Figure 2.26: Forces on a moving vehicle, [35].

Part II

Chalmers Hybrid Electric Vehicle for the Shell Eco-marathon

Chapter 3

The Eco-marathon competition

Chalmers participated for the first time in the UrbanConcept group in Shell Eco-marathon Europe 2009 with a series hybrid electric vehicle. Every year students from all over the world compete in the Shell Eco-marathon with their vehicles to go the farthest distance on one liter of gasoline.

The Shell Eco-marathon Europe competition consists of two categories; *Prototypes* and *UrbanConcept*. In the *Prototypes* category the main design criteria is to build the most aerodynamic and fuel-efficient vehicle as possible. In the *UrbanConcept* category, created in 2003, the vehicles are designed to better represent a conventional car, with certain roadworthiness criteria needed to be fulfilled.

The record in the UrbanConcept group using an internal combustion engine is 589 km/l and is held by a team from Technical University of Denmark.

3.1 History

The Shell Eco-marathon has been around since 1939, at that time named 'Shell Mileage Marathon'. The idea of the competition was found when employees of the shell Oil's research laboratory in the U.S. had an argument about whose car would give the best fuel mileage. The current form of the Shell Eco-marathon began in 1985 in France, which implies that this year the 25th edition of the competition was held. Since 2007 there is also an American version called The Shell Eco-marathon Americas and in 2010 the first Shell Eco-marathon Asia is scheduled to take place.

3.2 Shell Eco-marathon Europe 2009

The 2009 edition was held at the EuroSpeedway Lausitz in Germany, located 50 km north of Dresden, where 200 teams from more than 25 countries were competing.

3.3 Rules summary for UrbanConcept

Here follows, for the simulation, interesting rules of the Shell Eco-marathon Europe UrbanConcept group competition.

3.3.1 Fuel type and fuel tank

Regardless of energy type, the results will be expressed in kilometers per liter consumption of Shell Unleaded 95 (EU) / Shell Plus 89 (US) Petrol/Gasoline equivalent and corrected

to 15°C.

One of the following fuel or energy types may be used; *Shell Unleaded 95 (EU) / Shell Plus 89 (US)*, *Petrol/Gasoline*, *Shell Diesel*, *Liquefied Petroleum Gas (LPG)*, *Shell Gas To Liquid (100% GTL)*, *Fatty Acid Methyl Ester (100% FAME)*, *Ethanol E100 (100% Ethanol)*, *Hydrogen*, and *Solar*.

The vehicle must be equipped with one of the following fuel tanks, which are supplied and approved by Shell; 30, 100, 250 or 350 cc.

3.3.2 UrbanConcept vehicles using hybrid technology

It is only allowed to use a supercapacitor as energy storage device and it must be the only energy source for the electric motor driving the vehicle. It is allowed to have a regenerative braking system.

The voltage of the supercapacitor will be measured before and after the race. If the voltage registered after the run is less than before the race, the supercapacitor will be charged until the voltage has reached the start level. Due to safety reasons, the maximum voltage on board the vehicle must not exceed 48 V.

3.3.3 Miscellaneous

The maximum allowed weight of the vehicle (excluding the driver) is 160 kg and the driver must weigh at least 50 kg in full driving gear.

The UrbanConcept vehicles must have four wheels and the rims must have a diameter of 16 or 17 inches.

3.3.4 The Race

Each race consists of 7 laps, each lap being 3.173 km. The complete race will be 22.081 km since start and finish line is not at the same place. The race must be completed in 53 minutes including three pit stops of 10 seconds each. This means that one has to have an average speed of just above 25 km/h. Figure 3.1 shows the track for the UrbanConcept class.

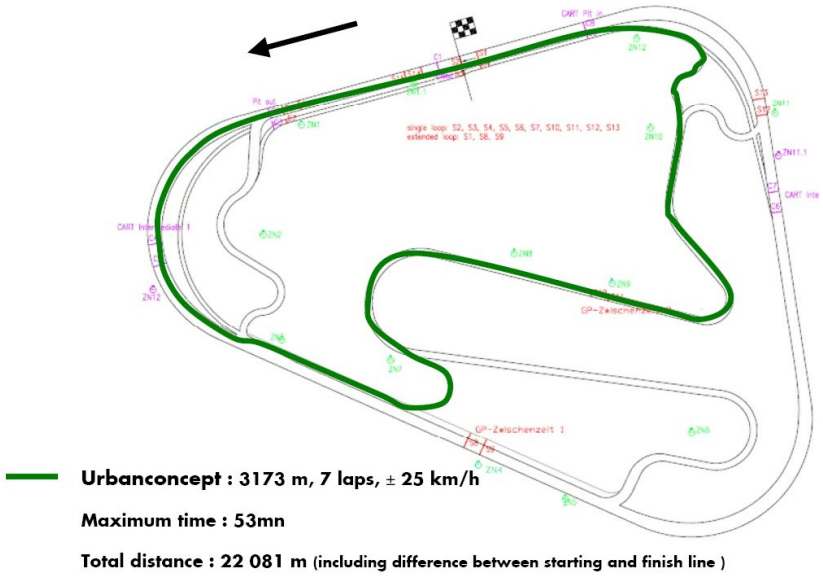

Figure 3.1: The UrbanConcept race track, [29].

Chapter 4

Chalmers vehicle; Smarter

Smarter, is the name of the series HEV, that Chalmers built for taking part in the Urban-Concept of the Shell Eco-marathon European competition in the spring of 2009.

In this chapter Smarter's driveline setup will be described. Necessary gathered information regarding the driveline components as well as other aspects of the vehicle, will also be presented. This information will then be the base for the MATLAB/Simulink modelling of the vehicle, that is presented in the next chapter.

4.1 The Smarter drive line

The drive line is thus a series hybrid, see Figure 4.1. This means that the ICE is not in direct contact with the wheels. Instead it is used for charging the electrical buffer, i.e. the supercapacitor, via one or two electrically paralleled DC generators. All the tractive effort is achieved using one or two electrically paralleled DC motors, each connected to one of the back wheels. A DC/DC-converter is placed between each tractive motor and the supercapacitor. The mechanical connection between the ICE and the generators as well as between the electric motor(s) and the wheel(s), are constant ratio chain gears.

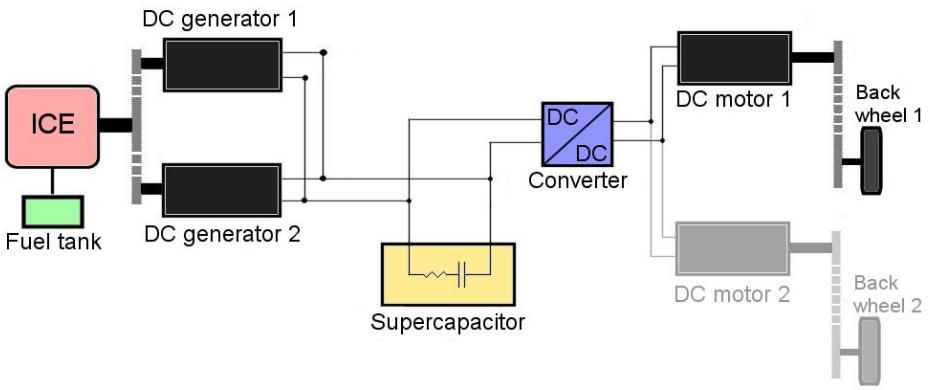

Figure 4.1: Smarters driveline. It can be run with one or two generators and one or two tractive motors.

4.2 ICE

There were two ICE's available for possible use in the vehicle; Honda GX25 and Honda GX35, two "mini" four-stroke, one cylinder, petrol engines of the same modell, but of different size, see Figure 4.2. Their data sheet specifications are listed in Table 4.1.

Figure 4.2: A Honda GX35 ICE, [25].

Table 4.1: ICE GX25 and GX35 data sheet specifications, [25].

	GX25	**GX35**
Displacement volume (cm^3)	25.0	35.8
Compression ratio	8:1	8:1
Max net power (kW) at 7000 rpm	0.72	1.0
Max net torque (Nm) at 5500 rpm	1.0	1.6
Dry weight (kg)	2.90	3.46 [1ex]

4.2.1 ICE modifications

Originally the ICE's had a carburetor, but comparison engine testing, conducted by master students at automotive engineering, showed that a fuel injection system was more fuel efficient. To increase the ICE efficiency, a control system called Versatile Engine Management System (VEMS), was used. The system uses four different sensors, including a lambda sensor, to monitor the engine performance. The external ignition timing was tuned via a software, as was the fuel injection. The lambda value was set to slightly less than 1 and the compression ratio was increased to 11:1, which should give a higher efficiency.

4.2.2 ICE performance measurements

Apart from the data sheet information from the manufacturer, Honda, a group of Chalmers Master students at automotive engineering has conducted measurements (2007) on the two engine's power and torque production as well as the specific fuel consumption, over a wide speed range . The tests were made with wide open throttle (100 %). The results are a bit rough, since the sensitivity of the fuel scale was relatively poor for these small differences in values. Also the engines were only run for about 10 s at each value of speed, and it was difficult to keep a constant speed below about 3000 rpm. It is not clear if or how the engines were modified at the time of these tests.

The results of the power and torque measurements along with data sheet values, can be seen in Figure 4.3 and Figure 4.4. Also the measurements of the engine's specific fuel consumption is presented in Figure 4.5. GX25 was run once at every speed level, but the

GX35 was run twice at five of the speed values (3000 - 5400 rpm). Thus the arithmetic mean value of those double values are presented in the figures.

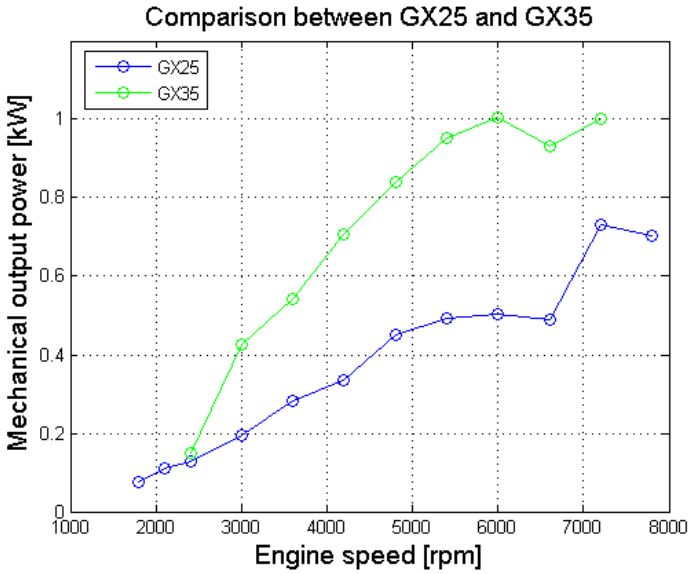

(a) Result from measurements.

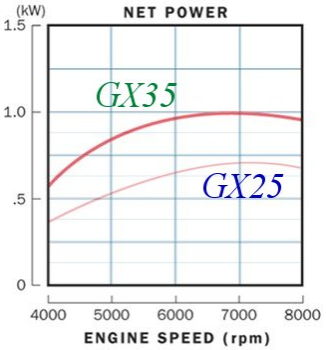

(b) Data sheet information.

Figure 4.3: Mechanical output power for GX25 and GX35.

The measurements of the power delivered by GX35 shows a stronger resemblance to the data sheet values than does the values for GX25. The GX25 measured power curve is slightly lower than the data sheet curve. Finally, the measurement series is a bit more consistent over the speed range for the GX35, with only one diverging value in the series.

Maximum power is delivered at about 6000 *rpm* for GX35 and 7200 *rpm* for GX25, according to the measurement data.

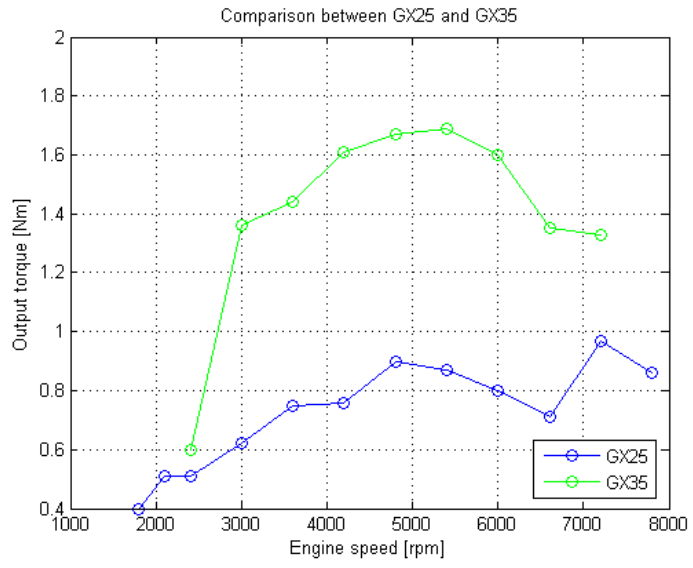

(a) Result from measurements.

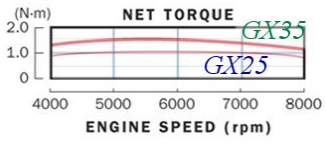

(b) Data sheet information.

Figure 4.4: Mechanical output torque for GX25 and GX35.

Due to the poor resolution of the data sheet values for the engine's torque production, it is difficult to compare it with the measured values. However, also here the GX35 measurement is closer to the data sheet values, than the GX25, which produces a lower torque than expected. The GX35 measurement values are more consistent, also for the torque production.

Maximum torque is delivered at about 5400 rpm for GX35 and 7200 rpm for GX25, according to the measurement data, which could be expected since also these speeds give the maximum power output.

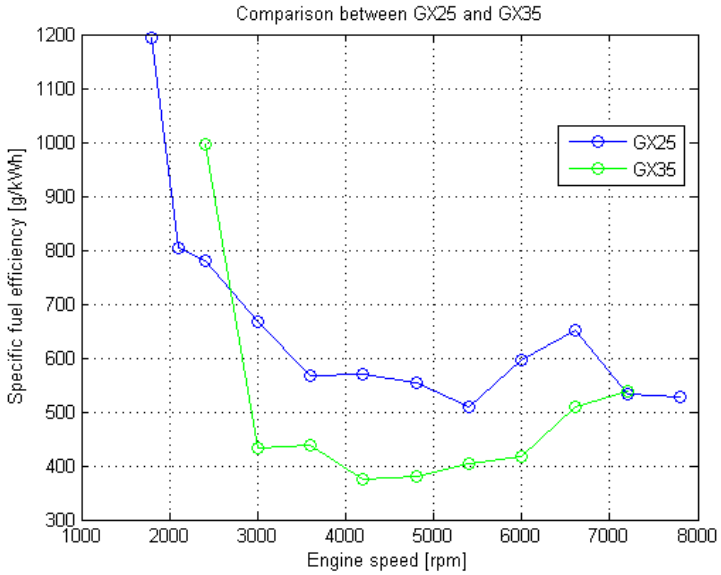

Figure 4.5: SFC for GX25 and GX35.

There was no information of the engine's SFC as a function of speed, from Honda. Nevertheless, the measurements shows a lower SFC for the GX35, compared to GX25, within the range of about 3000 rpm to 7000 rpm. The speed range with the lowest SFC is $4000-5000\,rpm$ for GX35 and about $5000-5700\,rpm$ as well as above 7000 rpm for GX25.

For a more comprehensive information regarding the engines SFC, torque and power production, several measurements at each operating point should be taken, also at different values of throttle positions. This would give, for example, one torque-speed curve for each value of the throttle position.

To start the ICE, either a Piaggio starter motor could be used, electrified by a Li-ion battery (also used for the vehicle's lights, horn and power electronics), or the DC generator(s) could be used, electrified by the supercapacitor. The starter motor has a mass of about 1 kg. According to measurements done by Master thesis students at Electric power engineering at Chalmers (spring 2009), the start of GX25 demanded about 75 J of energy over a time period of about 0.5 s. No similar measurement was conducted for the GX35 engine, but 10-20 % higher currents from the supercapacitor were observed during start tests.

Finally the engines will run in Smarter without any cooling system, in order to keep the weight of the vehicle as low as possible. Then, to avoid a temperature failure, the engines should not be run for more than about half of the time during the race.

4.3 Electric machines - generator and motor

The same type of electric machine was used both as generator and as tractive motor; a Maxon RE65, 250 W, DC motor (order number 353296), with permanent magnets and graphite brushes, see Figure 4.6. Some interesting operational parameters, given in the data sheet from the manufacturer, is presented in Table 4.3.

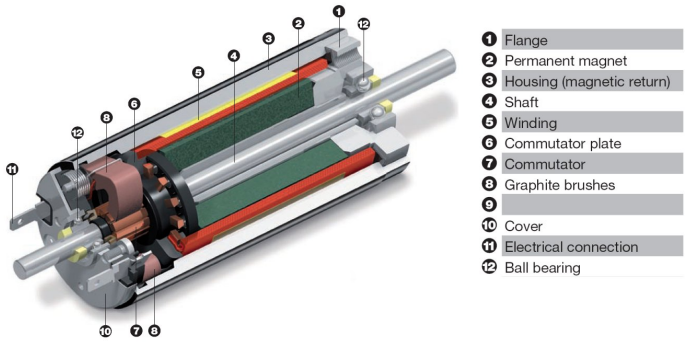

Figure 4.6: Maxon DC-motor RE65, [37].

Table 4.2: Specifications for the Maxon DC motor, [38].

Values at nominal voltage	
Nominal voltage	36.0 V
No load current	0.407 A
Nominal speed	3550 rpm
Nominal torque	0.654 Nm
Nominal current	7.74 A
Max efficiency	87.3 %
Characteristics	
Terminal resistance	0.173 Ω
Terminal inductance	0.848 mH
Torque constant	89.1 mNm/A
Speed constant	107 rpm/V
Rotor inertia	1380 gcm^2
Thermal resistance, housing-ambient	1.3 K/W
Thermal resistance, winding-housing	1.85 K/W
Thermal time constant, winding	127 s
Thermal time constant, motor	991 s
Max. permissable winding temperature	125 °C
Max. permissable speed	4000 rpm
Weight of motor	2.480 kg

The no load current is the current drawn by the motor at nominal voltage when unloaded. It represents the current needed to produce the torque that opposes friction in the brushes and bearings, which is increasing with speed.

Nominal torque and current are also the maximum permissable continuous values, in order to keep the winding temperature within acceptable limits.

The value for maximum efficiency does not necessarily represent the best operating point of the motor, but simply the highest efficiency at nominal voltage.

The maximum winding temperature should not be exceeded, not even temporarily. It is the winding temperature that limits the permissable motor current, and thus the amount of temporary motor overload.

Stated maximum speed is given with respect to thermal and mechanical considerations. Higher speed is possible, but will have a negative effect on the life expectancy of the motor. Through contact with the manufacturer, it was suggested not to exceed a speed of $5000\,rpm$, or the brushes would be damaged, and above $5500\,rpm$ even the winding will be damaged.

Finally the strength of the permanent magnet will be degraded with higher temperature, between $1-10\,\%$ at the temperature of 75 °C. [39].

Based on the information given in Table 4.3, the motor losses can be estimated and an efficiency map can be constructed, see Figure 4.7, for constant motor voltage. The losses that are being considered are the power loss in the terminal resistance, or copper losses,P_{Cu} , and the no load losses, $P_{no\,load}$. They are calculated as

$$P_{Cu} = R_{Cu}\, I^2 = R_{Cu} \left(\frac{T}{k_T} \right)^2, \tag{4.1}$$

and

$$P_{no\,load} = \omega\, T_{no\,load} = \omega\, k_T\, I_{no\,load}, \tag{4.2}$$

where R_{Cu} is the terminal resistance, I is the motor current, T is the produced torque, k_T is the torque constant, ω is the angular motor speed, $T_{no\,load}$ is the no load torque and $I_{no\,load}$ is the no load current.

As can be seen the efficiency is not the highest at the nominal operating point ($3550 rpm$, $0.654\,Nm$), but is increasing with motor speed. The friction losses are relatively large at lower torques, thus the efficiency is lower. The optimal operation point is thus a speed above $4000\,rpm$ and a torque between rated to about twice the rated torque of $0.6\,Nm$.

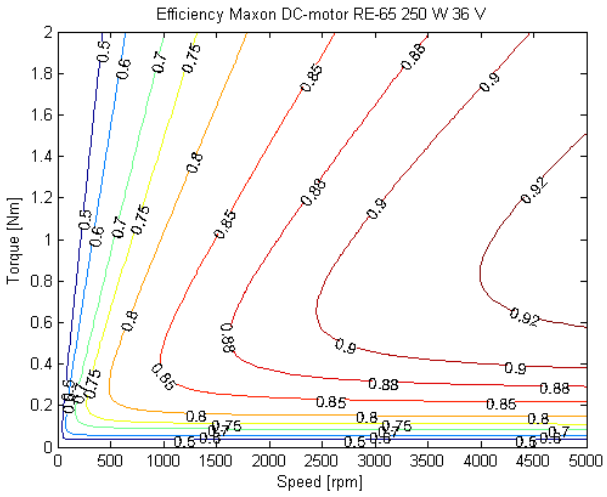

Figure 4.7: Efficiency plot of Maxon DC-motor RE65.

4.4 DC/DC converter

There were two different DC/DC converters available to use in Smarter, one was designed and manufactured by Maxon, and the other one was designed and realized by Master

students at the electric power department at Chalmers.

4.4.1 Maxon 4-Q converter

The Maxon converter was a 4-Q-DC Servoamplifier, ADS 50/10 (order number 201583), see Figure 4.8. It is a PWM controlled converter suitable to handle output powers of about $80 - 500\,W$.

The converter can handle voltages and currents that are both negative and positive. With negative voltage the motor can be run in reverse. But with both positive and negative current, the converter can deliver power in both directions in the driveline. From the supercapacitor to the motor and from the motor, through generative braking, to the supercapacitor.

Figure 4.8: The 4-Q maxon DC/DC converter.

Some of the specifications given in the data sheet of the converter, are stated in Table 4.3. The converter also has a protection for over current and over temperature. A warning red diode is lit at high temperatures, and finally the converter is shut down at temperatures above a certain critical value.

Table 4.3: Specifications for the Maxon DC/DC converter, [40].

Operating voltage, V_{CC}	12 - 50 V_{DC}
Max. output voltage	45 V (0.9 x V_{CC})
Max. output current	20 A
Continuous output current	10 A
Max. efficiency	95 %
Weight	0.4 kg

During a measurement by Master thesis students at Electric power engineering at Chalmers (spring 2009), the converter was tested during discharge of the Maxwell supercapacitor over a voltage controlled resistive load. At the capacitor input the power was $448.2\,W$ and the input voltage $48\,V$. On the output side, the maximum deliverable current by the converter was $16.6\,A$, that is not the fully $20\,A$ given by the manufacturer. In a lab room temperature of about 25 ℃, the converter was able to uphold this operation for over four and a half minute, without indicating over temperature or current, before the test was aborted. During the test, the converter case temperature rose about 12 ℃, (22.4 to 34.5 ℃).

Other measurements, also done by Master thesis students at Electric power engineering at Chalmers (spring 2009), shows that the converter efficiency varies during operation, between $82 - 92\,\%$.

4.4.2 Chalmers designed 2-Q converter

As a part of a Master thesis work at Electric power engineering at Chalmers (spring 2009), an alternative DC/DC converter was designed and produced. This converter is a one leg, 2Q converter, that is it can deliver only positive voltage, but both positive and negative current. Then the tractive motor can not be run in reverse, which is no real drawback for a vehicle in Eco-marathon, since it will not be needed. There is thus no benefit, in this case, in the Maxon 4Q operation over the 2Q operation.

The weight of the converter is $0.5\,kg$.

The aim of the converter was to have a higher efficiency and higher maximum current, compared to the Maxon converter. This is to be achieved with four paralleled MOSFET transistor per switch. With a higher current the tractive motor can deliver a higher torque and thus increase the acceleration of the vehicle. Measurements on the converter alone show an efficiency of about $99\,\%$, however it does have considerable output ripple, which may lower the over all efficiency when applied to the motor. The theoretical maximum power is as large as $50\,kW$, giving a maximum current of about $1\,kA$ with a voltage of $50\,V$.

Naturally the electrical parameters need to be better established to be able to, with some degree of certainty, evaluate the possible benefit of using this converter in Smarter.

4.5 Supercapacitor

In compliance with the Shell Eco-marathon's rules a supercapacitor was used as energy storage device. There were two options to choose between; one commercial and one student manufactured lithium-ion capacitor.

4.5.1 Maxwell supercapacitor

The commercial supercapacitor, with an operating voltage of 48.6 V, was Maxwell fabricated, see Figure 4.9. It has a maximum power density of 6.4 kW/kg, a maximum energy density of 3.40 Wh/kg and a mass of 13.5 kg [21]. It's operating temperature range is from -40 ℃ to +65 ℃.

Figure 4.9: Maxwell supercapacitor.

Some of the specifications were also measured at Chalmers, see comparison below. The measured values were the ones used in the simulation.

Table 4.4: Specifications for Maxwell supercapacitor, BMOD0140-P048

	Data sheet	**Measured at Chalmers**
C (F)	140	154.4
R (mΩ)	8.0	14.3

4.5.2 Student manufactured lithium-ion capacitor

This supercapacitor prototype was designed and produced by another, parallel ongoing, master thesis project.

It consists of 13 series-connected Standard 2200 F Lithium ion capacitor cells of JM Energy Corporation, see Figure 4.10.

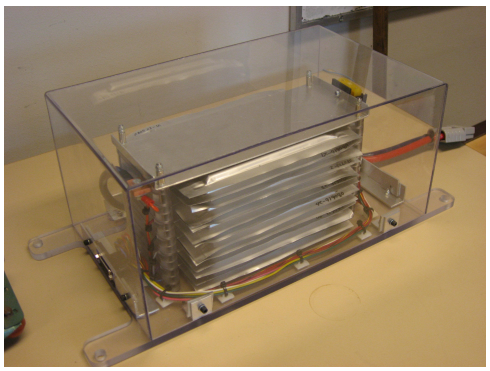

Figure 4.10: Li-ion capacitor.

Maximum voltage of each cell is 3.8 V [22], resulting in a maximum voltage of 49.4 V for the complete capacitor stack. Due to the Eco-marathon rules the maximum voltage on the vehicle was not allowed to exceed 48 V (due to safety reasons), therefore the supercapacitor had to be limited to 48 V. Minimum voltage of each cell is 2.2 V [22], resulting in a minimum voltage of 28.6 V for the complete capacitor stack. Maximum permissible current for each cell during charge and discharge is 250 A and the operating temperature range is from -20 ℃ to +70 ℃[22]. The characteristics of the capacitor stack is presented in the table below.

Table 4.5: Specifications for the student manufactured lithium-ion capacitor.

	Data sheet	**Measured at Chalmers**
C (F)	169.2	169.0
R (mΩ)	18.2	39.2
m (kg)	-	4.68

To calculate the maximum possible energy of the supercapacitor the following equation was used

$$W_{max} = \frac{CU_{max}^2}{2}, \tag{4.3}$$

where W_{max} (Ws) is the maximum energy, C (F) the capacitance of the supercapacitor and U_{max} (V) is the maximum voltage that the supercapacitor can have. The maximum

energy density was then calculated to be

$$\frac{169.2 \cdot 49.4^2}{2 \cdot 4.68 \cdot 3600} \approx 12.3 \text{ Wh/kg}. \tag{4.4}$$

When calculating the maximum possible power density of the supercapacitor the following equation was used

$$P_{max} = \frac{U_{max}^2}{4 \cdot R \cdot m} = \frac{49.4^2}{4 \cdot 18.2 \cdot 10^{-3} \cdot 4.68} \approx 7.2 \text{ kW/kg}, \tag{4.5}$$

where P_{max} (W) is the maximum power, U_{max} (V) the maximum voltage, R (Ω) is the equivalent series resistance at 1 kHz and m (kg) is the mass of the supercapacitor.

Consequently, the Li-ion capacitor has slightly higher power density and remarkably higher energy density compared to the commercial supercapacitor.

4.6 The transmission systems

Two transmission systems were used in Smarter, one between the ICE and the generator(s) and one between the electric motor(s) and the wheels.

4.6.1 Gear ICE-Generator

The construction of the gear between the ICE and the generators can be seen in Figure 4.11.

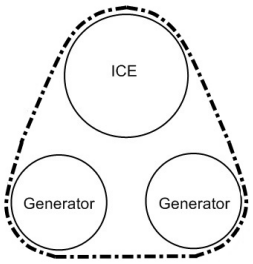

Figure 4.11: Gear ICE-Generators

The gear ratio from the ICE to the generators is 0.8 and the efficiency is assumed to be 90%.

4.6.2 Gear Motor-Wheels

The construction of the gear between the motor(s) and the wheels is shown in Figure 4.12, which also consists of sprockets and roller chains.

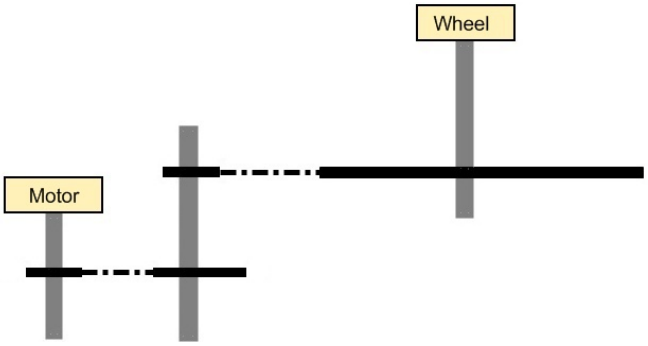

Figure 4.12: Gear Motor-Wheels

The complete gear ratio between motor and wheel is

$$\frac{21}{12} \cdot \frac{95}{12} \approx 13.9. \tag{4.6}$$

Also here is the efficiency assumed to be 90%.

4.7 Gas potentiometer

In order to save weight a linear sliding potentiometer was used instead of a gas pedal, see Figure 4.13.

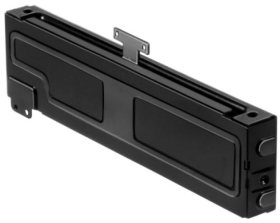

Figure 4.13: Sliding potentiometer Alps RSA0K11A1005-ELF, [31].

The sliding potentiometer sent a corresponding reference for the torque wanted at the electric traction motor, consequently the potentiometer acted both as a gas and brake pedal.

4.8 Wheels

The original rims were made of carbon fibre, which gives low weight and rotational inertia. Unfortunately they broke prior to the competition. Instead rims of aluminium were used.

The tires were delivered by Michelin (eco-tire) and had the dimensions 95/80 R16. That is, the tire width was 95 mm, the ratio of the tire hight to the width was 80 %, it was a radial tire and the diameter was 16 *inches* (1 in is 2.54 cm).

4.9 Smarter parameters

The chassis and body was made in one single piece, a monocoque, using an extra light carbon fibre, called TeXtreme®, manufactured by Oxeon in Borås, Sweden. In order not

to add unnecessary weight, no varnish was used on the chassis. The design of the vehicle chassis can be seen in Figure 4.14.

Figure 4.14: The Smarter chassis.

At the vehicle technical inspection, in Lausitz, for acceptance to take part in the Shell Eco-marathon, Smarter was equipped with the components listed in Table 4.6. This drive line set up gave the total weight of 74 kg.

The parameters that constitute Smarter's response to aerodynamic drag, rolling and climbing resistance as well as acceleration are also given in Table 4.6, where A is the cross sectional area at the widest spot, C_d is the aerodynamic air coefficient, C_r is the rolling resistance coefficient and m is the total vehicle mass.

Table 4.6: Smarter driveline components at the technical inspection in Lausitz, as well as the vehicle parameters.

$0.35\,l$	Petrol, Shell Unleaded 95		
1	GX35 Honda engine	A :	$1.4\,m^2$
2	Maxon DC generators	C_d :	0.28
1	Chalmers made Li-ion capacitor	C_r :	0.007
2	Maxon DC motors	m :	$74\,kg$
2	Maxon DC/DC converters		[1ex]

4.10 Driver vs control system

The car has no cruise control and therefor the driver needs to decide which speed is needed in order to complete the race in time. A digital display assists the driver with information about the current speed, which speed is needed to complete the race in time, average speed, distance driven and for how long time the race has been going on.

The display also shows the current voltage of the supercapacitor and if the ICE is on or off. The control system decides when the ICE needs to be on and off respectively. If the the voltage of the supercapacitor drops too low the control signal will send a start signal to the engine and when the voltage has reached its maximum allowed a stop signal will be sent from the control system. It is possible to operate in a manual mode, where the driver decides when the ICE should be on and off respectively.

The car is equipped with an emergency string which shuts everything down when pulling it, the string can be reached both from the inside and the outside of the car.

Chapter 5

Modelling and simulation of Smarter

To be able to evaluate Smarter's performance in the Shell Eco-marathon competition, the vehicle itself with its driveline components, as well as its behavior on the Lausitz race track, have been modeled in MATLAB/Simulink, and the race execution has been simulated using the same software. The main result from the simulation is Smarter's fuel economy, that is the predicted coverable distance per liter of fuel, km/l. In the next chapter, different vehicle parameters are compared, to find a set up that is probable to give a better fuel economy.

The level of complexity in the modelling depend both on the amount of available information of the object in question, but also on the desired resulting information from the simulation.

This chapter describes the structure of the simulator, and how Smarter and the race were modeled.

5.1 The simulator structure

The simulator structure is based on a vehicle propulsion simulation tool, developed by Chalmers University of Technology and Linköping University, within their cooperation CAPsim, Center for Automotive Propulsion Simulation, [28]. CAPsim is a simulator for conventional and hybrid vehicles, where the user can enter parameters for the vehicle and its components, and evaluate the vehicle performance when it comes to, for example, fuel consumption.

The modeled vehicle driveline consist of interconnected component blocks in Simulink, representing physical components, such as the ICE, the battery, the electric machine,and such. There is also a block for the driver model. All the necessary vehicle and component parameters are to be declared in an associated MATLAB m-file. The simulator is run by executing the m-file, which in turn calls the Smarter Simulink model-file, *SMARTER-sim.mdl*. The m-file also contain one time vector of the desired instantaneous vehicle speed during the race, and one vector of the momentarily track inclination depending on the instantaneous position on the track.

The top level in the Simulink modell consists of three subsystems, the *environment*,the Smarter *driver* and the Smarter *vehicle*, see Figure 5.1. The environment block handles both the speed and inclination vectors. The driver model gets information regarding both desired and current vehicle speed and gives an order to the vehicle to either accelerate, decelerate or maintain current operation. The vehicle model thus contain all the physical component blocks representing the driveline, where the operation of each component is

simulated in order to try to fulfill the wish of the driver. The next coming sections contain a more detailed description of the different blocks.

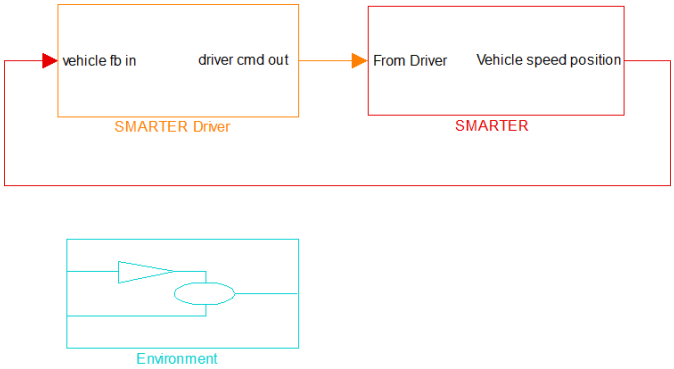

Figure 5.1: The top level in the Smarter simulator.

5.2 M-file including the simulation vector

As stated earlier, all the constants and parameters used in the modelling and simulation of Smarter for Shell Eco-marathon, are defined in a main m-file, *SMARTERsimrun.m*. The reference speed vector versus time, is defined in a function m-file, *FUNsimvect.m*, which is always called from the main m-file. There is also a function m-file, that calculates the maximum possible acceleration time for a given maximum tractive motor current; *FUNaccmax.m*. This function file may be called from FUNsimvect.m, if desired.

Finally there is an m-file that calculates the net vehicle mass, *Smarter_weight.m*, which is not called during simulation, but used as a precalculation.

All the m-files, used in the modelling and simulation of Smarter for Shell Eco-marathon, are available in Appendix A.

5.2.1 The main m-file

The main m-file, *SMARTERsimrun.m*, is divided into two parts or *cells*. The first cell defines all the parameters, calls the simulation vector representing the race, and runs the race simulation by calling the Smarter Simulink model. After the race simulation, interesting simulation parameters, by choice, are stored in the MATLAB workspace.

In the second cell, the ICE is run at vehicle stand still, to charge the supercapacitor to the starting voltage level, at which the simulation is stopped. The resulting fuel efficiency is then calculated by dividing the consumed fuel with the covered race distance. Finally the start/stop sequence of the ICE, as well as the supercapacitor voltage level, during the whole simulation, are graphically presented.

The parameter code structure is based on component block order. SI units are stated for all the parameters, as well as a comment regarding the origin of the information. Where two component choices are available, the one component not used in the current simulation, should have its parameters commented in the code.

5.2.2 Simulation vector

The race simulation vector, *FUNsimvect.m*, gives the Smarter reference speed as a function of time and position, through the 7 laps around the track, including the three mandatory pit stops of 10 seconds each.

For simplicity the speed reference is built up with constant accelerations and decelerations, and with a constant speed in between, see Figure 5.2. All the accelerations are assumed to be equally long in time, as are all the decelerations. The first pit stop is assumed to take place after the first lap, the second pit stop after the third lap and the third and final pit stop after the fifth lap.

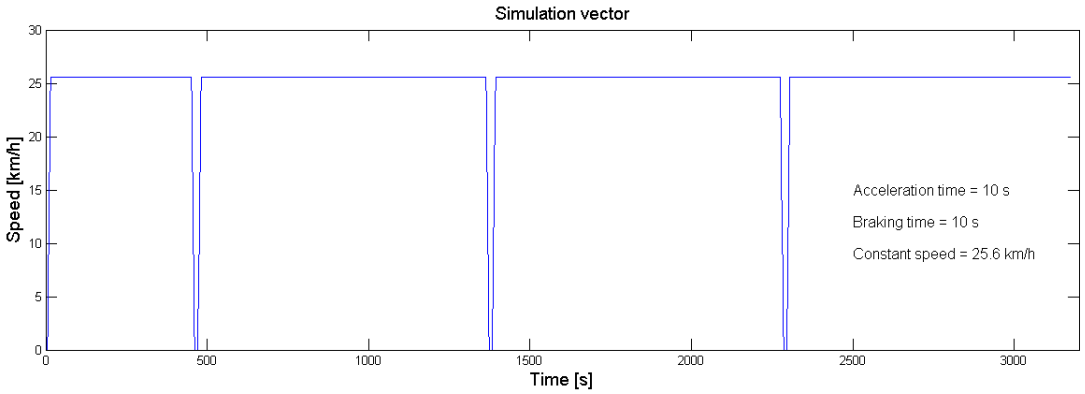

Figure 5.2: Race simulation vector, Smarter reference speed as a function of race time.

The total race distance is 22 081 m, and the maximum allowed race time is 53 min or 3180 s, which gives an effective race time of 3150 s excluding the pit stops. The mean speed during the race must then be at least $22081/3180 = 24.997\,km/h$, or $22081/3150 = 25.235\,km/h$. Depending on the time consumed during acceleration and deceleration, the constant speed must be high enough to make the race in time. However, the higher the constant speed, the higher the acceleration magnitude, to reach the constant speed in the same time intervall, hence the larger the amount of energy used during the race. That is, it is not only the driveline efficiency that may have influence on the result of the race, but perhaps also the manner in which it is executed.

When constructing the simulation vector, care must be taken, not only to the total race time, but also to make sure the whole race distance is actually covered. This is done by calculating the time to spend at constant speed based on the distance to be covered and at what speed, see Appendix A.2.

Another point to be made is that the start and the finish is not at the same place on the track, which makes the last lap 130 m shorter than the other laps.

A second part of the simulation vector is describing the inclination of the race track in radians as a function of position along the race track. This data is based on a topology map of Lausitz EuroSpeedway track, available at the Shell Eco-marathon internet homepage, [29]. The information on the topology map (declaring altitudes in meter along the track) was interpreted by master students at Automotive Engineering in the fall of 2008, and the resulting vector was received.

The resulting vector used during the simulations, covering all the seven laps, can be seen in Figure 5.3.

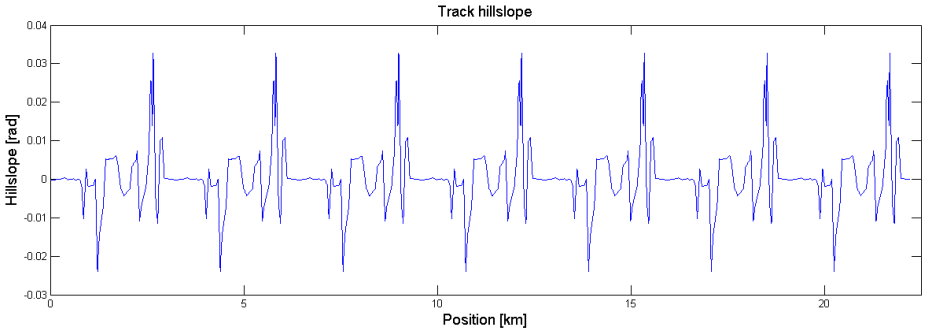

Figure 5.3: The Lausitz track hillslope in radians as a function of race position.

5.2.3 Maximum acceleration

All the tractive effort comes from the DC motor, which is fed by the DC/DC converter. Thus the maximum available acceleration/deceleration torque is limited by the maximum motor current.

The output current from the Maxon DC/DC converter is proven to be limited to about $16.6\,A$, which makes it interesting to investigate the effect of having limited amount of current.

The function m-file, *FUNaccmax.m*, calculates the maximum acceleration based on equation (2.27), and the information can then be used in the simulation vector to calculate necessary acceleration time.

The maximum acceleration, $a_{acc}\,(m/s)$, is calculated as

$$a_{max} = \frac{(I_{max}\,k_{torque} - T_{no\,load}) \cdot k_{gear} - T_{resistance} - T_{air\,drag}}{J_{tot}} \cdot r_{wheel} \tag{5.1}$$

where I_{max} is the maximum motor current, k_{torque} is the motor torque constant, T_{noload} is the motor no load torque, k_{gear} is the motor-wheel chain gear ratio, $T_{resistance}$ is the opposing rolling resistance torque, $T_{air\,drag}$ is the opposing aerodynamic drag torque, J_{tot} is the total Smarter rotational inertia, and r_{wheel} is the Smarter wheel radius.

The aerodynamic drag is calculated in FUNaccmax.m, based on the set constant speed, but the rolling resistance and the inertia are to be set as constant values, based on a presimulation with the same vehicle parameter set up.

5.2.4 Vehicle mass calculation

The total weight of Smarter is a key parameter for realistic simulation results. However not all the individual contributions to the total vehicle weight are known. What is known is the weight of the main driveline components, and the total weight of Smarter at the technical inspection at Shell Eco-marathon, as well as the driveline set up at that time. Based on this information, a base vehicle mass can be calculated, which is done in the m-file *Smarter_weight.m*, see Appendix A.4.

The net weight of the Smarter chassis, without; the ICE engine, initial fuel, generator, supercapacitor, converter, motors and the motor-wheel gear, is $54.3845\,kg$.

5.3 The environment model

The environment block contains a simulation clock, which is representing the race time in seconds, see Figure 5.4. It also receives information from the vehicle block, via the

From-block, regarding the vehicle current position, that is the traveled distance in meter. The vectors over desired instantaneous speed (m/s) and track inclination (rad), are available in the look-up tables, "speed-ref" and "Hillslope", both either as a function of time or of position. By setting the constant variables "Trig_speed_position_on" and "Trig_hillslope_position_on", in the m-file, to either 1 or 0, the time or the position function variable is chosen, via the switch-blocks. Thus the information about time and current position are input signals to the look-up tables, which then send information about current reference speed and track inclination, via the Goto-blocks "drivecycle" and "environment", to the driver and vehicle model respectively.

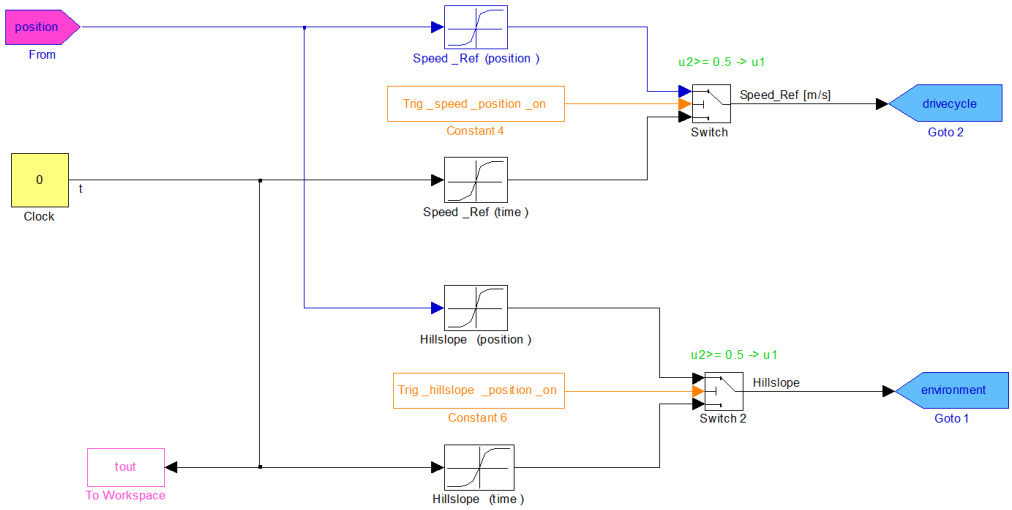

Figure 5.4: The environment model in the Smarter simulator.

5.4 The driver model

The driver model receives information about the current reference speed as well as the instantaneous vehicle speed and position, see Figure 5.5. To maintain the reference speed, the driver is modeled as a PI-controller with the speed error as an input, see equation 5.2 and Figure 5.6. The error, $e(t)$, is divided with the tyre radius, r, to be expressed in rad/s. The values of the controller parameters, K_i and K_p, are chosen to give a realistic torque reference value, T_{ref}, for the tractive DC motor, but also to keep the simulation stable. To keep the integrator from growing too large, a suitable upper limitation is added.

Since the mechanical brake is not intended to be used in Smarter during the race, its signal value is set to zero in the driver model. Hence the torque reference for the tractive motor is representing the signals from Smarter's gas potentiometer, that is positive values for acceleration and negative values for deceleration or generative braking.

Finally the driver model block also contains some "Scopes" for overlooking a few vehicle performance parameters as functions of time, see Figure 5.5.

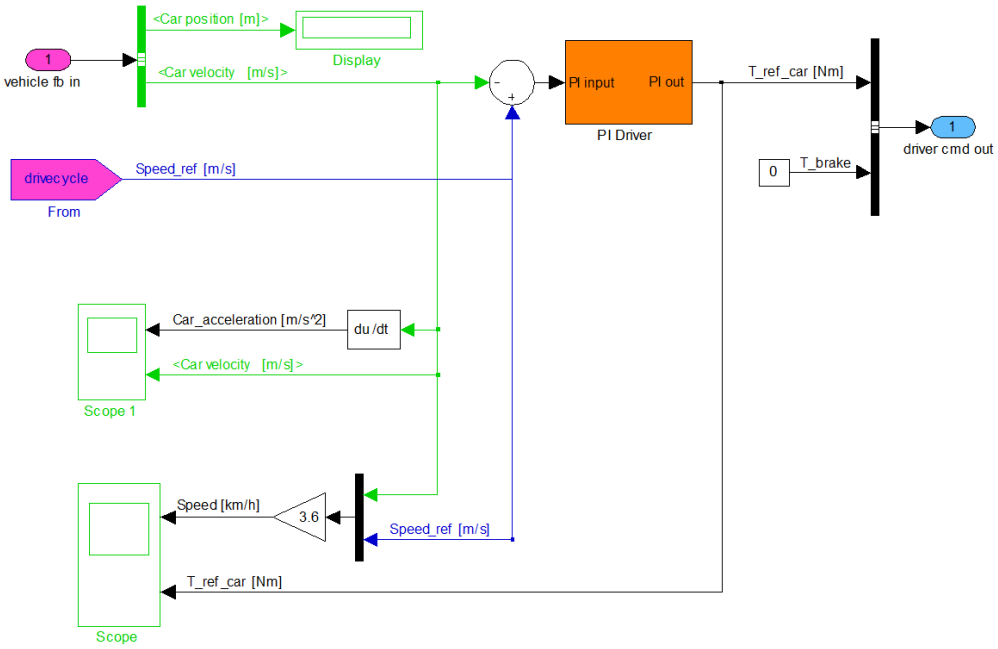

Figure 5.5: The Smarter driver model in the Smarter simulator.

$$T_{ref}(t) = K_p \frac{e(t)}{r} + K_i \int \frac{e(t)}{r}\, dt \tag{5.2}$$

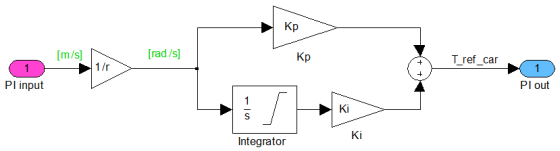

Figure 5.6: The Smarter driver PI-controller model.

5.5 The Smarter vehicle model

The vehicle model contains a *controller block*, which serve as a transition between the driver and the *component blocks* below. As mentioned earlier, the component blocks represent the physical components in the Smarter driveline, starting from the bottom left with the primary energy storage; the fuel tank, followed by the ICE, the chain gear between the ICE and the DC generator(s), the supercapacitor, the DC/DC converter, the DC tractive motor, the chain gear between the DC motor and the Smarter wheel, and finally the *chassis block*. In the chassis block the tractive force from the driveline is balanced towards the resistive forces acting on the vehicle.

The signals between the blocks represent physical values, such as; fuel flow rate, torque, speed, voltage and current. For each block the input and output powers are found via cross referencing the input and output signals.

The operating point of each component is depending on the adjacent component through the forward and backward fed signals. This may sometimes cause the problem of *algebraic loops*. Then the calculation of the next value of a signal depend on the very same value of the signal itself. To get around this, Simulink *memory blocks* have been used

when necessary throughout the simulator. Then the previous signal value is instead used to calculate the next value of the same signal. This may introduce a small error, or even an instability, in the simulation, which is here assumed to be negligible.

Next follows a more detailed description of each component block in the Smarter vehicle model.

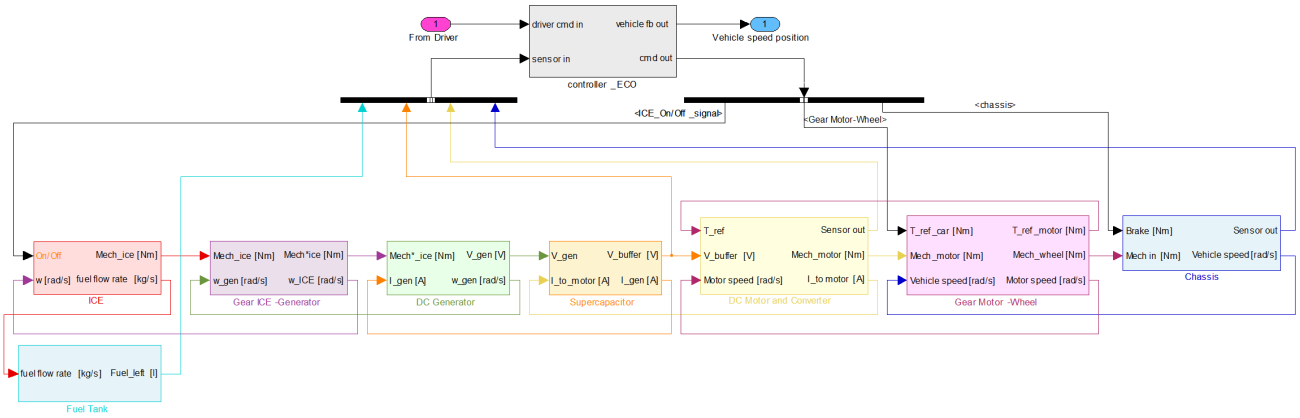

Figure 5.7: The Smarter vehicle model in the Smarter simulator.

5.5.1 Controller

The controller block which represents the control system of Smarter is presented in Figure 5.8.

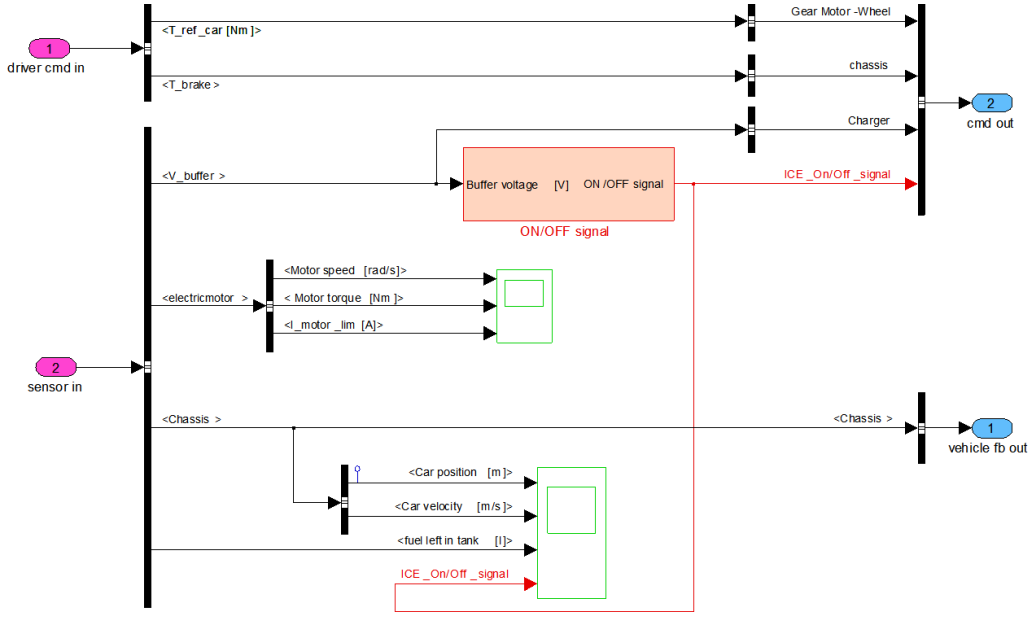

Figure 5.8: Block diagram model of the Smarter control system.

The block receives information from the driver model about the torque reference (Nm) and the braking torque (Nm) which are being sent right through the block to the gear motor-wheel block and the chassis block, respectively. The block also receives information about the current status of Smarter such as; supercapacitor voltage (V), motor speed (rad/s), motor torque (Nm), motor current (A), fuel left in tank (l), car position (m) and

car velocity (m/s). Most of these signals are just being either sent right through the block or being displayed, except for the supercapacitor voltage which is sent in to a sub-block controlling starts and stops of the ICE, see Figure 5.9. The position and the velocity of the car is sent to the driver model.

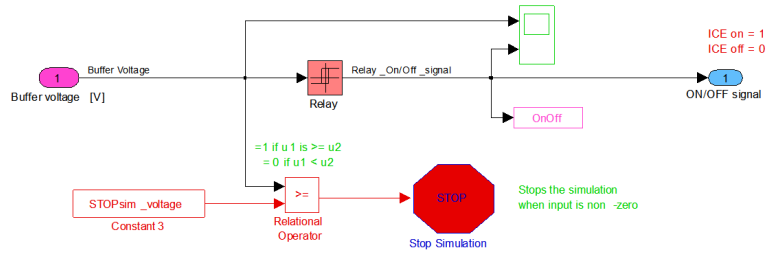

Figure 5.9: Block diagram model of the on-off control of the ICE.

When the voltage of the supercapacitor has dropped too low, a start signal will be sent to the ICE, and likewise when the voltage of the supercapacitor has reached its maximum allowed value, a stop signal will be sent. The block also has the functionality of starting the ICE, if the supercapacitor voltage is below the starting voltage level when the race is finished. The simulation then keeps running until the supercapacitor has been charged to the starting voltage level.

5.5.2 Fuel tank

The fuel tank is modeled having a starting mass of fuel. This mass is calculated with knowledge of the initial fuel volume ($0.35\,l$) and the fuel density. According to Shell, the density of the used gasoline Shell Unleaded 95 (EU) was about $0.73\,kg/l$.

The input to the fuel tank is the instantaneous fuel consumption of the ICE, $f_m\,(kg/s)$. The volume of fuel left, $v_{left}(t)\,(l)$, can then be calculated as in equation (5.3), where $m_0\,(kg)$ is the initial fuel mass and ρ_{fuel} is the fuel density. This parameter is also sent to MATLABs workspace to be available for result calculations.

The block diagram of the fuel tank model can be seen in Figure 5.10.

$$v_{left}(t) = \frac{m_0 - \int_0^t f_m dt}{\rho_{fuel}} \tag{5.3}$$

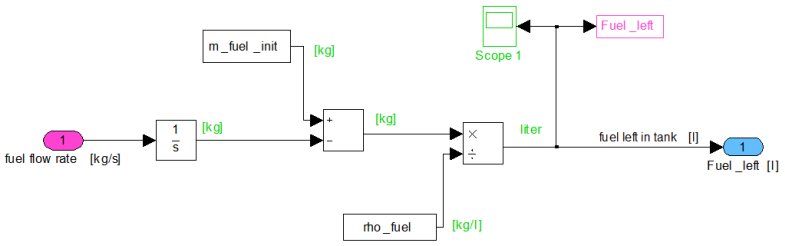

Figure 5.10: Block diagram model of the Smarter fuel tank.

5.5.3 ICE

At first the desire was to make a model of the ICE based on analytical expressions. To do that, many engine parameters and constants have to be known. Unfortunately these figures could not be found amongst the information from the manufacturer, or received

from other external sources. Also measurements on the engines were outside the scope of this master thesis work.

Therefore, the ICEs (both GX25 and GX35) were modeled using the received measurement data, or *mapped data*, discussed in the previous chapter, (section 4.2.2). This means the ICE models will not fully represent the actual engine performances, since the measurement data was gathered with no known modifications of the engines, but the engine used in Smarter was somewhat modified. Also the throttle position is not modeled, but assumed to be wide open.

The ICE model block can be seen in Figure 5.11. The input signals to the ICE block are the on/off signal from the controller block, and the ICE speed, $\omega_{ICE}\,(rad/s)$, from the Gear ICE-Generator block. The speed signal is then used as an input to the two look-up tables that give the expected ICE torque,$T_{ICE}\,(Nm)$, and fuel flow rate (kg/s), at the current speed, see Figure 5.12. Depending on which one of ICE's to model, their respective measurement data is read in the m-file.

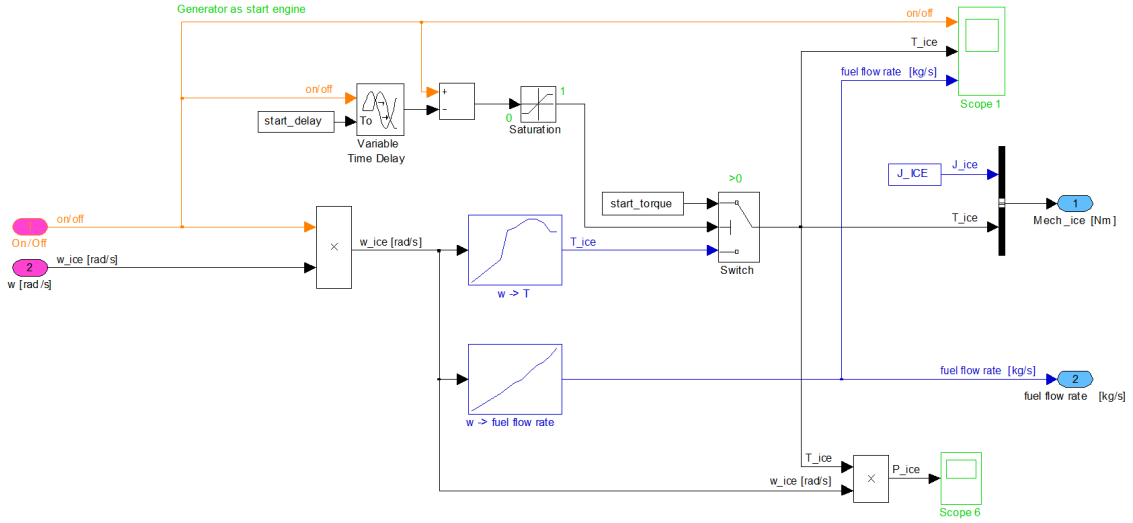

Figure 5.11: The model of the ICE, as well as start torque from generator when used as a starting motor.

The ICE's can be started using either a Piaggio start motor fed by a separate Li-ion battery, or by the DC generator(s) fed by the supercapacitor. Both of these cases were modeled.

When using the Piaggio start motor, simply an extra weight of about 1 kg was added to the total vehicle mass.

To simulate the energy loss from the supercapacitor, when starting the ICE with the generator(s), a representative negative torque, "start_torque", is applied from the ICE block on the generator(s) during $0.5\,s$, "start_delay", each time the ICE is turned on. For GX25 this torque is $-0.359\,Nm$ to represent an energy loss of $75\,J$. For the GX35 the torque is $-0.535\,Nm$, to represent an energy loss of $90\,J$ (assumed to be 20 % more than for the GX25).

The typical simulation characteristic of the ICE speed and torque during on and off mode can be seen in Figure 5.13. Here the negatively applied starting torque can be seen. It is also noticed that the speed does not start at zero, when the ICE is started. This is a consequence of the modelling of the generator-supercapacitor interconnection, which is based on a constantly "oscillating" nonzero voltage and thus generator speed. This

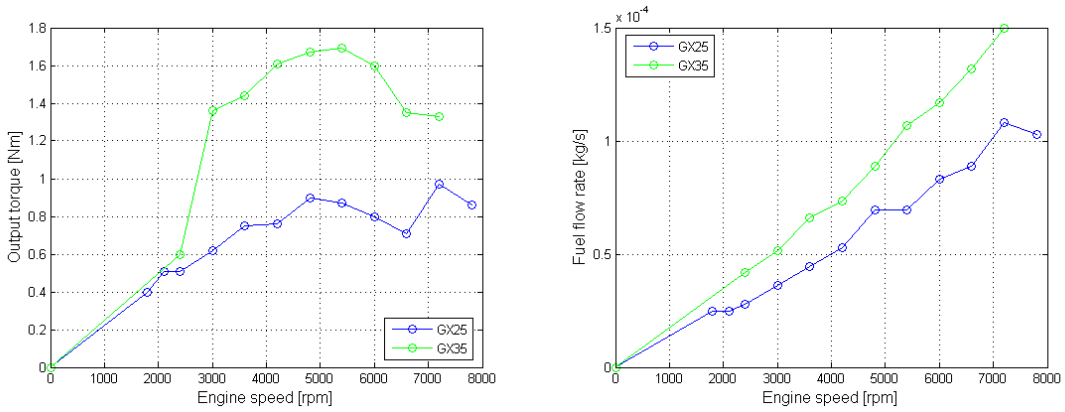

(a) Torque. (b) Fuel flow rate.

Figure 5.12: Measured engine output torque and fuel flow rate as a function of speed, for Honda GX25 and GX35.

is naturally a divergence from the real system, where both the generator and ICE are disconnected during the ICE off-time.

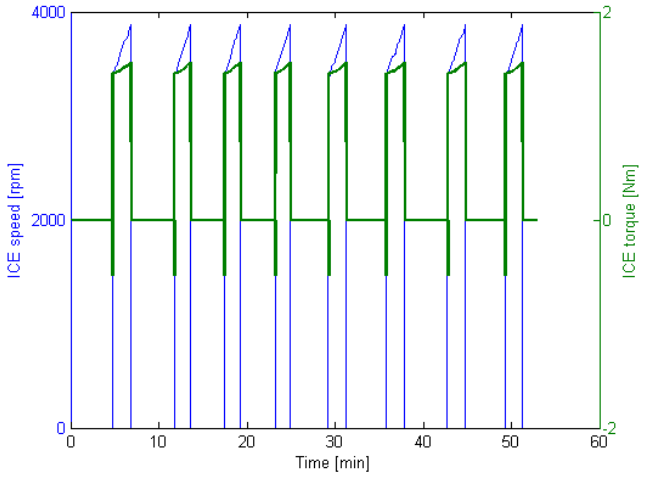

Figure 5.13: ICE torque and speed.

5.5.4 Gear ICE-Generator

The block representing the gear between the ICE and the generator(s) can be seen in Figure 5.14. The engine torque (Nm), engine inertia (kgm^2) and the rotational speed of the generator(s) are input signals to the block. Output signals are the input signals scaled with the gear ratio. *DrCh_ratio* is the gear ratio between the ICE and the generator(s) and *n_DrCh* is the efficiency of the gear.

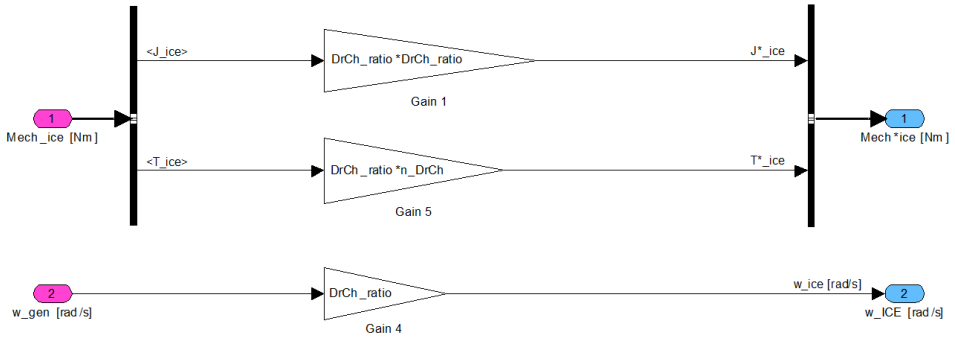

Figure 5.14: Block diagram model of the gear between the ICE and the generator(s).

5.5.5 Generator

The generator model can be seen in Figure 5.15. By setting the parameter, n_{gen} in the m-file, one or two generators can be modeled.

The input signals are the transformed torque, $T_{ICE}\,(Nm)$, and inertia, $J_{ICE}\,(kg\,m^2)$, from the ICE, and the generator current. By knowing the rotational inertia of the ICE and generator(s), J_{gen}, and by calculating the net generator torque, $T_{gen}\,(Nm)$, the generator speed, $\omega_{gen}\,(rad/s)$, can be calculated as

$$\omega_{gen}(t) = \int \frac{T_{ICE} - T_{gen}}{J_{ICE} + J_{gen}\,n_{gen}}\,dt. \tag{5.4}$$

The generator net torque is the torque produced by the generator current, subtracted by the no load torque, that is the no load current times the torque constant and the number of generators ($0.407A \cdot 89.1mNm/A \cdot n_{gen} = 0.036 \cdot n_{gen}\,Nm$). The no load torque is modeled to be constant over the whole generator speed range, only considering the direction of rotation. It is also ramped around the zero crossing, to avoid simulation problems around zero.

The other output signal from the generator block is the generator voltage. This is found using equation (2.3), but for the case of a generator. Then the generator terminal voltage, V_{gen}, is the generated emf, E, minus the voltage drop over the winding resistance, $I_{gen}R_a$; $V_{gen} = E - I_{gen}R_a$. The inductance is omitted, assuming the electrical time constant is much smaller than the mechanical one. The generator winding resistance is modeled as a function of the winding temperature, which in turn is depending on the generator load current.

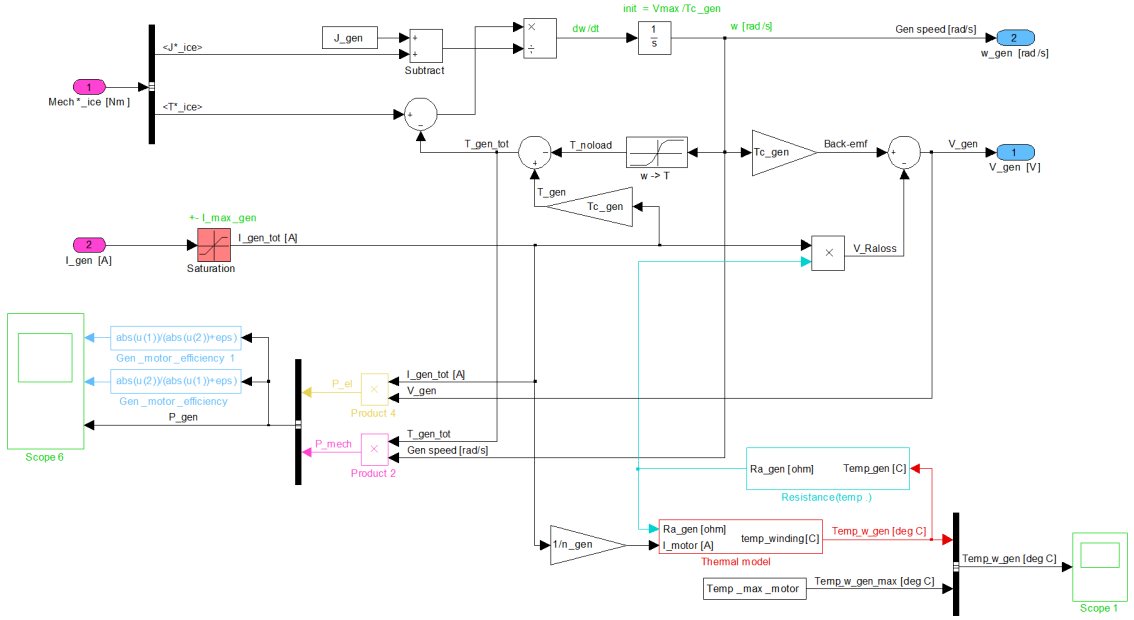

Figure 5.15: The model of the generator(s).

The generator temperature dependent winding resistance value can be calculated using equation (2.20). In the data sheet information from Maxon, the resistance at an ambient temperature of 25 °C, $R_{a\,25}$, is given (0.173 Ω). However, the ambient temperature, T_{amb}, can be set to an arbitrary value in the m-file. Therefore a new value for the reference resistance that corresponds to the set ambient temperature, must be found before the current winding resistance can be found, by also using information about the winding temperature, see Figure 5.16.

Consideration is also taken to the number of generators to be modeled.

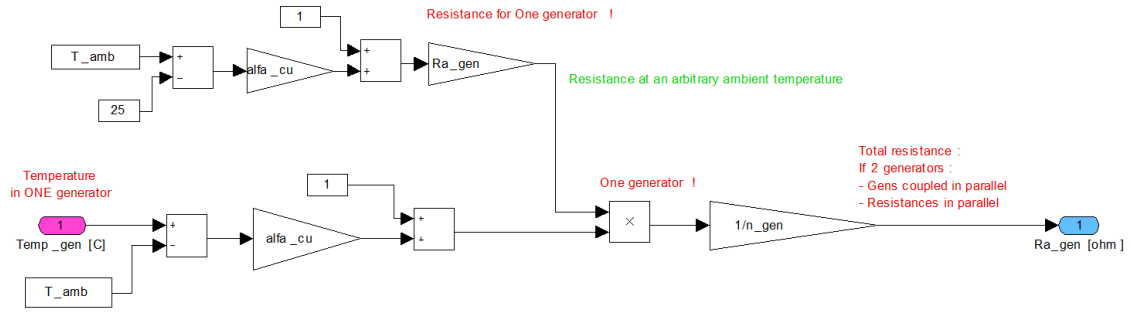

Figure 5.16: The model of the generator's winding resistance.

5.5.5.1 Transient thermal model of winding temperature

In the information from Maxon, the thermal resistances of winding to housing, $R_{th,wh}$, and of housing to ambient, $R_{th,ha}$, are given, as well as the time constants of the winding, $\tau_{th,w}$, and motor, $\tau_{th,m}$. Each time constant can be expressed as a product of a thermal resistance and a thermal capacity.

A lumped parameter transient thermal model of the motor thus includes two thermal resistances and two thermal capacitors. However, Maxon does not specify how such a lumped parameter circuit should be constructed, the Foster or the Cauer type, see section

2.4.3.1. Therefore the thermal step response of an equivalent Foster-type model is compared with the step response of equivalent Cauer-type model, see Figure 5.18. As can be seen the Foster-type model gives a shorter rise time of the equivalent thermal impedance, which may therefore serve as a "worst case" for the modeling of the motor, compared to the Cauer-type model. Thus the Foster-type model, see Figure 5.17, is implemented in the Simulink model of Smarter.

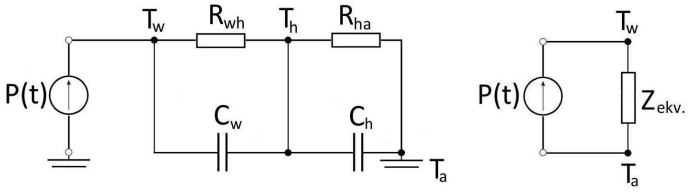

(a) Foster-type Maxon model.

(b) Equivalent transient impedance, Maxon model.

Figure 5.17: Thermal equivalent circuits for transient heat conduction, Maxon DC motor.

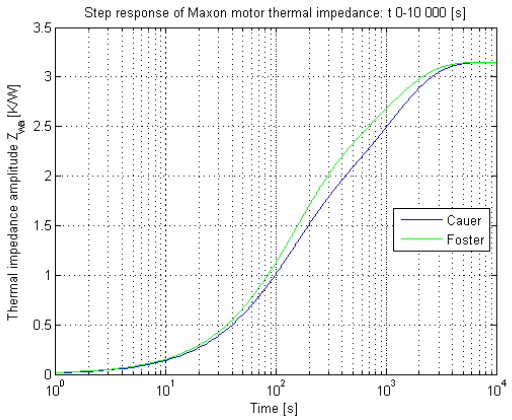

Figure 5.18: Step response for Foster vs. Cauer thermal model of the Maxon DC motor.

Thereby the value of the thermal capacity of the winding is assumed to be

$$C_{th,w} = \frac{\tau_{th,w}}{R_{th,wh}} = \frac{127\,s}{1.85\,K/W} = 68.65\,J/K,$$

and the thermal capacity of the housing to be

$$C_{th,h} = \frac{\tau_{th,m}}{R_{th,ha}} = \frac{991\,s}{1.3\,K/W} = 762.31\,J/K.$$

The equivalent transient thermal impedance of the motor, $Z_{th,eq}$, is implemented in Simulink as a transfer function, calculated as

$$Z_{th,eq}(s) = Z_{th,w} + Z_{th,h} = \frac{1}{\frac{1}{R_{th,wh}} + sC_{th,w}} + \frac{1}{\frac{1}{R_{th,ha}} + sC_{th,h}}. \tag{5.5}$$

The winding temperature can then be calculated as

$$T_w(t) = P(t) \cdot Z_{th,eq}(t) + T_{amb} = R_a I_{gen}(t)^2 \cdot Z_{th,eq}(t) + T_{amb} \tag{5.6}$$

where $P(t)$ is the dissipated power loss in the winding, R_a is the winding resistance of one generator, I_{gen} is the current in one generator and T_{amb} is the ambient temperature (temperature in the engine room) and considered to be constant. This is implemented in the generators "Thermal model" block, see Figure 5.19

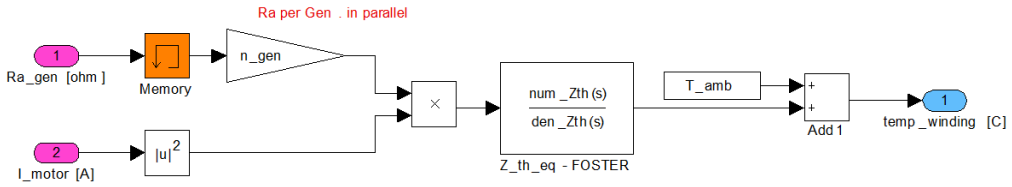

Figure 5.19: Transient temperature model of Maxon generator.

The simulated winding temperature is then compared to the maximum allowed winding temperature of 125 °C, in a scope in the generator model. An example of this can be seen in Figure 5.20, based on a simulation with the "original set up" described in chapter 6. Here the maximum winding temperature increase, above the initial temperature in the engine room of 25 °C, is about 10 °C.

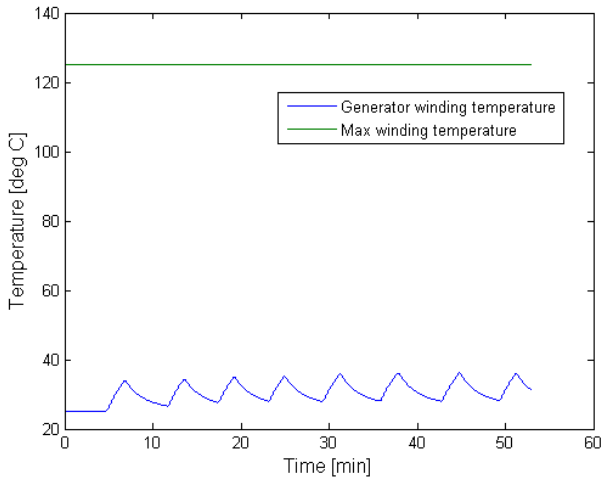

Figure 5.20: Temperature development in the Maxon generator.

5.5.6 Supercapacitor

The block diagram of the supercapacitor is shown in Figure 5.21. Input signals are the generator voltage (V) sent from the generator block and the current (A) required of the electric motor in order to produce the desired torque which is sent from the converter block. Output signals are the supercapacitor voltage (V) and the generator current which are being sent to the converter block and the generator block, respectively. C_cap is the capacity of the supercapacitor and $R\_cap + R\_fuse$ is the sum of the internal resistance of the supercapacitor and the resistance of the fuse.

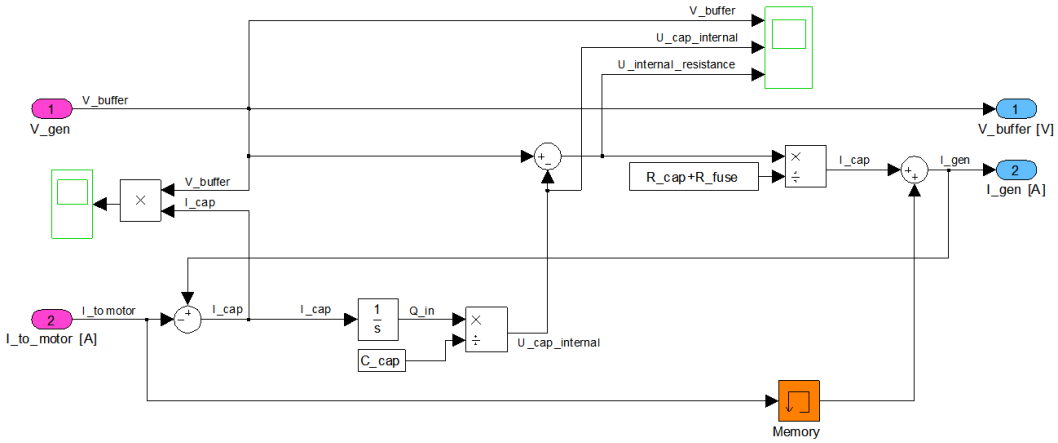

Figure 5.21: Block diagram model of Smarter supercapacitor.

In Figure 5.22 one can see how the voltage of the supercapacitor varies between 44 V and 38 V, which were set as the upper and lower limits, during the race.

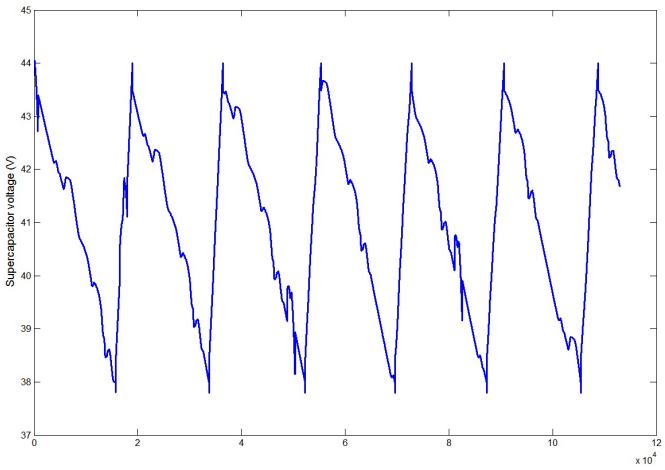

Figure 5.22: Variation of the supercapacitor voltage during the race.

5.5.7 Electric motor and DC/DC converter

The electric motor block consists of both a converter and the electric motor(s), see Figure 5.23.

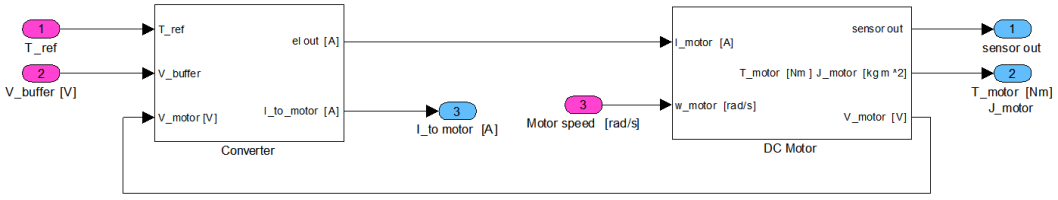

Figure 5.23: Block diagram model of the converter and the electric motor.

5.5.7.1 DC/DC-Converter

In Figure 5.24 the converter model is shown. It is a simple model just representing the converter with a power loss. The converter obtains information about the torque reference (Nm) from the gear motor-wheel block, the motor voltage (V) from the DC motor block and information about the supercapacitor voltage (V) from the supercapacitor.

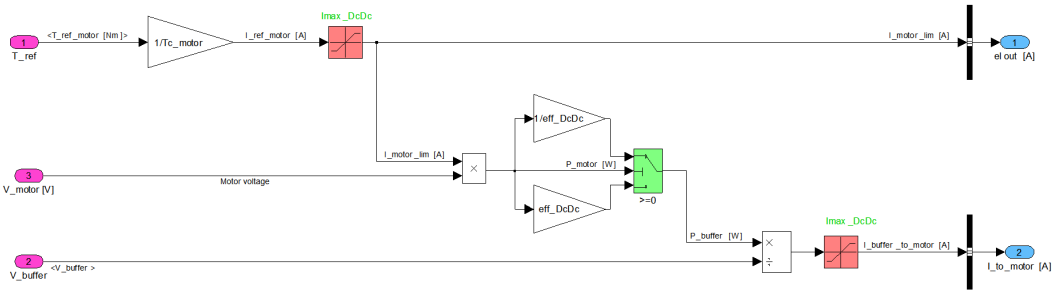

Figure 5.24: Block diagram model of the converter.

The block takes into account if the motor is operating as a motor or as a generator by changing the efficiency constant. *Tc_motor* is the motor constant and *eff_DcDc* is the efficiency of the DC-DC converter. From this block is motor current (A) being sent to the DC motor block and the current (A) needed to be sent to the DC motor which is sent to the supercapacitor block.

5.5.7.2 DC motor

Figure 5.25 shows the block diagram for the DC motor. Input signals are the motor current (A) sent from the converter block and the motor speed (rad/s) sent from the gear motor-wheel block.

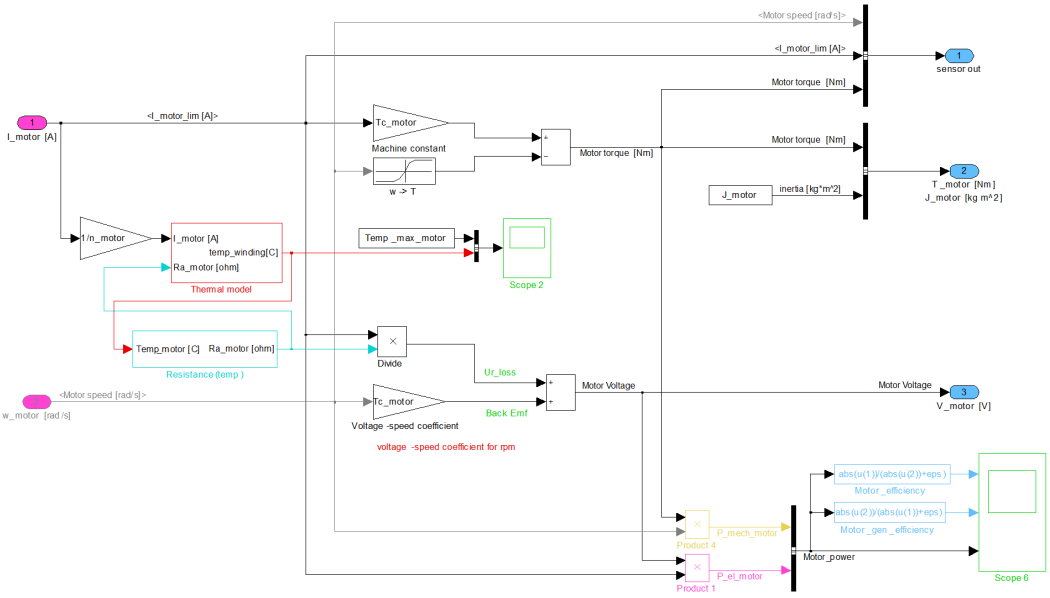

Figure 5.25: Block diagram model of the electric motor(s).

The block has two sub-blocks; *Thermal model*, which models the motor winding resistance temperature, and *Resistance(temp)*, which models the winding resistance's tem-

perature dependence. The Thermal model block is shown in Figure 5.26, and the Resistance(temp) block can be seen in Figure 5.27, and both blocks are modeled in the same way as in the generator model, and thus have the same function and resulting signals.

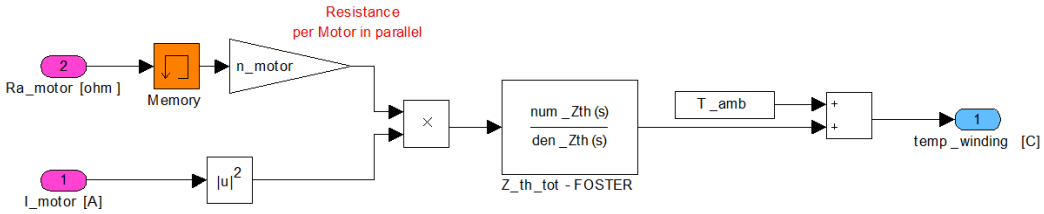

Figure 5.26: Block diagram model of the thermal model of the motor winding temperature.

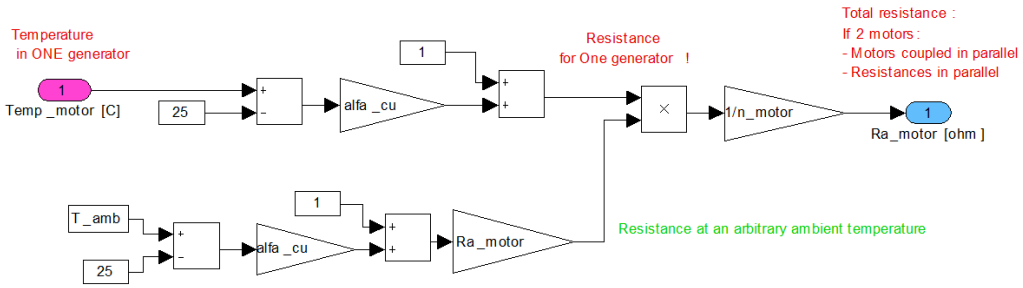

Figure 5.27: Block diagram model of the temperature dependence of the winding resistance.

An example of the winding temperature and resistance development during a race simulation can be seen in Figure 5.28

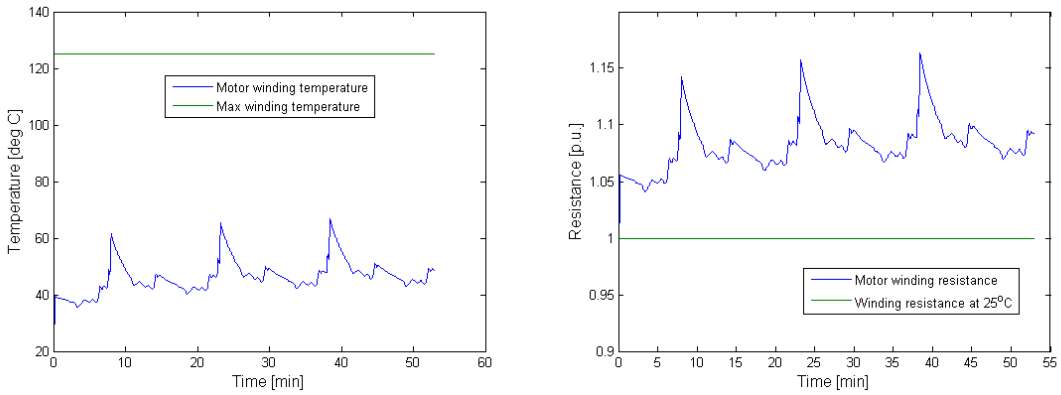

(a) Temperature development.

(b) Resistance change.

Figure 5.28: Winding temperature development and consequential resistance change in the Maxon motor.

Temp_ max_ motor is the maximum permissable motor winding temperature and *n_ motor* represents the number of parallel DC motors. The DC motor block sends information about the motor current (A) and the motor torque (Nm) to the controller block. It also sends information about the motor torque (Nm) and the motor inertia (kgm^2) to the gear motor-wheel block. Finally, the block also sends information about the motor voltage (V) to the controller block.

5.5.8 Gear Motor-Wheel

Figure 5.29 shows the block diagram model for the gear between the DC motor(s) and the wheels. The block receives information about the car torque reference (Nm) from the controller block, the motor torque (Nm), the motor inertia (kgm^2) from the DC motor block and the vehicle speed (rad/s) from the chassis.

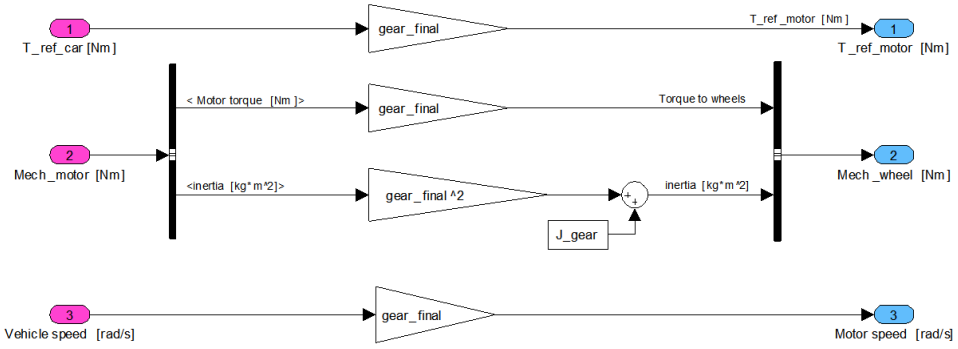

Figure 5.29: Block diagram model of the gear between the electric motor(s) and the wheels.

The input signals are transformed to the following output signals; motor torque reference (Nm), torque on wheels (Nm), inertia (kgm^2) and motor speed (rad/s). These signals are being sent to the converter, the chassis and the DC motor respectively.

5.5.9 Chassis

The block diagram model representing the chassis of Smarter can be seen in Figure 5.30, representing the different forces acting on a moving vehicle. The block receives signals about the braking torque (Nm) from the controller block, the torque acting on the wheels (Nm), the "so far" inertia (kgm^2) from the gear motor-wheel block and information about differences of altitude on the track (rad) from the environment model.

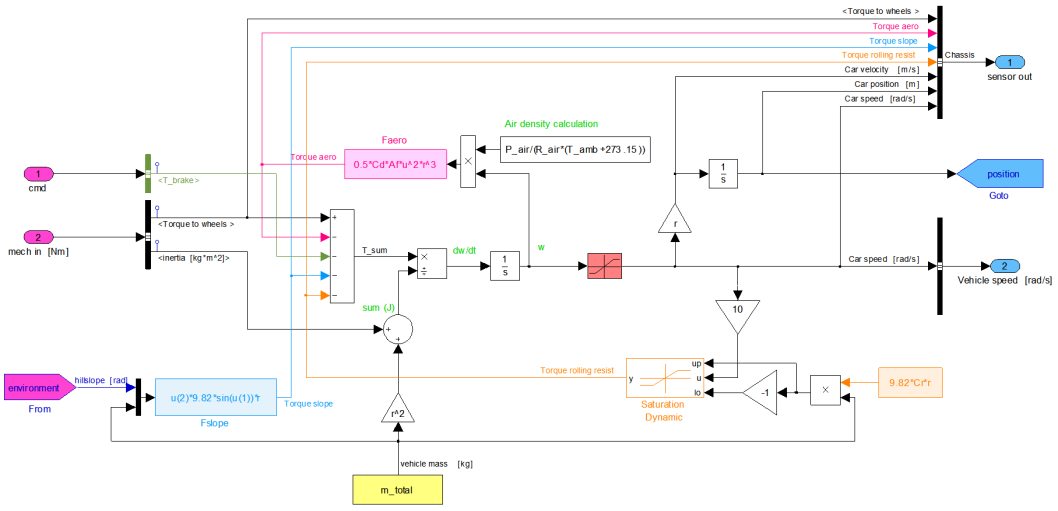

Figure 5.30: Block diagram model of the chassis.

Opposing torques due to braking, rolling resistance, aerodynamic drag (which depends on air density, i.e. air temperature) and slope resistance are subtracted from the driving

torque acting on the wheels. The resultant torque is then the net torque that propels the vehicle. The speed of the car is found by dividing the resultant torque with the vehicle's total inertia and then integrating.

From this block information about; torque to wheels (Nm), opposing torques (Nm) due to aerodynamic, slope and rolling resistance, car velocity (m/s), car position (m) and car speed (rad/s) is sent to the controller block. Information about the position of the car (m) is sent to the environment model and finally the vehicle speed (rad/s) is sent to the gear motor-wheel block.

Chapter 6

Performance evaluation of the simulated Smarter

In this chapter a series of simulations are run, using different components and/or component parameters. The fuel efficency (km/l) is compared between the different cases, as well as other results which may be considered interesting.

All the simulations are based on an original vehicle driveline setup, see Table 12.1, which was the one used in Smarter during the Shell Eco-marathon competition in EuroSpeedway Lausitz, Germany 2009.

Table 6.1: Original vehicle setup

Simulation vector		**ICE**	
Constant speed	25.6 km/h	Type	GX35
Acceleration time	10 s	ICE inertia	0.0069
Deceleration time	10 s	ICE starter	Generator(s)
Gear ICE-generators		**Gear motor-wheels**	
Gear ratio	0.8	Gear ratio	13.9
Efficiency	90 %	Efficiency	100 %
Supercapacitor		**Miscellaneous**	
Type	Li-ion capacitor	Nr. of generators	2
V_{max}	44 V	Nr. of motors	1
V_{min}	38 V	DC/DC converter	Chalmers designed
V_{init}	44 V	Driver weight	50 kg
		Engine room temperature	25 ℃
Chassis		**Simulation results**	
C_r	0.007	Fuel efficiency	**255.24 km/l**
C_d	0.28	Regenerated energy	1.13 %
A_f	1.4 m^2	Motor speed	3372 rpm
Air temperature	25 ℃	Generator speed range	4018 - 4840 rpm
Tire radius	0.2754 m	ICE speed range	3215 - 3872 rpm

6.1 Modelling and simulation aspects

Here follows some aspects when it comes to the modelling or the simulation.

6.1.1 Estimation of the ICE's rotational inertia

No data sheet or estimated values of the ICEs moment of inertia were achieved. Therefore the values for both engines were initially simply assumed to be five times larger than the value for one DC-motor.

Simulations with the original Smarter set up were then run with different values of the moment of inertia on the GX35 ICE, and the results are presented in Table 6.2, where η_{fuel} is the fuel efficiency and, $\Delta\eta$, is the difference in fuel efficiency compered to the original set up. As can be seen the differences in results are rather small. Thus, even though the value of the engines moment of inertia may be erroneously estimated, the relevance is negligible.

It was however noticed that the simulation time, t_{sim}, was much longer when using the lowest value of inertia (these figures are to be seen as relative figures, as the simulation time strongly vary depending on the calculation power of the system used). Since the difference in simulation result is rather small, but the gain in simulation time is relatively large, the rotational inertia of the ICE is modeled to be $0.0069\,kg\,m^2$.

Furthermore, for simplicity it is assumed that GX25 och GX35 have the same rotational inertia.

Table 6.2: Comparison between different values of moment of inertia of GX35.

Multiplication factor	**0.1**	**1**	**10**	**100**
$J_{ice}\,(kgm^2)$	0.0006900	0.0069	0.069	0.69
$t_{sim}\,(s)$	68 (100%)	12 (18%)	7 (10%)	7 (10%)
$\eta_{fuel}\,(km/l)$	255.19	255.24	256.76	258.63
$\Delta\eta\,(km/l)$	-0.05	-	1.52	1.87

6.1.2 Generator speed, supercapacitor voltage

When operating the generator at the recommended maximum speed of $5000\,rpm$, the maximum generated voltage, $V_{max} = \frac{w_{gen}}{k_\omega} = \frac{5000\,rpm}{107\,rpm/V} = 46.7\,V$. With the original Smarter set up, the approximate resistive voltage drop is shown to be about about; $1.7\,V$ for GX25 and $1.2\,V$ or GX35. This means the maximum terminal voltage, and thus supercapacitor voltage, is either about $45\,V$ or $45.5\,V$.

For this reason, and based on test rig measurements done by master thesis students at Electric Power Engineering at Chalmers, a maximum voltage of $44\,V$ was decided to be used in Smarter during Shell Eco-marathon.

6.2 Component and vehicle optimization

Here follows the results, from running simulations with varying parameters and different components.

6.2.1 With or without ICE start motor

To get an indication whether it is more fuel efficient to use the Piaggio start motor, or whether the generators should be recommended as start motors, both set ups were simulated and their results compared.

The Piaggio ICE starting motor was simply modeled as an extra kilo mass to the total vehicle mass, which then became 72.22 kg. The fuel efficiency when using the start motor was 255.70 km/l, while the fuel efficiency when using the generators was 255.24 km/l. This shows a very small difference in favor of using the Piaggio start motor. However it was not used in Smarter during the Shell Eco-marathon.

6.2.2 GX25 or GX35 and one or two generators?

To find out which engine is preferable over the other and whether one or two generators should be used, the results from simulations with each engine is presented in Table 6.3, where $m_{Smarter}$ is the vehicle weight without driver, t_{ICEon} is the total time during the race that the ICE is running, η_{fuel} is the fuel efficiency and, $\Delta\eta$, is the difference in fuel efficiency compered to the original set up.

As can be seen the resulting fuel efficiency is improved when using the GX35, in spite of the quite moderate increased weight. However, when using only one generator, the maximum winding temperature increase, ΔT_{max}, is rather high since one generator then receives the whole power from the ICE. This can be a problem if the engine room temperature is higher than the simulated 25 ℃, which very well may be the consequence as the race progresses in time.

Using two generators, prove not only to be better in a thermal point of view, but also shows to be the most fuel efficient choice. That is in spite of the extra weight added by the second generator.

The speed range is about the same for all cases; $4000 - 4800/5000\,rpm$. But the current, torque and power production from the GX35 is about two times higher than with GX25, which then gives a faster charge of the supercapacitor.

As can be seen, the most fuel efficient choice, using GX35 with two generators, is also the case where the ICE is running for the shortest total time. In both cases when the GX25 is used, the running time for the ICE is almost doubled, which is also reflected in the lower number of ICE-starts. Since the GX35 fuel flow rate is less than two times the GX25 fuel flow rate in almost the whole speed range, it is then evident that these circumstances will lead to a higher efficiency for the GX35.

Table 6.3: Comparison between GX25 and GX35, with one or two generators.

	GX25		**GX35**	
	One gen.	**Two gen.**	**One gen.**	**Two gen.**
$m_{Smarter}\,(kg)$	68.18	70.54	68.74	71.22
$ICE\ starts$	5	5	9	9
$t_{ICEon}\,(s)$	1938	1764	1032	925
ΔT_{max} (℃)	21	5.5	50.4	11.3
$\eta_{fuel}\,(km/l)$	178.43	198.09	228.98	255.24
$\Delta\eta\,(km/l)$	-76.81 (69.9 %)	-57.15 (77.6 %)	-26.26 (89.7 %)	- (100%) [1ex]

6.2.3 Gear ratio: ICE-Generators

The specific fuel consumption of the used GX35 ICE varies over its speed range and has a measured optimal operation range somewhere between $4000 - 5500\,rpm$, see Figure 4.5. Since the speed of the generator is more or less dependent on the capacitor voltage, one can adjust the speed range of the ICE by adjusting the gear ratio between the ICE and the generators. With the original gear ratio of 0.8 between the ICE and the two generators

this speed range is about $3400 - 3900\,rpm$, which may not be the best working range for this GX35, as can be seen in Figure 4.5. In this set of simulations, an attempt has been made to perhaps find a gear ratio which is more fuel efficient than the one used in Smarter.

However, the higher the working speed range of the ICE, the higher its output torque and thus its mechanical output power will be. This means that the generator current will be higher and therefore also the temperature rise in the winding. This may be a problem depending on the engine room temperature.

The simulation results are presented in Table 6.4. According to the simulations, the temperature rises are in general rather moderate, hence there should be no thermal problem. As can be seen, the unity gear ratio will keep the ICE in the preferred speed range and thus gives the best result, i.e. the highest fuel efficiency.

Table 6.4: Comparisons of gear ratios between the ICE GX35 and the two generators.

Gear ratio	**0.7**	**0.8**	**0.9**	**1**
$ICEstarts$	8	9	10	10
$\Delta speed_{ICE}\,(rpm)$	2900-3400	3400-3900	3800-4400	4300-4900
ΔT_{max} (°C)	9.5	11.3	14.1	15.4
$\eta_{fuel}\,(km/l)$	251.79	255.24	279.76	286.17
$\Delta\eta\,(km/l)$	-3.45	-	24.52	30.93 [1ex]

6.2.4 Maxwell versus Li-ion capacitor

Simulations have been done to compare the commercial supercapacitor and the Li-ion capacitor, see Table 6.5.

Table 6.5: Fuel efficiency comparison between Maxwell supercapacitor and the Li-ion capacitor.

Supercapacitor	Fuel efficiency	Number of ICE starts
Maxwell	246.10	9
Li-ion	255.13	9

With the Li-ion capacitor Smarter can go 9 km longer per liter. The difference in the vehicle's total fuel efficiency, when comparing the commercial and the Li-ion one, is mainly due to the fact that when saving one kg Smarter can go 1 km/l longer and that the Li-ion capacitor is 8.8 kg lighter than the commercial one. With that, the student manufactured Li-ion capacitor is with advantage chosen.

6.2.5 Maxon or Chalmers designed converter

The main difference between the Maxon and the Chalmers designed converter, is the maximum possible output current. For the Maxon converter the current is limited to $16.6\,A$, while it, in this context, can be regarded as unlimited for the Chalmers designed.

First the two converters are compared, when using the same drive cycle.

By utilizing FUNaccmax.m, and entering the necessary constant velocity for this current, the maximum possible acceleration is calculated. This value is then used to run the simulation with the shortest possible acceleration and deceleration time; $15\,s$, and the

constant speed value; $25.7\,m/s$. The results can be seen in Table 6.6.

As can be seen, the temperature development is the same in both cases, since the current need is the same.

There is however a difference between the two converters, when it comes to the running time of the ICE, and the number of starts. Clearly, the higher efficiency of the Chalmers designed converter makes the system more fuel efficient.

When running the simulation using the Chalmers designed converter and a current limit set to $200\,A$, and an acceleration time of $10\,s$, the peak current in the motor is $25\,A$ during acceleration and $17.4\,A$ during deceleration.

According to the simulations, there is no difference in fuel efficiency between the case with the lower current limit and the one with the higher limit, even though the running time of the ICE is about $20\,s$ longer in the second case. This result raises the interest to compare different acceleration and deceleration times, to find the most fuel efficient time.

Table 6.6: Comparison between Maxon and Chalmers designed converter.

	Maxon	**Chalmers designed**	
	16.6 A	**16.6 A**	**200 A**
ΔT_{max} (°C)	33	33	42.0
$t_{ICEon}\,(s)$	1098	903.8	924.8
$ICEstarts$	9	8	9
$\eta_{fuel}\,(km/l)$	211.57	255.49	255.24
$\Delta\eta\,(km/l)$	-43.92	-	-0.25

6.2.6 One or two driving DC motors?

It is not evident whether it is preferable to use one driving DC motor or whether it is more fuel efficient to use two. There may also be another aspect to consider, i.e. the peak power, drawn by the motor in order to accelerate and brake the vehicle, which inherently will lead to a temperature development, ΔT_{max} in the motors winding. With two motors, this power will be split between the two and thus the temperature development much more moderate compared to using only one motor, as can be seen in Table 6.7.

Another aspect is the over all efficiency of the motor package, η_{motor}, which is not the same in the two cases. Since the motor speed range is dictated by the speed of the vehicle, it will be the same regardless of the number of motors, which then will give the same total output torque ($2.18\,Nm$) in both cases. When using two motors, the total output torque will be shared by the two motors, but in the same time the total friction torque will be doubled, resulting in a lower efficiency compared to using only one motor.

One may also consider the total electrical power, $P_{el}\,(W)$, drawn by the motors. Naturally, the two motors will consume a bit more power to compensate for the extra losses, a prediction that was then seen in the simulations. This means that the ICE must run for $61.9\,s$ longer during the race, to charge the supercapacitor, when using two motors.

According to simulations, not only is the power conversion more efficient when using only one motor, but the system is also the one that proves to be the most fuel efficient choice. However, when using two motors a slightly higher ratio of energy is regenerated, $1.15\,\%$, than when using only one, $1.12\,\%$.

Table 6.7: Comparison of using one or two driving motors.

	One motor	**Two motors**
$P_{el,peak}\,(W)$	900	860
$t_{ICEon}\,(s)$	924.8	986.7
$\Delta T_{max}\,(\text{℃})$	42.0	10.7
$W_{e,regen}(\%)$	1.12	1.15
$\eta_{motor}\,(\%)$	90	85
$\eta_{fuel}\,(km/l)$	255.24	239.59
$\Delta\eta\,(km/l)$	-	-15.65 [1ex]

6.2.7 Gear: Electric motor(s)-Wheels

Here follows simulations on how the fuel efficiency is dependent of gear ratio and gear efficiency.

6.2.7.1 Gear ratio

Smarter's gear ratio between the electric motor(s) and the wheels is according to simulations a bit low, a gear ratio of 15 would be optimum giving a fuel efficiency of 255 km/l, see Figure 6.1.

The purple circle in the graph indicates the gear ratio used in Smarter, which was 13.9.

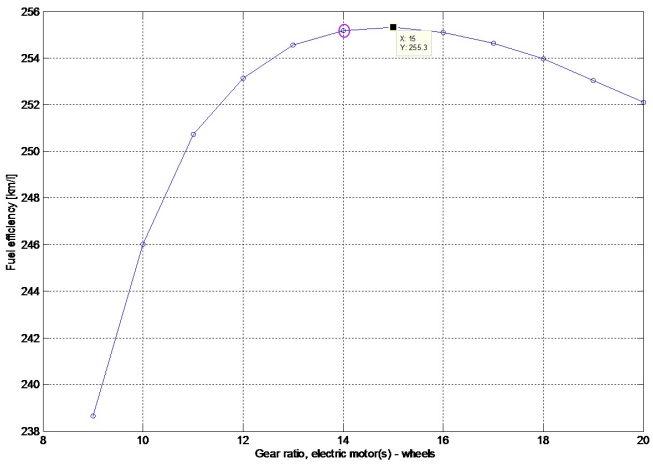

Figure 6.1: Fuel efficiency as a function of gear ratio between electric motor(s) and wheels.

6.2.7.2 Gear efficiency

The gear between the electric motor(s) and the wheels is modelled having an efficiency of 100 %. However, Figure 6.2 shows how the fuel efficiency is dependent on the efficiency of the gear between the motor(s) and the wheels.

The purple circle indicates perfect efficiency, which was used when modelling the gear.

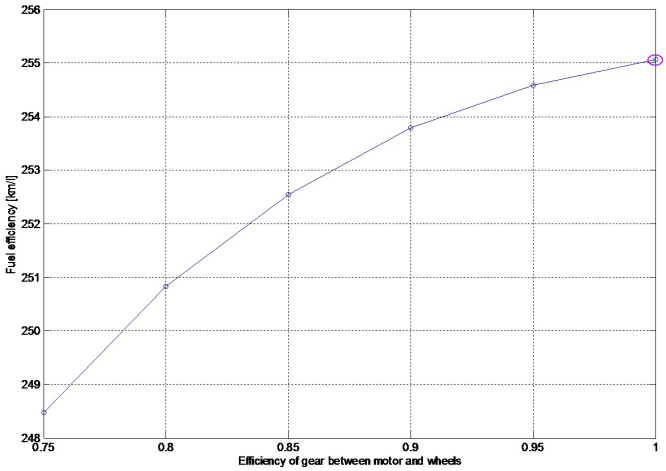

Figure 6.2: Fuel efficiency as a function of the efficiency of the gear between the motor(s) and the wheels.

6.2.8 Chassis

In this section follows some simulations regarding characteristic parameters of the Smarter chassis.

The current relation between the tractive torque from the motor, *"to wheels"* and resistive torques acting on the vehicle can be seen in Figure 6.3. As can be seen, the main resistive torque is the air drag.

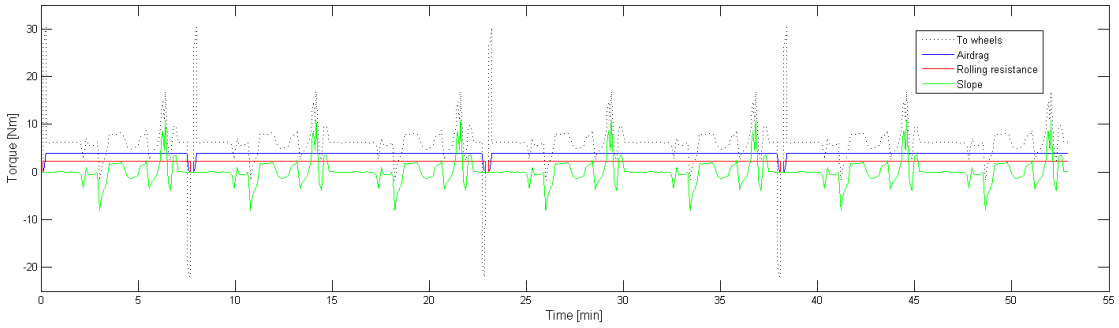

Figure 6.3: Torques acting on the vehicle.

6.2.8.1 Rolling resistance coefficient, C_r

The fuel efficiency is inversely proportional to the rolling resistance coefficient, C_r, see Figure 6.4.

Smarter's rolling resistance coefficient was estimated to be 0.007 and is marked with a purple circle in the graph. As can be seen in the figure the rolling resistance coefficient has a large impact on the fuel efficiency.

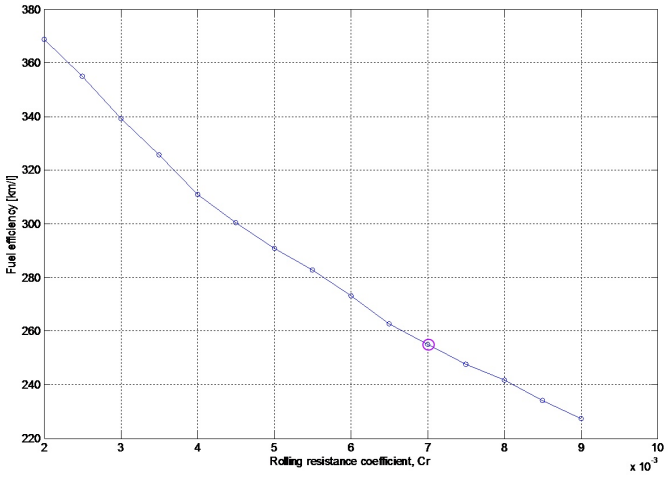

Figure 6.4: Fuel efficiency as a function of rolling resistance coefficient, C_r.

6.2.8.2 Tire radius

The Shell Eco-marathon's rules states that the rims should have a diameter between 16 and 17 inches. Smarter's rims have a diameter of 16 inches and according to simulations it is the best choice to choose rims of 16 inches. Even if it would have been preferable to have a tire which had a bit smaller radius, see Figure 6.5.

Again, the purple circle represents the parameter value chosen in Smarter.

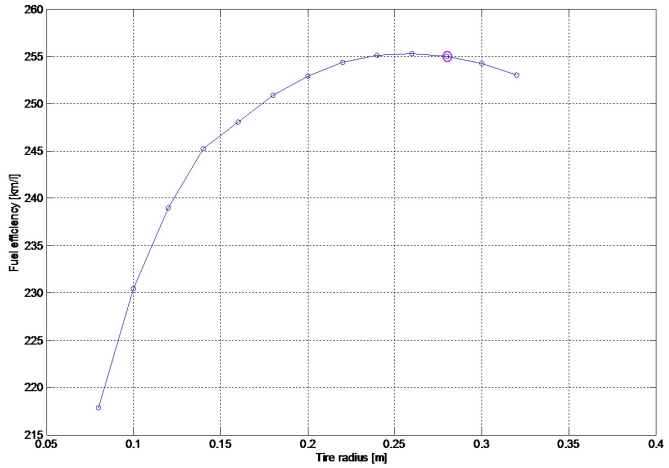

Figure 6.5: Fuel efficiency as a function of tire radius.

6.2.8.3 Aerodynamic drag coefficient, C_d

Figure 6.6 shows how the fuel efficiency is dependent on the aerodynamic drag coefficient, C_d.

The purple circle in the graph indicates Smarter's estimated aerodynamic drag coefficient, $C_d = 0.28$. The aerodynamic drag coefficient has a huge impact on the fuel efficiency.

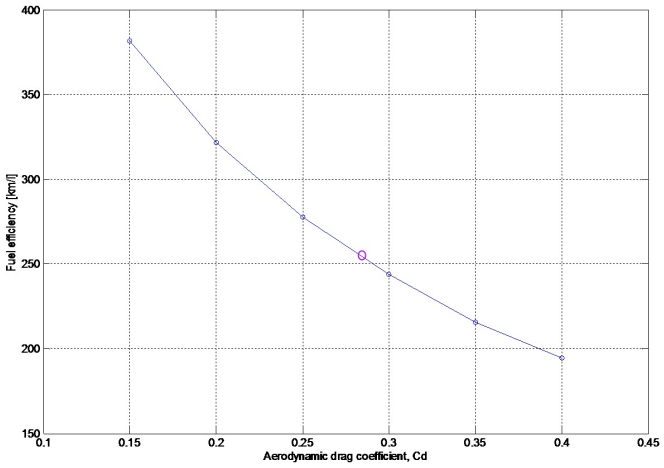

Figure 6.6: Fuel efficiency as a function of aerodynamic drag coefficient, C_d.

6.2.8.4 Cross-sectional area, A_f

The fuel efficiency is exponentially proportional to the cross-sectional area, A_f, see Figure 6.7.

Smarter's cross-sectional area was estimated to be 1.4 and is marked with a purple circle in the graph. As the rolling resistance coefficient and the aerodynamic drag coefficient also the cross-sectional area has a major influence on the fuel efficiency.

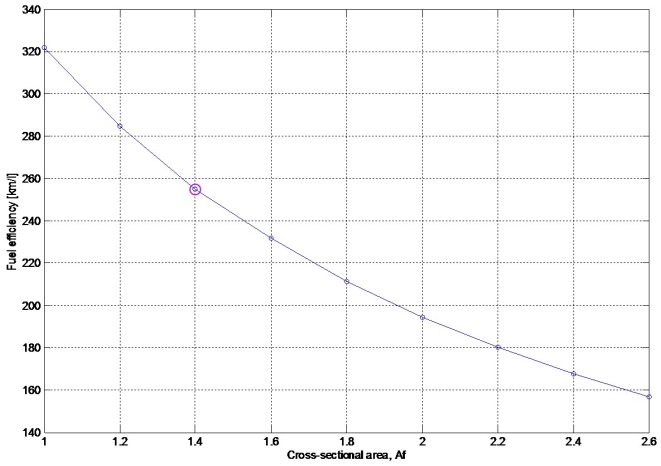

Figure 6.7: Fuel efficiency as a function of cross-sectional area, A_f.

6.2.9 Fuel efficiency dependency of vehicle mass

Figure 6.8 shows how the fuel efficiency is almost linearly dependent of the vehicle mass. For every added kg of mass, the fuel efficiency decreases about $1.1\,km/l$.

With the above mentioned general setup, Smarter had a mass of 121 kg, which is indicated with a purple circle in the graph.

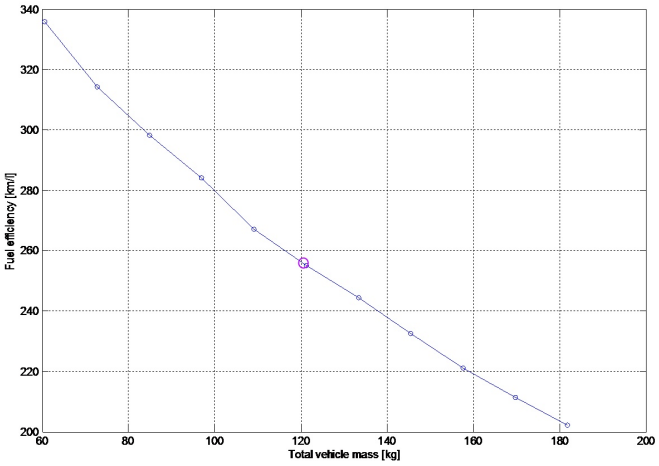

Figure 6.8: Fuel efficiency as a function of vehicle mass. The mass includes a driver of $50\,kg$.

6.3 Analysis of different (control) strategies

6.3.1 Discharge level for the Li-ion capacitor

The next question is then how much we should allow the Li-ion capacitor to discharge before turning on the ICE and starting to charge the capacitor again. During the race in Lausitz the maximum and minimum allowable capacitor voltages was 44 V and 38 V, respectively.

The minimum permissable capacitor voltage has been varied to see how the fuel efficiency is dependent on how much the supercapacitor is allowed to discharge. Figure 6.9 shows simulations where the minimum voltage has been varied from 65 % to 95 % of the maximum voltage, 44 V. 65 % of maximum capacitor voltage is 28.6 V which is the minimum permissable voltage of the capacitor according to the manufacturer of the Li-ion capacitor cells [22].

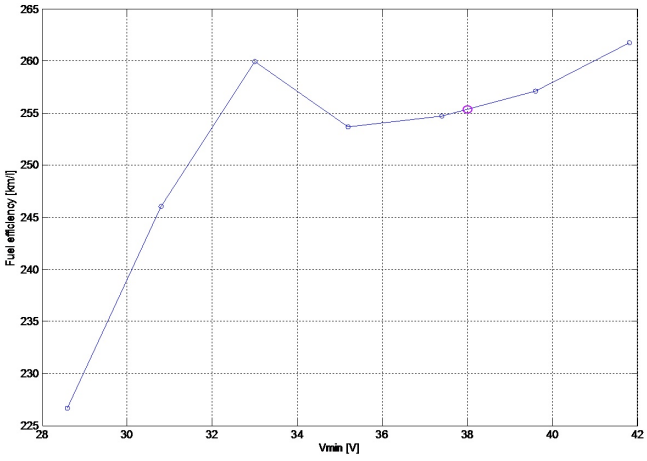

Figure 6.9: Fuel efficiency as a function of minimum voltage of the Li-ion capacitor.

The general trend which can be seen in the graph is that it is better, in a fuel efficiency point of view, to only allow such a small discharge as possible. However, a very low

permissable discharge results in longer on-time for the ICE which in turn could lead to overheating of the engine, thus it should be investigated. Only allowing the capacitor to discharge to a voltage level of 95 % of maximum voltage level (41.8 V) results in 26 starts of the ICE and an race-on-time of 893.4 s, whereas allowing the capacitor to discharge to 38 V results in only 8 starts and an race-on-time of 924.8 s, that is only 32.4 s longer.

6.3.2 Initial charge level for the Li-ion capacitor

To examine the relationship between the initial charge level and fuel efficiency a set of simulations, from 65 % to 100 % of maximum possible charge level, were done, see Figure 6.10.

Apart from worse fuel efficiency, it can be harmful to the supercapacitor to have too low Q_{init}.

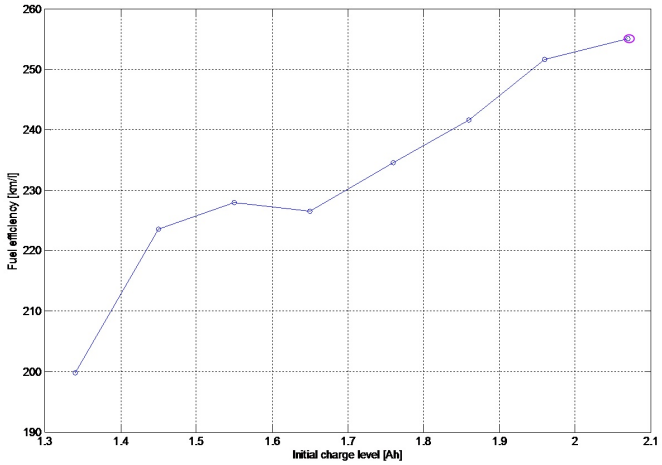

Figure 6.10: Fuel efficiency as a function of Q_{init} of the Li-ion capacitor.

6.3.3 Acceleration and deceleration time

So far the acceleration and deceleration times have been set to 10 s each, and the constant speed has been 25.6 km/h. Here follows an investigation of how the fuel efficiency depends on the drive cycle, that is variations of the acceleration and deceleration time as well as the constant speed.

The results from the simulations are presented in Table 6.8. The total race time for most simulations was 3180 s, and for a few 3179 s and the acceleration and deceleration times were set to be equally long.

As can be seen, the results are very similar for the different runs, with a difference of only one or a few km/l more or less. The highest fuel efficiency was reached with an acceleration and deceleration time of 12 s, and a speed of 25.6 km/l. For both shorter and longer acceleration times the trend is a slightly lower fuel efficiency.

Since no major improvement is indicated in the results, there will be no further investigation regarding different drive cycles and their effect on the system, in this thesis.

Table 6.8: Comparison between different drive cycles.

Acceleration time (s)	Speed (km/h)	Fuel efficiency (km/l)
4	25.38	252.62
6	25.43	255.06
8	25.49	255.88
10	25.55	256.12
12	25.60	256.18
14	25.66	255.64
16	25.73	255.25
18	25.79	254.85
20	25.85	254.40
25	26.00	253.38
30	26.14	252.23
35	26.29	250.80
40	26.44	249.45

6.4 Impact of air temperature

The aerodynamic drag is inversely proportional to the air temperature, that is the lower the air temperature, the larger the aerodynamic drag and thus the lower the fuel efficiency. Simulations have been run to find the magnitude of this effect, see Figure 6.11.

According to the simulations, the difference between 15 ℃ and 25 ℃, is about 11.5 km/l, and as much as 17.4 km/l between 10 ℃ and 25 ℃. That is, for every increased degree, the fuel efficiency increases about 1.15 km/l. The aerodynamic drag is about 4.30 Nm at 10 ℃, 4.16 Nm at 15 ℃ and 3.88 Nm at 25 ℃.

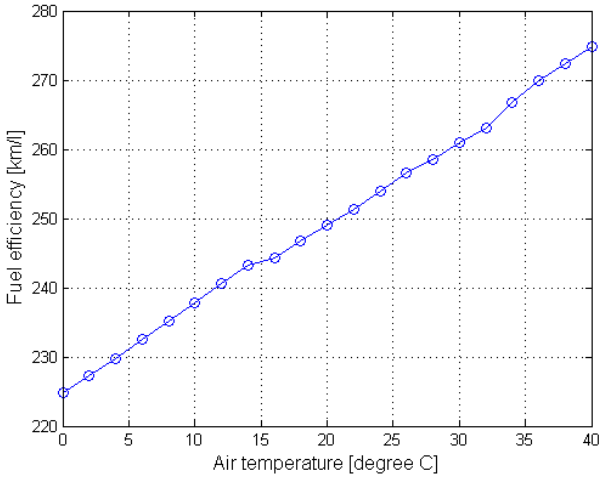

Figure 6.11: Fuel efficiency as a function of air temperature.

6.5 Evaluation with improved parameters

In previous sections, different vehicle parameters and components have been altered one by one, to investigate their influence on the simulated Smarter fuel efficiency.

In this section, simulations have been run where more than one parameter or component have been altered, still to investigate the fuel efficiency.

6.5.1 Multiple improved parameters

Here all the previously found most preferable parameter values have been used in a single simulation run, see Table 6.9. With this set up the fuel efficiency is 278.19 km/l, which is an improvement by 22.95 km/l compared to the original set up.

Table 6.9: Optimal vehicle setup

Simulation vector		**ICE**	
Constant speed	25.6 km/h	Type	GX35
Acceleration time	12 s	ICE inertia	0.0069
Deceleration time	12 s	ICE starter	Generator(s)
Gear ICE-generators		**Gear motor-wheels**	
Gear ratio	1	Gear ratio	15
Efficiency	90 %	Efficiency	100 %
Supercapacitor		**Miscellaneous**	
Type	Li-ion capacitor	Nr. of generators	2
V_{max}	44 V	Nr. of motors	1
V_{min}	33 V	DC/DC converter	Chalmers designed
V_{init}	44 V	Driver weight	50 kg
		Engine room temperature	25 ℃
Chassis		**Simulation result**	
C_r	0.007	**Fuel efficiency**	**278.19 km/l**
C_d	0.28	$t_{ICEon}\,(s)$	694.5 s
A_f	1.4 m^2	ICE starts	6
Air temperature	25 ℃		
Tire radius	0.2792 m		

6.5.2 Lower fuel flow rate

The information regarding the ICE fuel consumption is relatively uncertain, see section 4.2.2. Firstly, the measurements were conducted with a rather poor resolution. Secondly, the real engine had most probably been further modified, thereby reaching higher efficiency. Therefore some simulations have been run where the fuel flow rate have been scaled from 5 to 20 %, to represent a possible error in data. The scaling was applied with the same factor to the whole speed range. This is naturally a simplification of the problem, but still gives an indication of the effect on the result, which can be seen in Figure 6.12.

According to the simulation results, a 10 % lower fuel flow rate, gives a slightly more than 10 % increase in the fuel efficiency.

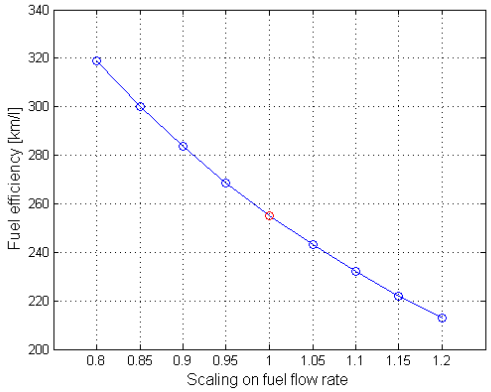

(a) Fuel flow rate in km/l.

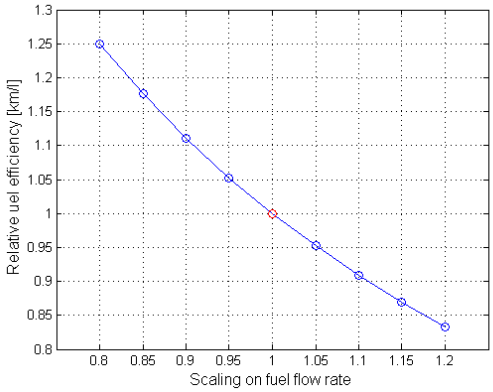

(b) Fuel flow rate in per unit value, with 255.4 km/l as a base.

Figure 6.12: Fuel efficiency as a function of weighted fuel flow rate, with different units on the y-axis. The red circle marks the original set up value.

6.5.3 Better body and wheels

In this section follows an investigation of how the fuel efficiency is effected if the Smarter body and wheels are redesigned for improved performance.

An improved body has a smaller cross sectional area, less friction, and a more aerodynamically friendly shaped body. It may be interesting to get a rough estimation of how much could be gained in fuel efficiency, if all these three parameters were made as beneficial as possible.

Here it is assumed that the cross sectional area can be decreased from 1.4 to $1\,m^2$. It is also assumed that the rolling resistance coefficient can be as small as 0.004 instead of 0.007, which demands different tires. Finally it is assumed that the aerodynamic drag can be reduced to 0.2 from 0.28, which needs a more streamlined design of the body. No further investigation on what needs do be done in order to achieve these improved parameters have been done. It is however assumed that these parameters can not be improved further than what is here estimated.

The simulations shows that the fuel efficiency, with the given more beneficial parameters, is about **548 km/l**.

Finally, a simulation was run where improved parameters for both the drive line and the body was used. In this run, the fuel flow rate was decreased to 80 % of the original value, the ICE-generators gear ratio was set to unity, the gear ratio between the DC motor and the wheel was set to 15, the lower voltage limit on the supercapacitor was set to $33\,V$, the aerodynamic drag was set to 0.2, the rolling resistance was set to 0.004, and the cross sectional area was set to $1\,m^2$.

With all these improvements, the fuel efficiency of the vehicle is **732.95 km/l**. This is an improvement of $477.71\,km/l$ compared to the original set up, and the ICE needs only to be started three times and run for 311 seconds.

This result can serve as an "as good as it gets"-result. That is, according to the simulations, the given driveline is assumed to be performing at its best, and according to assumptions, the body and wheels can not be further improved.

Chapter 7

Smarter's performance in Shell Eco-marathon 2009

Here follows a short summary of Smarter's performance in the competition at Eurospeedway Lausitz Racing Circuit.

7.1 Smarter's race execution

The assembly of Smarter was not finalized in time to take part in the first race. It was however done in time for the second race.

After hardly two laps, the driver pulled the emergency stop when receiving a warning signal from the control system, of under voltage in the supercapacitor. Thus the race was aborted.

After the second race it was found that the wheels had been wobbling so much during the race, causing the brakes on the back wheels to become locked in the on-state. This may have added an extra load on the driveline, that it had not been able to support.

In the third and last race, Smarter almost finalized the first lap, before the left front wheel sprung loose from the system, and also the third and last race had to be aborted.

7.2 Driver experience

When simulating the race, the speed of Smarter between the pit stops were simulated to be constant. However, during the actual races it was impossible due to the fact that there were about 15 to 20 vehicles to share the track with and that some of the curves were pretty sharp.

7.3 Top 10 results of UrbanConcept

Here are the top ten results in the UrbanConcept, overall and in the ICE class, see Figure 7.1 and Figure 7.2.

Rank	Country	Institute	Best Run (km/l)	Energy Source
1		NTNU (Norges Tekniske og Naturvitenskapelige Universitet)	1246 km	Hydrogen
2		Haagse Hoge School/TH Rijswijk Academie voor Engineering	804 km	Hydrogen
3		Technical University of Denmark	589 km	Liquid Petroleum Gas (LPG)
4		University of Sakarya	568 km	Hydrogen
5		National University of Singapore	484 km	Hydrogen
6		EMAC Albi Carmaux - Ecole des Mines	480 km	Hydrogen
7		Faculdade de Engenharia da Universidade do Porto	343 km	Gasoline (Petrol)
8		LP Louis Delage Cognac	339 km	Gasoline (Petrol)
9		Instituto Politécno da Guarda	297 km	Gasoline (Petrol)
10		Lycée Jean-Baptiste de Baudre Agen	245 km	Diesel

Figure 7.1: Top 10 results amongst all UrbanConcept participants.

Rank	Country	Institute	Best Run (km/l)	Energy Source
1		Technical University of Denmark	589 km	Liquid Petroleum Gas (LPG)
2		Faculdade de Engenharia da Universidade do Porto	343 km	Gasoline (Petrol)
3		LP Louis Delage Cognac	339 km	Gasoline (Petrol)
4		Instituto Politécno da Guarda	297 km	Gasoline (Petrol)
5		Lycée Jean-Baptiste de Baudre Agen	245 km	Diesel
6		IPSA Kremlin Bicêtre - Institut Polytechnique des Sciences Avancées	244 km	Gasoline (Petrol)
7		Lycée Niepce Chalon sur Saone	243 km	Diesel
8		IES Alto Nalón	241 km	Diesel
9		I.T.I.P. "I.BUCCI"	240 km	Gas to Liquid (GTL)
10		Faculté Polytechnique	206 km	Liquid Petroleum Gas (LPG)

Figure 7.2: Top 10 results amongst the UrbanConcept Internal Combustion Engine participants.

Chapter 8

Conclusions and future work proposals

The goal for this first part of the thesis, was to make a model of the current Smarter vehicle, and to simulate its performance in Shell Eco-marathon. By adjusting different parameters in the vehicle model, further performance investigations were also to be conducted.

Here follows some conclusions on how well the goal of the thesis was fulfilled and what needs to be done still. Furthermore, a discussion regarding the performance of the simulated Smarter vehicle is also presented.

8.1 Modelling aspects

The Smarter vehicle and its driveline components have been modeled, and thus this part of the goal is considered fulfilled.

A model can never be an exact replica of reality, but it should give about the same output as in the real world, based on the same input. The main weakness of the Smarter model is that almost no data or parameter has been confirmed or adjusted by measurements and/or test runs, but they are simply based on manufacturer data sheet values. Nor have any model been verified. In order to have a more reliable result, this ought to be done.

Another weakness is that some loss parameters, such as the gear and converter efficiencies, are modeled as constant factors, when in reality it most probably varies between different working points.

Also, the Maxon DC motors' and generators' no load torque is assumed to be constant over the speed range, while in reality it is probably speed dependent. The value given in the data sheets are valid at nominal voltage and speed; $3550\,rpm$. The simulated generator speed is about $4000 - 4800\,rpm$, and the motor speed about $3400\,rpm$. This means that the simulated fuel efficiency may be slightly higher than the real one, due to the two generators.

8.1.1 Non modeled parameters and aspects

What is not represented in the model in general are different kinds of losses; electrical resistance in cables, mechanical friction during rotation and rotational inertia of the ICE-generator gear and the wheels. The main reason for this is lack of information regarding the magnitude of these. Naturally, the more loss parameters that one adds to the model, the more complex the model becomes, making it more delicate while analyzing the result.

There may also be unexpected losses in reality, that are not discovered until the vehicle is finalized. One example of this are the wobbling wheels of the real Smarter in Shell Eco-marathon 2009, a loss that is not represented in the model.

8.1.2 Future work proposals: Modelling

Since the ICE is modeled using measurement data, the only way to improve the model is to improve this data. The measurements should then be done on the very specific engine that will actually be used in Smarter, with all its modifications. A larger series of more accurate measurements are needed to establish a more reliable torque(rpm)-curve, as well as an SFC(rpm)-curve to draw conclusions of the optimal ICE speed range. Also the fuel flow rate as a function of speed could be reinvestigated, as the current information shows rather inconsistent curves.

Other interesting parameters to investigate are the efficiencies of the gears, both the ICE-generator and the motor-wheel gear. The gear losses could be larger than here assumed, causing an even lower fuel efficiency than simulated. It could also be that it varies in the speed range.

As mentioned in section 4.4.2, the Chalmers designed converter currently has a rather large output ripple, which may cause increased losses in the dc motor. This phenomenon should be further investigated to find a more reliable loss modeling.

Finally, as a relatively small decrease of the parameters of the body can have a rather large effect on the vehicle fuel efficiency, it is recommended that these parameters are carefully measured.

8.2 Simulation aspects

In compliance with the set goal, the Shell Eco-marathon race was simulated. However, the race simulation speed-time-vector is quite simplified, simulating an ideal race with no disruptions. In the real race, collisions with other participants must be avoided and thus the speed may vary during the race. With the current speed-time-vector, one can preferably compare different vehicle set ups to find an optimal one, but it is rather difficult to make reliable predictions of the Smarter resulting fuel efficiency in the real Shell Eco-marathon.

Due to the relatively large level of influence that the air temperature has on the aerodynamic drag, it is perhaps more appropriate to run the simulations using an air temperature that is closer to the typical local track temperature. Since the competition is set in Germany in the beginning of May, somewhere around $10 - 15$ °Cshould be more accurate.

The winding temperature is modeled for both the generator(s) and the motor(s), using a constant engine room (ambient) temperature. This temperature is though most probable to increase during the race, as all the components will dissipate power. A more detailed temperature model of the whole driveline is desired, but naturally rather difficult and complicated to accomplish. Perhaps a compromise could be to test run Smarter with a thermal sensor placed in the engine room. This information could then be enough to make a time-vector of the engine room temperature, to run it in the race simulation.

8.2.1 Driveline operational aspects

In the simulator, the generator voltage is in every moment also dictating the voltage over the supercapacitor, since they are coupled in parallel. This means that if the generator

speed goes down to zero, so will the voltage over the supercapacitor. In the same time, the main control system of the simulator is the one controlling the voltage level on the supercapacitor; turning the ICE off at V_{max} and turning it on at V_{min}. That is, even though the ICE is off, the voltage over the capacitor is always non zero, hence the generator speed is always non zero. In fact the generator speed has the same profile as the generator and supercapacitor voltage, i.e. it is going linearly up and down over time.

As a consequence of this, the ICE will never start its operation at zero speed, when it is simulated to start, but it will be the minimum speed of the generator speed profile, which is directly proportional to the set lower voltage limit of the supercapacitor.

In the real Smarter, there is a turn off switch, causing the speed of the generator and of the ICE, to always go down to zero, as the ICE is turned off. The difference in operation between the real Smarter and the simulated Smarter, may result in a slightly higher simulated fuel consumption, than what is expected in the real vehicle.

8.2.2 Future work proposals: Simulation

According to simulations the fuel efficiency did not vary much for different parameters in the speed-vector. It could still be interesting to further vary the speed vector, to simulate the influence of other vehicles, and evaluate the resulting fuel efficiency.

It may also be a good idea for the Shell Eco-marathon 2010, to have a GPS in Smarter during the race, and then use the gained information regarding speed and time, to make a more reliable speed vector. Perhaps then, an optimal driving strategy can be developed and investigated.

8.3 Smarter performance aspects

Throughout the whole process of designing and manufacturing Smarter, one of the main issues was to keep the total mass of the vehicle to a minimum, in order to maximize the fuel efficiency. Much thanks to the carbon fibre chassis, but also chosen components such as the electric machines and the Li-ion capacitor, this has been a successful work. The consequence is that some tens of kilogram mass have probably been saved, which according to the simulations means about as many km/l in fuel efficiency.

However, the simulations indicate a somewhat smaller dependence on the vehicle mass than what was probably first expected by the designers. This can be seen for example, when the generators were chosen to serve as start motors for the ICE, instead of adding an external start motor with one kg of mass. In fact the simulations shows that it would be somewhat more favorable to use the external start motor, even though the difference was rather minimal.

Furthermore, the original driveline set up would give Smarter a fuel efficiency of $255.24\,km/l$, according to simulations. This result would have placed Smarter as number 10 in the overall UrbanConcept, and as number 5 in the ICE class, if the vehicle had finished a race in the 2009 edition of Shell Eco-marathon.

Even though the driveline parameters are set to their proven most optimal values, the improvement in final result is rather limited; only about $23\,km/l$. This would not mean any climbing in the result list. Not to forget; the model is not verified, and many mechanical and electrical losses are not represented in the model. This means that the real result for this set up, is probably lower than indicated by the simulator.

Simulations show, that if the ICE manage to consume only 80% of the current fuel consumption, one spot in each of the Eco-marathon result lists could be gained. But to reach 80 % of the fuel consumption may mean quite a lot of work on the engine, together with more careful measurements.

As can be seen in section 6.2.8 and 6.5.3, variations of the chassi parameters (C_d, C_r and A_f) have the possibility to increase the vehicle fuel efficiency quite a lot. With the body improvements alone, given in section 6.5.3, Smarter would place as number 5 in the overall UrbanConcept, and as number 2 in the ICE class.

Finally, even if some of the modeled parameters are erroneous and not fully representative of the real Smarter, a simulation has been run with all the found necessary improved parameters, see section 6.5.3. This includes gear ratios, the body and using 80 % of the ICE fuel flow rate. The resulting fuel efficiency would place Smarter on the third place in the overall UrbanConcept and on first place in the ICE class. This simulation is intended to indicate the potential of the vehicle, with the current driveline component set up.

8.3.1 Future work proposals: Smarter

The simulations indicate that the possible modifications of the parameters in the current Smarter driveline only give moderate improvements in fuel efficiency. Instead it seem to be modifications of the Smarter chassis and body that will help Smarter to reach a higher position in the result list in the next coming editions of Shell Eco-marathon.

Another possibility for Smarter, is to investigate the use of a parallel driveline, instead of the current series driveline. That would mean one less mechanical-electrical energy conversion, and thus it could yield a higher fuel efficiency.

A parallel driveline most likely also mean that, both the ICE and the electrical machine will be connected to the vehicle wheels, probably via a few chain gears. Then both of them may be exposed to the lower speed range, during the start and the pit stops. In this operating area, the efficiency is essentially lower, for both the ICE and the electrical machine.

Another problem will be to manage to find an optimal gear ratio such that both the ICE and the generators can operate in their most optimal speed range during the most part of the race, as they will probably be connected via the same gears.

It it thus not obvious whether a parallel driveline in fact is favorable over the current series one, and if so by how much. However, due to the shown limitations of the series driveline, it is strongly recommended to model and evaluate a parallel driveline for Smarter.

Part III

QRTECHs Electric Go-Kart

Chapter 9

Introduction to go-karting

Karting originates from the 1950's USA and has spread to other countries, especially European ones, becoming an entrance to the world of motor sports due to its relatively low costs to perform.

The different classes in karting are divided depending on the age of the driver, the size of the motor, costs and if the kart has a gear or not. The lowest class is from age seven, but is only a presentation class. There exists competition classes from age ten and upwards.

The chassis of a go-kart is made of a steel tube and is characterized by not having any wheel suspension and having a stiff rear axle. The intention with these limitations is to keep the expenses down. A regular private car has a so called differential which facilitates different speeds of the driving wheels when turning, this is not the case for a go-kart.

Electric go-karts have a number of advantages over the conventional go-kart, such as; no emissions, lower maintenance and no gasoline handling. Still, they have just started to come into the market and then mainly in recreation.

Chapter 10

The go-kart

At the time of working on this master thesis, QRTECH had not yet constructed their planned go-kart. However, during the spring of 2009 a group of undergraduate students at Chalmers Electric Power Engineering division were building an electric go-kart, as a part of their bachelor thesis. This go-kart was the starting point for our work. Parallel with this, another group of bachelor thesis students were working on an alternative motor control system for the go-kart, based on technology from QRTECH.

This chapter describes the go-kart build by the undergraduate students, but also the go-kart QRTECH is planning to build. Finally there is a description of the go-kart that was chosen to be modelled for this simulator. It contains components from both the Chalmers and the QRTECH go-karts.

10.1 The Chalmers go-kart

The built go-kart was in size of the national internal combustion engine go-kart class *Mini*. In this class the minimum allowed age is eleven, the minimum vehicle and driver weight is $115\,kg$. The allowed engine cylinder volume is $85\,cc$, and the top power about $8\,hp$, or about $5.9\,kW$. The reached top speed can be about 90 to $100\,km/h$, depending on the track shape.

The primary goal of the undergraduate project was simply to make a functional electrical go-kart, that is not necessarily an optimal designed driveline. Therefore the components were selected from a rather limited source of choices and one main supplier; ETP Kraftelektronik AB.

The go-kart chassis was made of a red steel pipe frame, and it was powered by a NiMH battery pack feeding an induction machine. The induction machine was connected to one of the back wheels via a chain gear. To make sure that the go-kart would be finalized within the time frame of the project, a ready combined converter and motor control system was chosen. Unfortunately this also meant that very few details were accessible regarding the design and structure of this control system. Furthermore, a simple gas pedal at the foot side was connected via a wire, to a gas pedal and a potentiometer system, which was translating this gas pedals' position to a control signal for the electric machine control system. There was also a simple brake pedal at the left foot side, directly connected to a disc brake. The go-kart can be seen in Figure 10.1.

Next follows a more detailed description of some of these components.

(a) Go-kart without battery packs. (b) Go-kart with battery packs.

Figure 10.1: The Chalmers undergraduate go-kart.

10.1.1 The NIMH battery

The battery system consists of eight modules of the NiMH, *Nilar Membrane Battery*, $24\,V$, $9\,Ah$, see Figure 10.2. They are connected two and two in series, forming four pairs. All four pairs are then coupled in parallel, and placed with two pairs on each side of the go-kart, inside a plastic box, see Figure 10.1(b).

Figure 10.2: One Nilar battery unit.

Parameter manufacturer data for one module, as well as for the whole battery pack can be seen in Table 10.1. The ratio of the power density over the energy density, $277\,(W/kg)/55\,(Wh/kg)$, is about 5, which is less than 10. According to the Nilar battery application manual, this battery is thus designed in favor of high energy storage capability, rather than high power deliverability.

During a constant current discharge, the terminal voltage is decreasing according to Figure 10.3. Higher discharge currents give rise to a larger voltage drop over the internal resistance, thus reducing the terminal voltage, thereby the different curves in the figure.

Table 10.1: Nilar battery data.

	One module		Total battery pack	
Nominal voltage	24	$V_{(d)}$	48	V
Rated capacity at C/20	9	$Ah_{(d)}$	36	Ah
Nominal current at 5C	45	$A_{(d)}$	180	A
Peak current at 10C for 10 sec.	90	$A_{(d)}$	360	A
Nominal power	1 080	$W_{(d)}$	8 640	W
Peak power	2 160	W	17 280	W
Energy content	216	$Wh_{(d)}$	1 728	Wh
DC resistance	100	$m\Omega_{(d)}$	50	$m\Omega$
Weight	3.9	$kg_{(d)}$	31.2	kg
Nominal power density	277	$W/kg_{(d)}$		
Energy density at C/20	55	$Wh/kg_{(d)}$		
Temperature range	-10 to 45	$°C_{(d)}$		

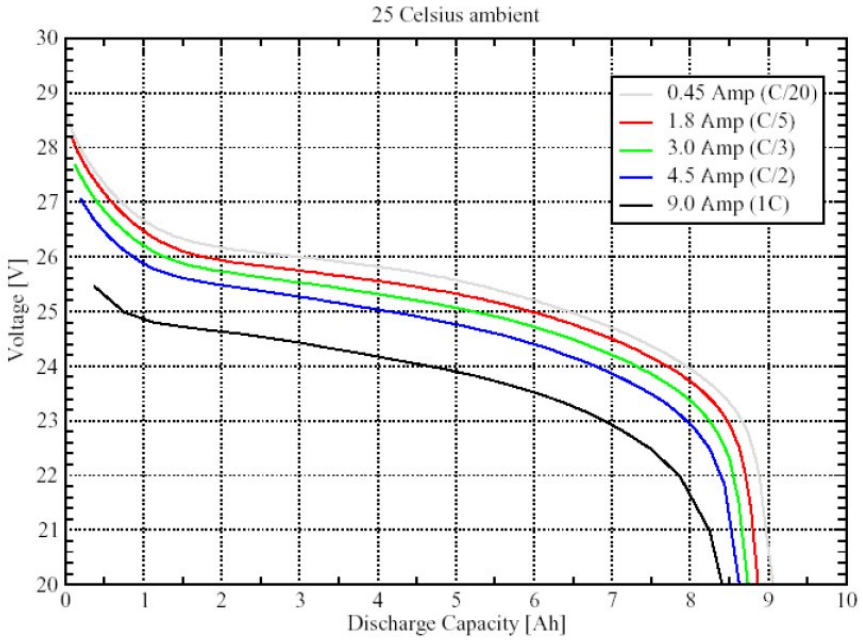

Figure 10.3: Terminal voltage dependence of different constant discharge currents, for one Nilar battery module, taken from the Nilar battery application manual.

In the application manual Nilar gives the following cell voltage levels for a NiMH battery; the nominal cell voltage $1.25\,V$, the fully charged cell $1.35 - 1.45\,V$ and the fully discharged cell $1.17\,V$. With 20 cells in each module that means module voltage levels of; nominal $25\,V$, fully charged $27 - 29\,V$ and fully discharged $23.4\,V$. However, through contact with Nilar it was understood that during discharge, the voltage level of each module should not go below about $22\,V$, depending on the load situation.

In the same time the individual cell voltages may differ somewhat from each other. That is, some cells may be closer to the lower voltage limit than others. Therefore, the battery should not be further discharged when the lower voltage limit is reached, or it may cause individual cell voltages to drop rapidly, and possibly cause the cell polarity

change. That would irreversibly reduce the energy storage capability of the battery, due to oxidation of the negative electrode.

During charge it is important not to overcharge the battery, or the aging will be accelerated, but most importantly the internal pressure may rise and cause the battery to become permanently damaged. There is a pressure vent on each unit, to ease the problem. Furthermore, higher charge current rates will cause higher temperature rises, and thus contribute to an accelerated aging. Nilar also claims in their battery application manual, that the charging efficiency is decreasing as the SOC passes 80 %. In the same time the internal pressure is increasing when going above 80 %.

Based on this information, the recommendation in the Nilar battery application manual, is that the battery should be kept within the SOC limits of 20 % to 80 % for best operation. It is also in this range of SOC that the internal resistance is at its lowest.

It is difficult to predict the cycle life of the battery, since it depends on the cycle depth, the charge and discharge rates and the environmental conditions in which the battery is operated. But according to Nilar a NiMH battery has a typical cycle life of about 500 to 1000. Nilar also declares that shallow cycles, for example with SOC between 50 % to 60 %, give longer cycle life.

More details regarding the operational recommendations and behavior of this battery, can be found in the Nilar battery application manual, which may be requested via the Nilar homepage; www.nilar.com.

10.1.2 The induction machine

The electric go-kart induction machine was delivered by ETP Kraftelektronik AB. Its weight was 19.2 kg. Furthermore it has the following name plate and electrical parameters:

Table 10.2: Name plate for the induction machine

AM173.0081 C.F.R. Modena Italy	
Watt	6000
V	3x27
Amp	168 IF
r.p.m.	2850
Hz	100
np (pole pair)	2

Table 10.3: Measured electrical parameters for the induction machine

AM173.0081 C.F.R. Modena Italy	
R_s	6.4 $m\Omega$
R_r	7.1 $m\Omega$
L_{sl}	22.371 μH
L_{rl}	22.371 μH
L_m	438.71 μH

10.1.3 Other components

The inverter and motor controller was a Zapi S.p.A. ACE-2 $36 - 48V$ transistor inverter, which was also delivered by ETP Kraftelektronik AB. This is thus a complete system, intended for control of battery fed electric working vehicles such as electric trucks. Little design information is given by Zapi in the user manual. Mostly it contains information regarding the operation of the device.

Together with the inverter a gas pedal system was also delivered from ETP Kraftelektronik AB. This system transforms the physical position of the wire from simple gas pedal, via a potentiometer, to control signals for the motor.

Between the induction motor shaft and the back wheel axle, there was a constant chain gear, with the gear ratio of 55/23 or 2.3913, that is the speed of the motor is about two times the vehicle wheel.

The tires are manufactured by Vega and the modell used was Cadetti 10x4.00-5, with a diameter of $252\,mm$.

10.2 The QRTECH go-kart

QRTECHs go-kart driveline is planned to have the same set up as the Chalmers go-kart, but with different components when it comes to the battery, inverter and motor controller and electrical machine. That is, QRTECH is planning to use a Li-ion battery, an inverter and motor control system designed by QRTECH and a synchronous three phase electrical motor. At the time of writing this thesis, the battery system and electrical machine had not yet been chosen. But a prototype inverter had been designed and manufactured as well as the control system hardware. The planned overall drive system can be seen in Figure 10.4. Details such as gas and brake system as well as the gear ratio was not yet worked out at the time of writing this thesis.

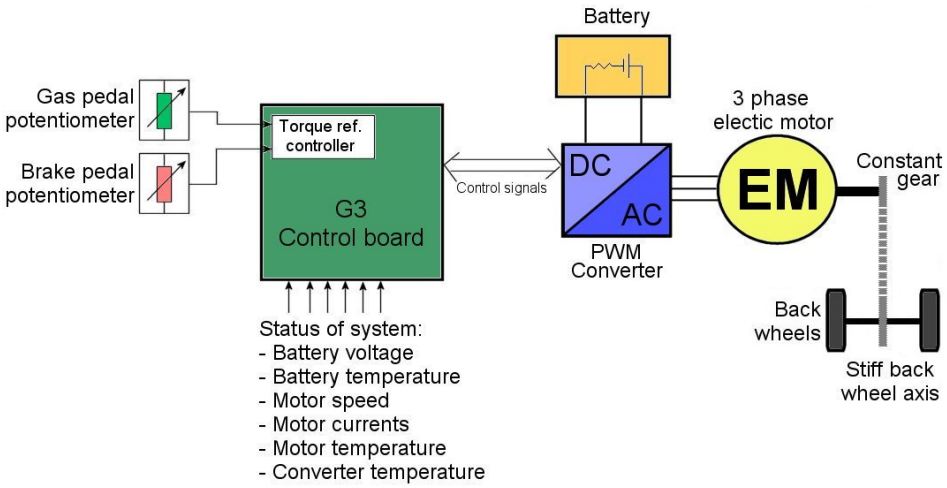

Figure 10.4: System overview of QRTECHs planned go-kart.

10.2.1 The inverter

The inverter is a four quadrant three phase PWM inverter, utilizing International Rectifier (IR) MOSFETs (HEXFET IRFS3107-7PPbF). Each phase leg has two switches, one upper and one lower, according to Figure 10.5, and each switch consists of five MOSFET transistors coupled in parallel. The MOSFETs internal parasitic diode functions as the switches' parallel diodes. Paralleling MOSFETs is no problem due to their positive temperature dependence. According to an application note from IR, paralleling the transistors will reduce the junction to case thermal resistance, and perhaps even the conduction losses. A small resistive value ($3.3\,\Omega$) at each transistor gate is added in order do reduce possible oscillations from parasitic impedances. Parallel to each of the five upper and lower transistor pairs, are two parallel coupled capacitors ($680\,\mu F$) for voltage stabilization. The switching frequency intended to be used is $15 - 20\,kHz$, to keep above the frequency range that is detectable by the human ear. The maximum current and voltage is about $1\,kA$ ($260\,A$ per transistor) and $60\,V$ respectively. The HEXFET operating temperature range is up to 175 °C, but according to a general MOSFET information the temperature should not pass about 90 °C, or the transistor performance and lifetime will be degraded.

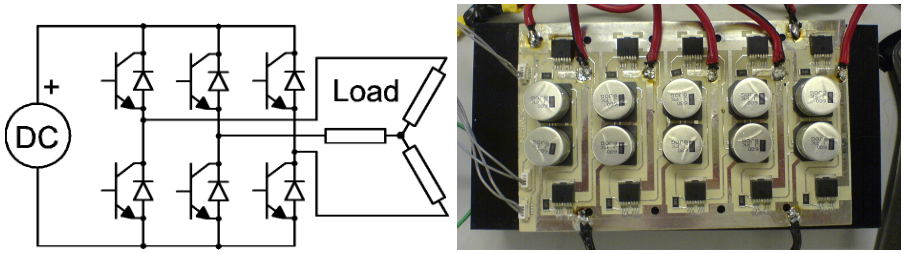

(a) A simplified schematic of QRTECHs prototype go-kart inverter, [41].

(b) One phase leg inverter and heat sink.

Figure 10.5: QRTECHs prototype inverter.

This inverter is realized as three separate pieces, one for each phase leg with ten transistors, five upper and five lower. The components are mounted on *Thermal Clad* circuit bords from the manufacturer The Bergquist Company. These substrates are designed to have a very effective thermal transport, and consist of three layers. The first layer is the *circuit layer*, which consist of a $140\,\mu m$ thin copper layer forming an application specific conduction pattern. The middle layer is an electrically isolating *dielectric layer*, made of a $75\,\mu m$ thin mix of polymers and ceramics. The bottom layer or *base layer*, is made of a $1.6\,mm$ thick aluminium plate.

Finally, each of the three inverter pieces are placed on a black anodised aluminium heat sink (SK 47/ 100/ SA), manufactured by Fischer Elektronik, see Figure 10.6.

More details regarding the inverter properties will be given in the next chapter, as the modelling of the inverter is presented. Then properties of the MOSFET transistors, and the dimensions and thermal parameters of the circuit boards, will come to use.

Figure 10.6: The heatsink for one inverter leg.

10.2.2 The control system

The control system of the go-kart will be made up of a control unit which will receive status information about e.g. motor currents, battery voltage and current, battery temperature, converter temperature, motor temperature, gas and brake pedal positions. The control unit will consist of QRTECH's G3 control board based on MPC5567. MPC5567 is a 32-bit PowerPC microcontroller, from Freescale Semiconductor's MPC55xx family, designed for engine management. The intention of the Simulink block *Controller GoKart* was not only to represent the control of the go-kart in the simulation environment, but also to be used to generate C code which could be downloaded on the control unit of the physical go-kart. C code can be generated from the Simulink model by the use of MATLAB's Real-Time Workshop.

10.3 The thesis work modeled go-kart

In order to construct the simulator it is in practise necessary to also have a model of a go-kart to at least make test runs. Since the QRTECH go-kart was not ready, and the Chalmers go-kart contained a "black box" inverter and control system, a mix of the two go-karts was chosen to be modeled. The base of the modeled go-kart was the Chalmers go-kart with its induction machine and NiMH battery pack. The modeled inverter and motor control is based on the inverter designed by QRTECH and the FreeScale implementation of vector control for an induction machine. Also the gear ratio was set to unity.

Chapter 11

Modelling and simulating the electric go-Kart

This chapter describes the structure of the simulator, and how the electric go-kart and a typical race were modeled. The level of complexity in the modelling depend both on the amount of available information about the object in question, but also on the desired resulting information from the simulation.

11.1 The simulator structure

Just like the simulator described in the previous part of this thesis, this simulator structure is based on the vehicle simulation tool; CAPsim, where the modeled vehicle driveline consist of interconnected component blocks in Simulink, representing physical components. There is also a block for a driver model. All the necessary kart and component parameters are to be declared in an associated MATLAB m-file, *GoKart_param.m*. In contrast to the previous simulator, this simulator is run by executing the go-kart Simulink model-file, *GoKart.mdl*, which in turn calls the m-file. The m-file also contain one time vector of the desired instantaneous vehicle speed during one lap of a race.

The top level in the Simulink modell consists of three subsystems, the *Environment*,the go-kart *Driver* and the go-kart *Vehicle*, see Figure 11.1. The environment block handles the speed vector. The driver model gets information regarding both desired and current vehicle speed and gives an order to the vehicle to either accelerate, decelerate or maintain current operation. The vehicle model thus contain all the physical component blocks representing the driveline, where the operation of each component is simulated in order to try to fulfill the wish of the driver. The next coming sections contain a more detailed description of the different blocks.

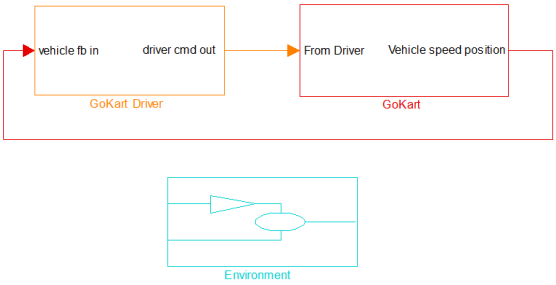

Figure 11.1: The top level in the go-kart simulator.

11.2 The m-file and the simulation vector

As mentioned, all the constants and parameters used in the modelling and simulation of the go-kart, are defined in the main m-file, *GoKart_param.m*, which is available in Appendix B. The parameter code structure is based on component block order. SI units are stated for all the parameters

The race simulation vector gives the go-kart reference speed as a function of time. The information is based on a measurement of one lap around a go-kart track in Göteborg made by an ICE go-kart, see Figure 11.2(a). It was received from a parallel master thesis project dealing with energy consumption of an electric go-kart. This lap is here assumed to represent a typical track profile, even though go-kart tracks more often than not are quite different from each other.

Since the speed in this one lap does not start from zero, a modified version of the time vector was made, see Figure 11.2(b). It has an initial speed of $0\,km/h$ followed by a $10\,s$ constant acceleration up to the current speed of the original time vector.

To simulate a whole go-kart race of about 10 *minutes* for the Mini class, the modified first lap was followed by twelve of the original laps, that is 13 laps in total, see Figure 11.3.

One lap is $969.4239\,m$ long, and takes $48.778\,s$. That makes the whole race $12\,602.5107\,m$ and $634.114\,s$.

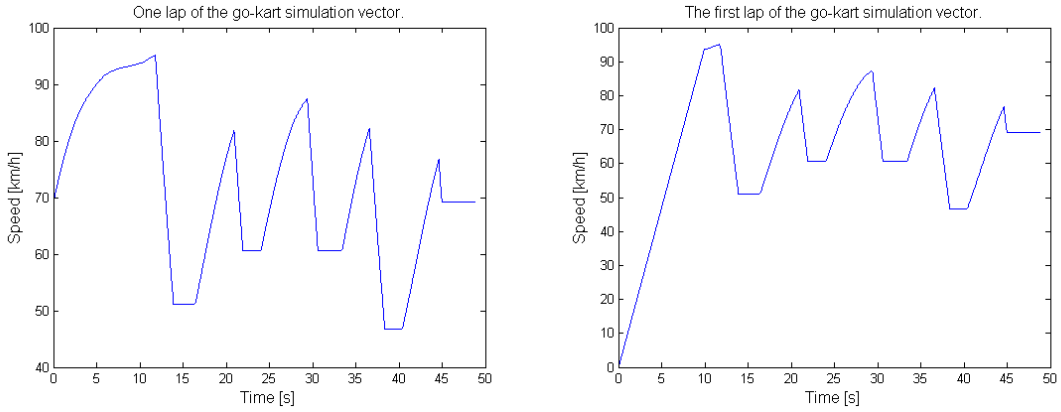

(a) One lap.

(b) The first lap.

Figure 11.2: Go-kart reference speed as a function of race time.

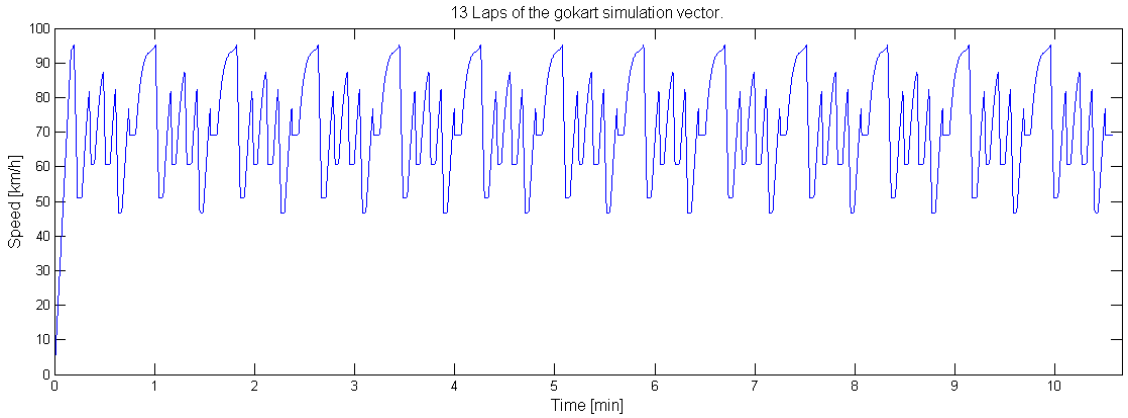

Figure 11.3: Race simulation vector, showing the modelling of thirteen laps.

11.3 The environment model

The environment block contains a simulation clock, which is representing the race time in seconds, see Figure 11.4. The vector over desired instantaneous speed (m/s) is available in the look-up table *speed-ref* as a function of time. Then the information about time is input signal to the look-up table which then sends information about current reference speed via the Goto-block *drivecycle* to the driver model.

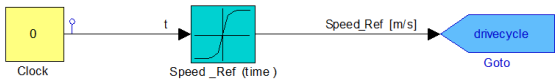

Figure 11.4: The environment model in the Go-kart simulator.

11.4 The driver model

The driver model receives information about the current reference speed and the instantaneous vehicle speed, see Figure 11.5. To maintain the reference speed, the driver is modeled as a PI-controller with the speed error as an input, see equation (5.2) and Figure 11.6. The values of the controller parameters, K_i and K_p, are chosen to give a control signal value between -1 and 1. To keep the integrator from growing too large, a suitable upper limitation (20) is added. The PI-controller output has a saturation block that keeps the signal between -1 and 1. The positive part of this signal symbolizes the position of the gas pedal, and the negative part symbolizes the position of the brake pedal. Therefore the signal is split up in a positive and a negative part before it is sent to the go-kart control system block, where it is scaled to represent physical torque signals in the vehicle, see section 11.5.1.

Finally the driver model block also contains some *Scopes* for overlooking a few vehicle performance parameters as functions of time, see Figure 11.5, such as speed and acceleration.

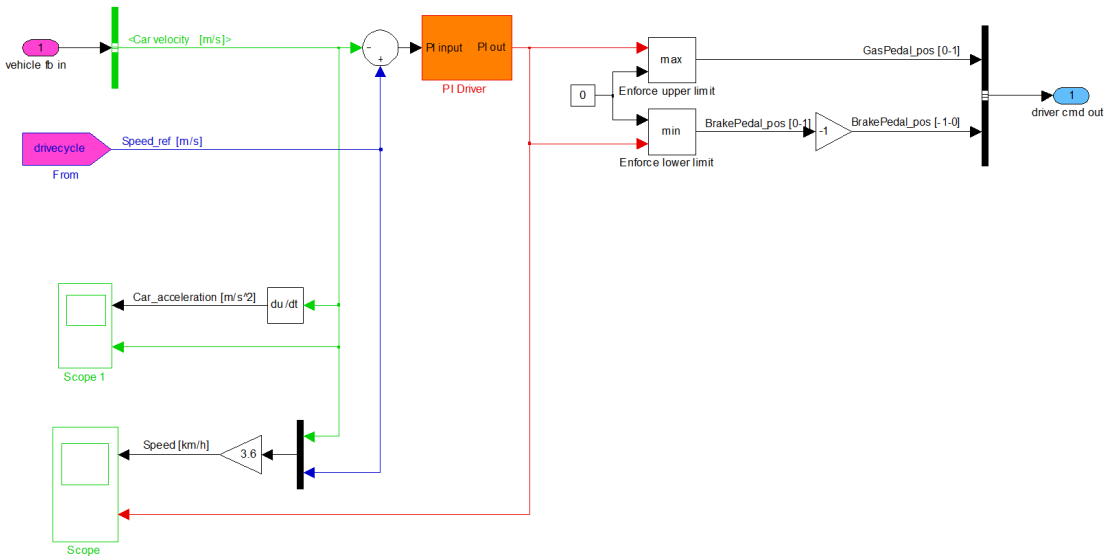

Figure 11.5: The go-kart driver model in the go-kart simulator.

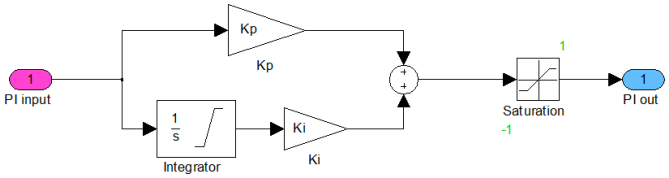

Figure 11.6: The go-kart driver PI-controller model.

11.5 The electric go-kart model

The vehicle model contains a *controller block*, which serve as a transition between the driver and the *component blocks* below. As mentioned earlier, the component blocks represent the physical components in the go-kart driveline, starting from the bottom left with the primary energy storage; the battey, followed by the DC/AC inverter, the AC tractive motor and its control system, the chain gear between the AC motor and the go-kart wheel, and finally the *chassis block*. In the chassis block the tractive force from the driveline is balanced towards the resistive forces acting on the go-kart.

The signals between the blocks represent physical values, such as; torque, speed, voltage and current. For each block the input and output powers are found via cross referencing the input and output signals.

The operating point of each component is depending on the adjacent component through the forward and backward fed signals. This may sometimes cause the problem of *algebraic loops*. Then the calculation of the next value of a signal depend on the very same value of the signal itself. To get around this, Simulink *memory blocks* have been used when necessary throughout the simulator. Then the previous signal value is instead used to calculate the next value of the same signal. This may introduce a small error, or even an instability, in the simulation, which is here assumed to be negligible.

Next follows a more detailed description of each component block in the go-kart model.

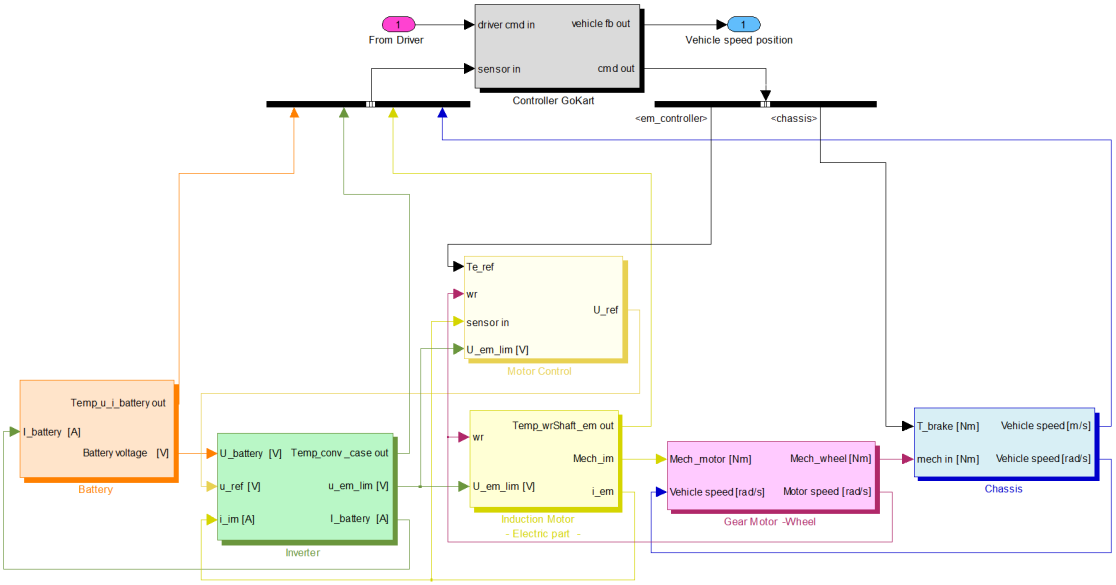

Figure 11.7: The go-kart vehicle model in the go-kart simulator.

11.5.1 Controller

The controller block, see Figure 11.8, is intended for torque reference control of the electric go-kart with the possibility to limit or even to set the torque reference to zero when needed. Such a situation can arise if, for example, the battery voltage and/or the SOC is too high or too low. The torque reference will then be set to zero to protect the battery from e.g. getting shorter cycle life in the case of too low SOC. However, this situation should normally not be occurring if the battery is dimensioned properly.

As mentioned earlier in the report, the components in the driveline are non-ideal and with that generate heat. If the temperature in the converter, the motor or the battery would rise too high the torque will be limited by the PI-regulators to lower the temperature to acceptable levels.

Another function is the possibility to limit the maximal permissible motor speed, a function which could be interesting if the same go-kart will be driven in different competition classes or by children.

The values of the regulator parameters, K_p and K_i, are not obvious but need to be tuned when the go-kart is built. A large value of the proportional gain, K_p, normally means a fast response but a too large value would lead to oscillations and instability. A larger value of the integral gain, K_i, implies a quicker elimination of the steady-state error at the cost of higher overshoots. Estimation of the regulator parameters was not done since the go-kart was not finalized at the time of the writing this thesis, at present the parameter values are set to one.

For future work the intention is to generate C-code from this particular block in the Simulink model and then implement it in the physical go-kart. Such a generation can be made by the use of Real-Time Workshop.

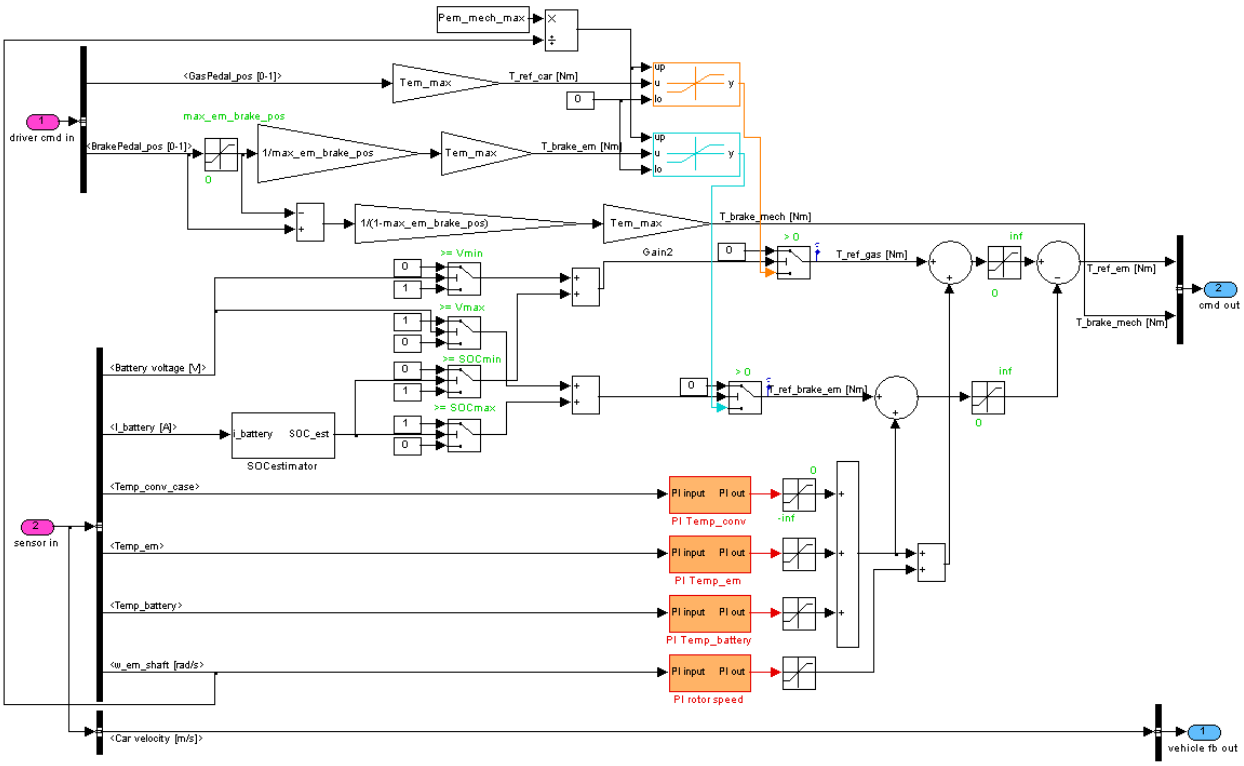

Figure 11.8: Block diagram model of the torque reference control block.

The *driver cmd in* input block receives information from the driver block about the positions of the gas and brake pedals. The position of the gas pedal, which is a value between zero and one is multiplied by the maximum torque, *Tem_max*, that can be produced by the electric motor. The position signal of the brake pedal first needs to pass a saturation block which only let signals between zero and *max_em_brake_pos* through. If the constant is set to e.g. 0.25 that would signify that as long as the brake pedal only is pushed at maximum 25 % of the maximum possible then the electric motor alone can provide all the needed braking torque and hence the mechanical brakes are not needed.

The signal is now scaled to be a value between zero and one and is then multiplied with *Tem_max*. *T_ref_car* and *T_brake_em* then enter a saturation dynamic block each which makes sure that the torque reference value does not exceeds the maximum torque that can be produced by the electric machine when operating in field-weakening. If the brake pedal is pushed more than 25 % of the maximum possible then the excess above the 25 % will result in a mechanical braking torque.

Note that the constant *Tem_max* is used in this case too, however the maximum possible mechanical braking torque has nothing to do with the maximum torque that can be produced by the electric machine.

The *sensor in* input block receives information from the battery, the inverter, the induction motor and the chassis of the go-kart about battery voltage, battery current, temperature of the inverter case, electric machine and the battery and from the chassis the rotational speed of the electric machine and the speed of the go-kart are given.

The battery voltage is sent to two switches which send out the value one if the battery voltage either exceeds or is below the maximum or minimum allowed. The battery current is sent to the *SOC estimator* block which calculates the corresponding SOC, more infor-

mation about the SOC estimator is given later. The estimated SOC is also sent to two switches which send out the value one if the SOC either exceeds or is below the maximum or minimum allowed.

The values being sent from the switches checking that the battery voltage and the SOC does not drop too low is added and if the sum is larger than zero then the torque reference, T_ref_gas, is set to zero. On the other hand, if the sum is zero then the reference torque corresponding to the position of the gas pedal is being sent further.

The values being sent from the switches checking that the battery voltage and the SOC does not exceed its maximum allowed are added and if the sum is larger than zero then the braking torque reference is set to zero. In the case of this situation it will not risk the safety, it only implies that the mechanical brakes need to work harder. If the sum is zero the braking reference torque corresponding to the position of the brake pedal is being sent further.

The temperatures in the inverter case, the electric machine and the battery and the rotational speed of the electric machine are each being sent to a PI-regulator, the function of the PI-regulator blocks will be described later. The possible negative torques that are sent out from the first three PI-regulators are being added and then added to $T\_ref\_brake\_em$. The summation of the negative torques from all four PI-regulators are added to T_ref_gas. These two actions result in the driving reference torque and the braking reference torque to be decreased when necessary.

Finally, $T\_ref\_brake\_em$ is drawn from T_ref_gas resulting in T_ref_em where the sign of the torque decides if the electric machine is operating as a motor or as a generator. The output signals are then the reference torque which is sent to the controller of the electric machine and the necessary mechanical braking torque which is sent to the chassis. The speed of the go-kart is just being sent right through to the GoKart Driver.

11.5.1.1 SOC estimator

The SOC estimator block diagram is shown in Figure 11.9.

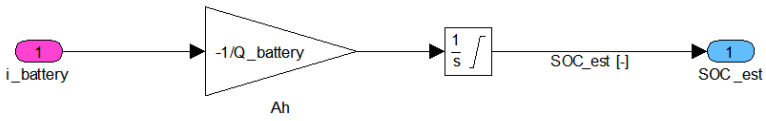

Figure 11.9: Block diagram model of the SOC estimator block.

The input signal, the battery current is multiplied by minus one and divided by the capacity of the battery, $Q\_battery$. Integrating the result gives the estimated SOC, SOC_est, which is the output signal. The integrator has an initial condition, $SOCinit$, which is the initial state of charge of the battery. The SOC estimator can be derived from equation 2.15.

11.5.1.2 PI-regulator

Figure 11.9 shows the function of the PI-regulators.

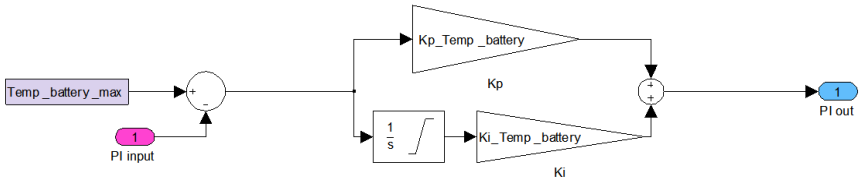

Figure 11.10: Block diagram model of one of the PI-regulators.

The input signal, which in this case is the temperature of the battery, is drawn from a constant, which in this case is the maximum permissible temperature in the battery. This gives an error which the PI-regulator tries to compensate for. However, it is not desired that the PI-regulator affects the torque references when the error is positive, this is worked out by letting the output values from the PI-regulator pass a saturation block only letting values between zero and negative infinitive through.

11.5.2 Battery

The battery model is based on the simple circuit in Figure 2.17(a), with an SOC dependent open circuit voltage source (OCV) and a constant internal resistance, see Figure 11.11. The SOC is calculated using equation 2.15, where SOC_{init} is the initial SOC level which is set in the m-file, Q_{tot} is the battery capacity of 36 Ah, and $i(t)$ is the battery current and also the input signal to the battery block. The OCV dependence of SOC is implemented as a look-up-table based on the discharge characteristics given in Figure 10.3. The output signal of the battery block is the positive result of the OCV voltage minus the IR voltage drop over the internal resistance. The battery temperature development is not modeled, but represented as a constant value, and thus plays no role in the simulation.

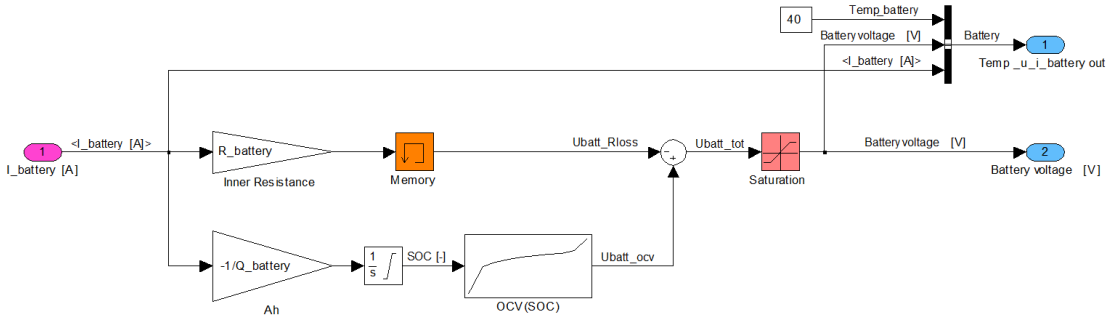

Figure 11.11: The go-kart battery model.

To find the OCV dependence of the SOC, eleven points were used on the $0.45\,A$ $(C/20)$ discharge characteristics in Figure 10.3. The x-axis was transformed to values of SOC by assuming that 100 % equates a charge of $9.05\,Ah$. Then the internal voltage drop was compensated for by adding $0.045\,V$ $(0.45\,A * 0.1\,\Omega)$ to each point. Finally all values were multiplied by two to represent the whole battery pack. The result can be seen in Figure 11.12.

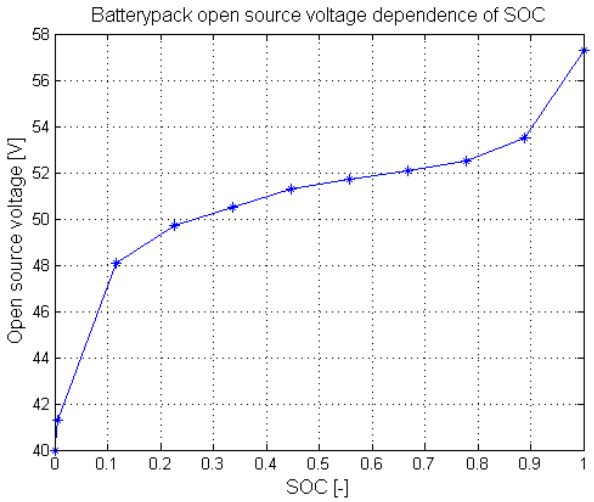

Figure 11.12: The go-kart battery pack open source voltage dependence of SOC.

11.5.3 Inverter

The main functions of the inverter block, see Figure 11.13, are to limit the inverter output voltage in order not to exceed the available battery voltage, to calculate the inverter temperature development, to calculate and then subtract the inverter losses from the power transport between battery and motor, and to calculate the drawn battery current.

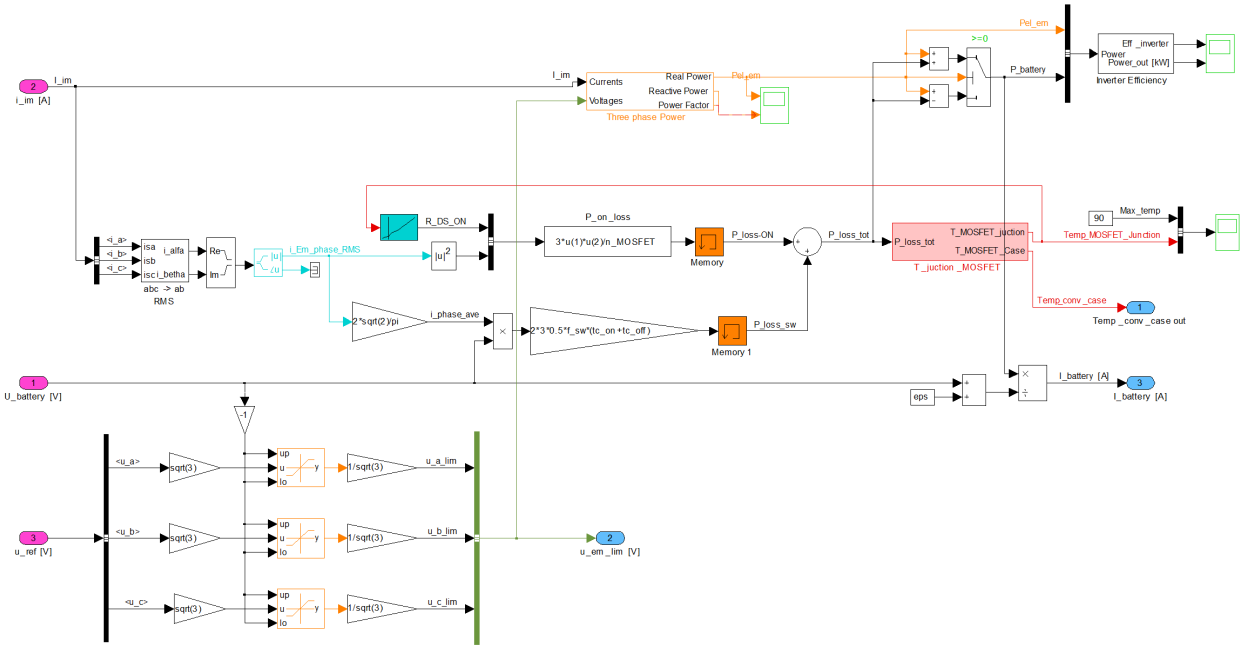

Figure 11.13: The go-kart inverter model.

Naturally the inverter output voltage can not be of larger magnitude than that of the available battery voltage. As can be seen in Figure 10.5(a) the line to line voltage of the load, i.e. the three phase AC induction motor, is equal to the battery voltage. Therefore the input containing the motor phase voltages are first scaled up to the magnitude of the line to line voltages, whereby all three phases are limited one by one, before they are scaled

down to phase voltage magnitudes again. The limited phase voltages are then one of the inverter block outputs and they are sent to feed the induction machine.

The instantaneous three phase active, $P(t)$, and reactive, $Q(t)$, induction machine power is calculated in the subblock seen in Figure 11.14, according to equation 11.1 and 11.2, where $v_{a,b,c}(t)$ and $i_{a,b,c}(t)$ are the instantaneous three phase motor voltages and currents respectively. Also the power factor, $PF(t)$, is calculated according to equation 11.3.

$$P(t) = v_a(t)i_a(t) + v_b(t)i_b(t) + v_c(t)i_c(t) \tag{11.1}$$

$$Q(t) = \frac{1}{\sqrt{3}}\Big[v_a(t)\Big(i_c(t) - i_b(t)\Big) + v_b(t)\Big(i_a(t) - i_c(t)\Big) + v_c(t)\Big(i_b(t) - i_a(t)\Big)\Big] \tag{11.2}$$

$$PF(t) = \cos\Big(\arctan\left(\frac{Q(t)}{P(t)}\right)\Big) \tag{11.3}$$

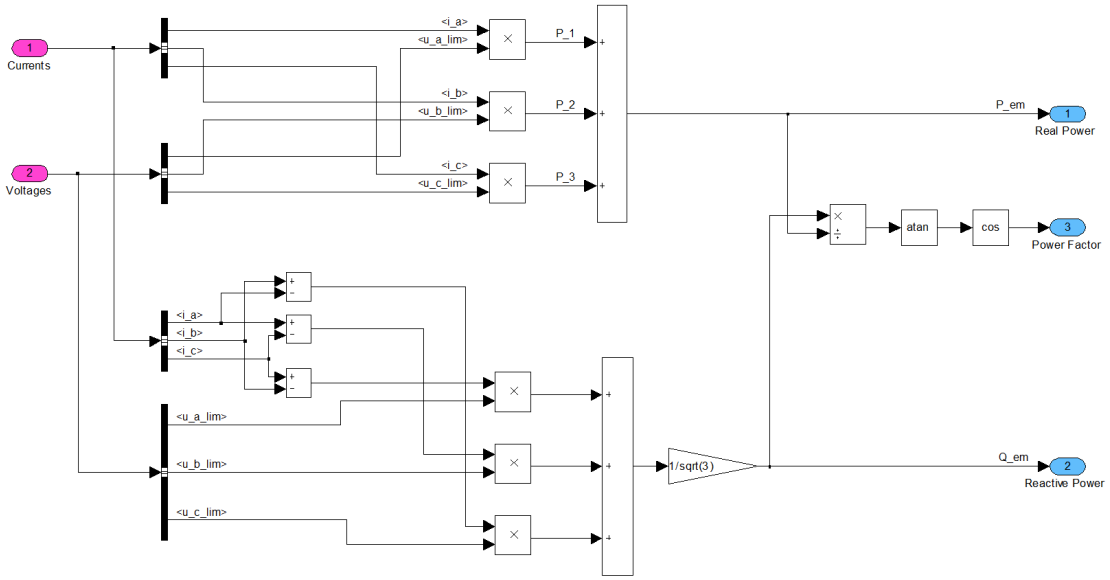

Figure 11.14: The calculation of the three phase real and imaginary power, as well as the power factor.

The inverter efficiency is simply calculated by dividing the motor power by the battery power. This result is naturally not valid during regenerative braking. However the efficiency is assumed to be about the same in the two cases, which is why it is not calculated during regenerative braking.

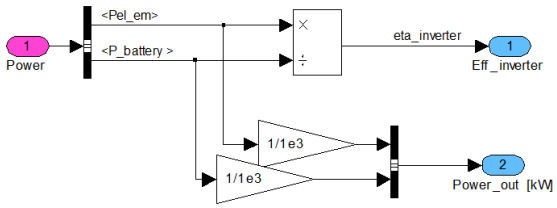

Figure 11.15: The inverter efficiency calculation.

The last output, the battery current, is calculated by dividing the battery power by the battery voltage, where the battery power is assumed to be the sum of the motor power and the inverter power losses. During regenerative braking the battery power is the motor power minus the inverter losses.

11.5.3.1 Inverter losses

Both the inverter on-state or conduction losses and the switching losses are calculated by using the information in chapter 2.3.4. To simplify the simulations the inverter was not modeled on switching level, which is why the loss calculation was simplified as well.

During real operation of the inverter, the two switches on each leg takes turn in conducting the current. There is also a short time duration, called *blanking time*, in between these turns when neither switch is conducting. This is to make sure the other switch have enough time to stop conducting before the next one starts to conduct. If both switches would be conducting at the same time, the battery would be short circuited. However, to simplify the simulations no care has been taken to this blanking time, but it is assumed that at all times, either one of the switches on each leg is conducting.

On-state losses

The on-state losses are simply calculated as a resistive power development, RI^2, one for each leg or phase, with the total drain-source resistance per switch, and the motor rms phase current. With five transistors per switch, the total on-state resistance is the transistor $R_{DS_{on}}$ divided by five. Even the temperature dependence of the on-state resistance is modeled, see section 11.5.3.2. The rms phase current can be found by transforming the phase currents to the alpha-beta reference frame, using rms value scaling, see Figure 11.16. Then the magnitude of the complex alpha-beta-vector equals the rms value of the phase current.

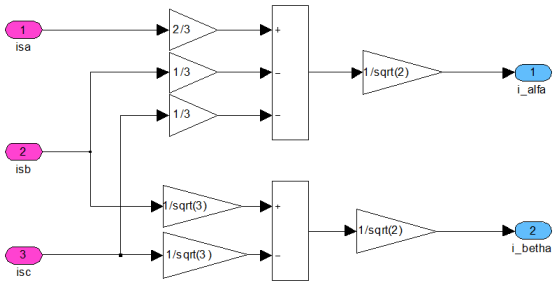

Figure 11.16: The transformation from three phase to alpha-beta in RMS value scaling.

Switching losses

The switching losses are calculated using equation 2.18, where V_d is the battery terminal voltage, I_o is the mean value of the phase current over one period of the current, f_s is the switching frequency, and $t_{c(on)}$ and $t_{c(off)}$ are transistor turn on and turn off times respectively.

The mean value of a sinusoidal signal of arbitrary frequency can be described as the rms value times the form factor $\frac{2\sqrt{2}}{\pi}$. This factor is multiplied with the rms phase current to find the mean value of the phase current.

The switching frequency was set to $20\,kHz$, which is the higher value in the thought range, to serve as a "worst case".

The transistor turn on and off times are not explicitly declared in the transistor data

sheet, at least not in compliance with the parameters for turn on and turn off times in Figure 2.22. For example there is no information regarding the rise and fall times of the drain current. However, there is information about the rise and fall times of the drain source and the gate source voltages, see Figure 11.17. Based on this information, the transistor turn on and off times are assumed to be two times t_r and t_f respectively, to serve as a "worst case", since the external gate resistors most probably will add to these times.

Finally the expression is multiplied by three since there are three legs, and by two since there are two switches per leg and the losses occur in each switch.

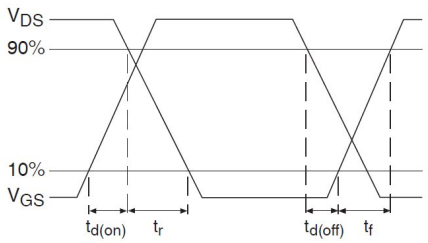

Figure 11.17: Switching waveforms of the used inverter transistor.

11.5.3.2 Inverter temperature model

In an application like this, with occasional large power demanding accelerations, the component temperature development may become quite large. It is therefore interesting to simulate the inverters transistor junction temperature, to get an indication wether the heat transport of the inverter is sufficient or not. This is done by modeling the inverter transient thermal behavior, see section 2.4.3.1.

In reality it is difficult to measure the junction temperature during operation of the inverter, but rather the transistor case temperature is measured. Therefore also the case temperature is modeled and the information is sent to the go-kart controller block.

Only one leg of the inverter is modeled. Since several transistors are mounted on the same circuit board, it is not enough to only consider one transistor, but all ten must be included.

In this section follows a description of how the inverter components were thermally modeled and how these models were put together to represent the whole inverter. All components are modeled according to the Cauer network, see section 2.4.3.1, since real material data were used in the modelling. It is also assumed that the whole power loss in the transistor dissipates as heat, and is transported from the HEXFET junction to the ambient air purely through the circuit board and the heatsink without any leakage to sides.

HEXFET thermal model

It is desirable to model a HEXFET as only one value for the thermal resistance and one for the thermal capacity. This simplifies the calculation of the equivalent thermal impedance for all the ten transistors, which will then be $C_{th_{tot}} = 10C$ and $R_{th_{tot}} = R/10$, since they are parallel coupled. Therefore it would be preferable to find a more simple representation of the thermal behavior of the transistor instead of using the suggested 8-parameter model in the data sheet from the manufacturer IR, see Figure 11.18.

By utilizing the fact that after one time constant a step response has reached about 63 % of its final value, a rough estimation of the transistors total time constant can be found. This can be done using the diagram for the single pulse measurement of the transient

thermal impedance, depicted in the transistors data sheet, see Figure 11.18. The step response final value is the total junction to case thermal resistance, $R_{th_{JC}} = 0.4022\,K/W$, which makes the 63 % value equal to $0.2534\,\Omega$. Thus the time constant, τ_{th}, is estimated to be about $7\,ms$, which is where most of the measurements cross the 63 % value. Then the thermal capacity can be calculated as the ratio of the time constant and the thermal resistance, $C_{th} = \tau_{th}/R_{th} = 0.0174\,J/K$.

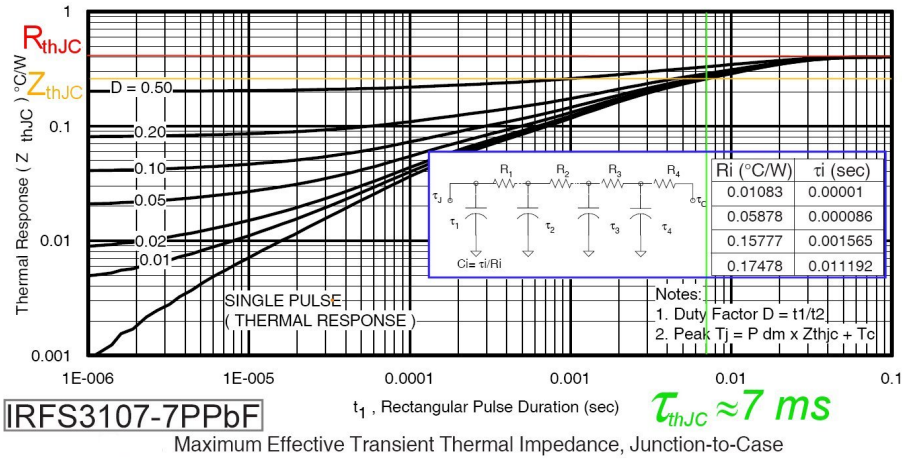

Figure 11.18: Thermal behavior of the HEXFET according to the IR data sheet.

The above described assumption, was also compared with the 8-parameter model in the data sheet, calculating the equivalent impedance in two different ways. One called *sum*, where the parallel equivalent is calculated for each of the four RC couples and then summed up. And the other one called *parallel and series*, where the total equivalent impedance is calculated like an electrical circuit, by paralleling the forth right RC pair, and then put them in series with R_3, and so on. Finally the three different calculation methods were compared, see Figure11.19. Since the step response of the first assumption reaches the final value sooner than the others, this is chosen to represent the thermal behavior of one HEXFET, to serve as a "worst case".

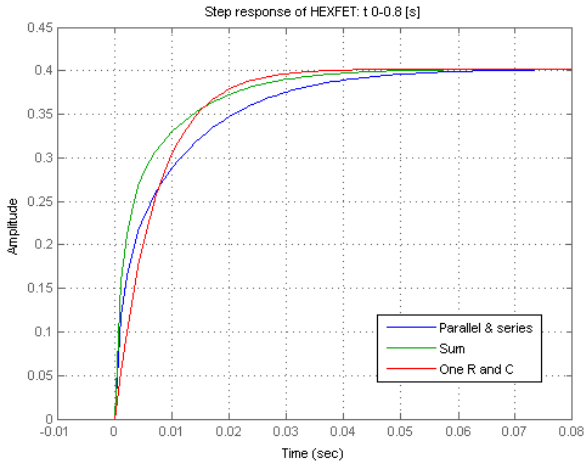

Figure 11.19: Comparison of step responses for different thermal calculations.

Circuit board thermal model

The circuit board consist of three different layers; an aluminium, a dielectric and a current conducting copper layer. Each layer can be thermally represented by a thermal resistance in parallel with a thermal capacity, except for the dielectric layer which is chosen to only be represented by a thermal resistance, since the capacity was negligibly small. Then the two RC circuits are series connected with the single resistance in between.

The base plate is $100 \times 160\,mm$, which is also the size of the dielectric and aluminium layers. The copper layer is only partly covering the surface, see the metallic material in Figure 10.5(b). The copper surface area is approximated by rough measurements.

As declared in section 2.4.2, the thermal resistance $R_{th}\,(K/W)$ of a material is dictated by the path length of the transported heat which in this case means its thickness $d\,(m)$, the materials thermal conductivity $\lambda\,(W/mK)$ and its cross sectional area $A\,(m^2)$. These parameters and the final values for all three layers are presented in Table 10.1.

Table 11.1: Thermal resistance parameters of the circuit board.

	Copper	**Dielectric**	**Aluminium**
$d\,(\mu m)$	140	75	1574.8
$\lambda\,(W/mK)$	380	2.2	150
$A\,(mm^2)$	8 324.75	16 000	16 000
$R_{th}\,(K/W)$	$4.43 \cdot 10^{-5}$	$2.13 \cdot 10^{-3}$	$6.56 \cdot 10^{-4}$

The thermal capacity $C_{th}\,(J/K)$ is calculated using the copper and aluminium thermal capacity per unit mass $C_m\,(J/kgK)$, their volumes $d \times A\,(mm^2)$ and their densities $\rho\,(kg/m^3)$. The found parameters are presented in Table 11.2.

Table 11.2: Thermal capacity parameters of the circuit board.

	Copper	**Aluminium**
$C_m\,(J/kgK)$	380	1 256
$\rho\,(kg/m^3)$	$8.958 \cdot 10^3$	$2.71 \cdot 10^3$
$d\,(\mu m)$	140	1574.8
$A\,(mm^2)$	8 324.75	16 000
$C_{th}\,(K/W)$	3.97	95.20

Heatsink thermal model

According to Elfa who is the heat sink retailer, the thermal resistance is 0.7 (K/W). The thermal capacity is calculated using the aluminium heat capacity per unit of mass times the mass. That is, $C_{th(Al)} = 896(J/kgK) \cdot 1.071(kg) = 959.62(J/K)$.

Implementing the thermal model

At this point all the necessary thermal parameters for making a thermal model of the inverter, are found. As mentioned an equivalent R and C have been found for the ten transistors that are coupled in parallel. The transistor RC-network is then coupled in series with the RC-R-RC-network of the circuit board, which in turn is coupled in series with the heatsink RC-network, see Figure 11.20.

The complete RC-network of the modelled inverter leg is then implemented in the m-file as a laplace transfer function, receiving one third of the calculated power loss, see Figure 11.21. The equivalent transfer function is calculated much like an equivalent electrical circuit; paralleling the heatsink RC, in series with the aluminium R and then paralleling

the result with the aluminium C, adding the result to the dielectric and copper R's, paralleling it with the copper C, in series with the total transistor R and finally in parallel with the total transistor C.

Also the case temperature is calculated using the same method, but without adding the RC-network of the transistors.

The ambient temperature is set to 25 °C.

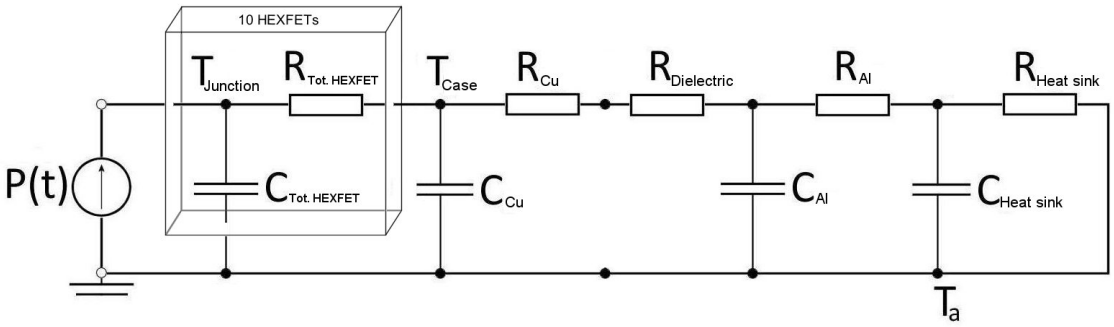

Figure 11.20: Thermal model of one leg of the inverter.

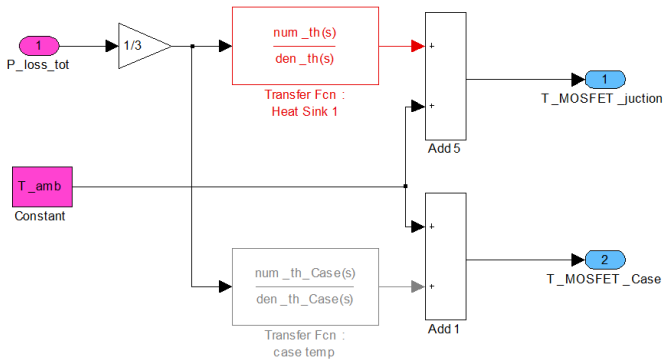

Figure 11.21: The calculation of the inverter junction temperature.

On-state resistance thermal model

The real on-state resistance is increasing with increasing junction temperature. Therefore it is modeled to be temperature dependent, see Figure 11.22. The red point marks the 25 °Cvalue, 2.1 $m\Omega$, which is the base of the normalization.

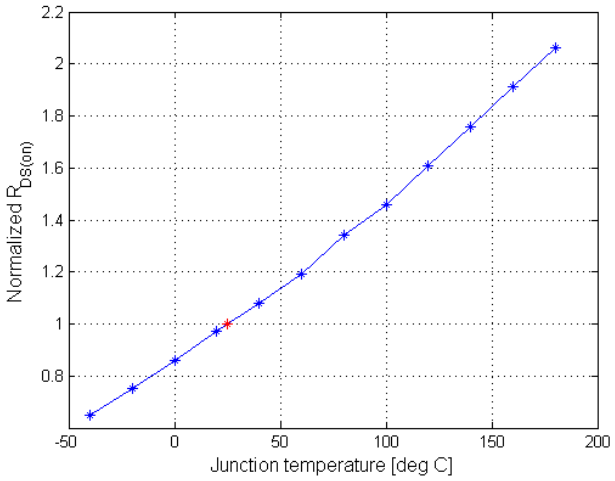

Figure 11.22: The implemented transistor on-state drain source resistance dependence of the junction temperature according to the HEXFET data sheet. The red point marks the 25 ℃value, 2.1 $m\Omega$, which is the base of the normalization.

11.5.4 Induction machine

A model representing the induction machine, see Figure 11.23, used in the Chalmers go-kart was first created. However, during the progress QRTECH realized that a PMSM would be preferable.

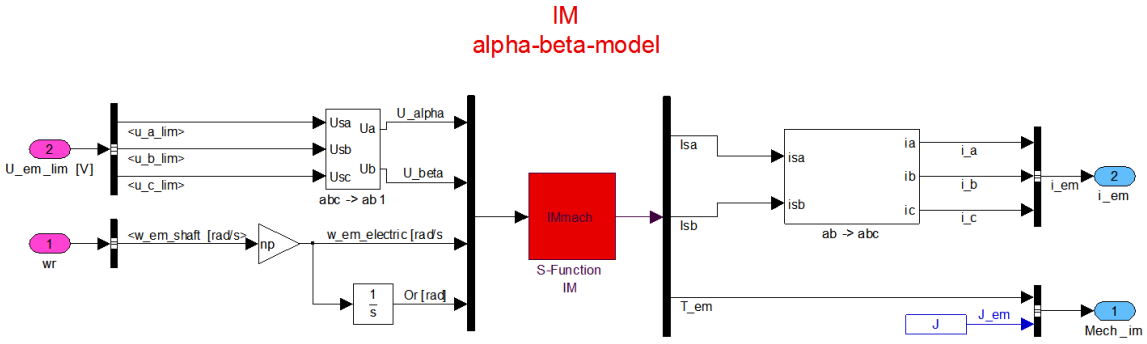

Figure 11.23: Block diagram model of the induction machine.

The desired three-phase voltages of the induction machine is sent from the inverter to the induction machine as the input signal, U_em_lim. The second input signal is the motor speed, wr, which is sent from the gear block. The three-phase voltages are transformed into equivalent two-phase voltages in $\alpha\beta$-coordinates. The motor speed is transformed into the equivalent electrical speed by the multiplication of the pole-pair number, np, and by integrating the electrical speed the rotor position is obtained.

The induction machine itself is modeled as an S-function, which is a computer language describing a Simulink block. The S-function is derived from the state-space representation of the dynamic T-equivalent model of the induction machine in $\alpha\beta$-coordinates. The state-space representation is derived from the general state-space equation:

$$\dot{\mathbb{X}} = A\mathbb{X} + B\mathbb{U}, \tag{11.4}$$

where

$$\mathbb{X} = \begin{bmatrix} i_{s\alpha} \\ i_{s\beta} \\ i_{r\alpha} \\ i_{r\beta} \end{bmatrix} \tag{11.5}$$

is the state vector and

$$\mathbb{U} = \begin{bmatrix} u_{s\alpha} \\ u_{s\beta} \\ 0 \\ 0 \end{bmatrix} \tag{11.6}$$

is the input vector.

$$U = \underbrace{\begin{bmatrix} L_s & 0 & L_m & 0 \\ 0 & L_s & 0 & L_m \\ L_m & 0 & L_r & 0 \\ 0 & L_m & 0 & L_r \end{bmatrix}}_{\text{Lmat}} \begin{bmatrix} \dot{i}_{s\alpha} \\ \dot{i}_{s\beta} \\ \dot{i}_{r\alpha} \\ \dot{i}_{r\beta} \end{bmatrix} + \underbrace{\begin{bmatrix} R_s & 0 & 0 & 0 \\ 0 & R_s & 0 & 0 \\ 0 & \omega_r L_m & R_r & \omega_r L_r \\ -\omega_r L_m & 0 & -\omega_r L_r & R_r \end{bmatrix}}_{\text{Rmat}} \begin{bmatrix} i_{s\alpha} \\ i_{s\beta} \\ i_{r\alpha} \\ i_{r\beta} \end{bmatrix} \tag{11.7}$$

$$\dot{\mathbb{X}} = \underbrace{-L^{-1}R}_{\text{Amat}}\mathbb{X} + \underbrace{L^{-1}}_{\text{Bmat}}\mathbb{U} \tag{11.8}$$

Output signals from the induction machine block are the three phase currents, which have been transformed from two-phase currents in the $\alpha\beta$-coordinates, the induction machine torque and inertia.

11.5.4.1 Induction machine controller

The next block to be considered is the block controlling the induction machine, see Figure 11.24. The block contains several sub-blocks, such as; current reference calculation, flux estimation and current controller. The vector control of the induction machine in the model is imitating Freescale's vector control drive based on Freescale's PowerPC MPC5500 microprocessor, which will be used in the physical go-kart.

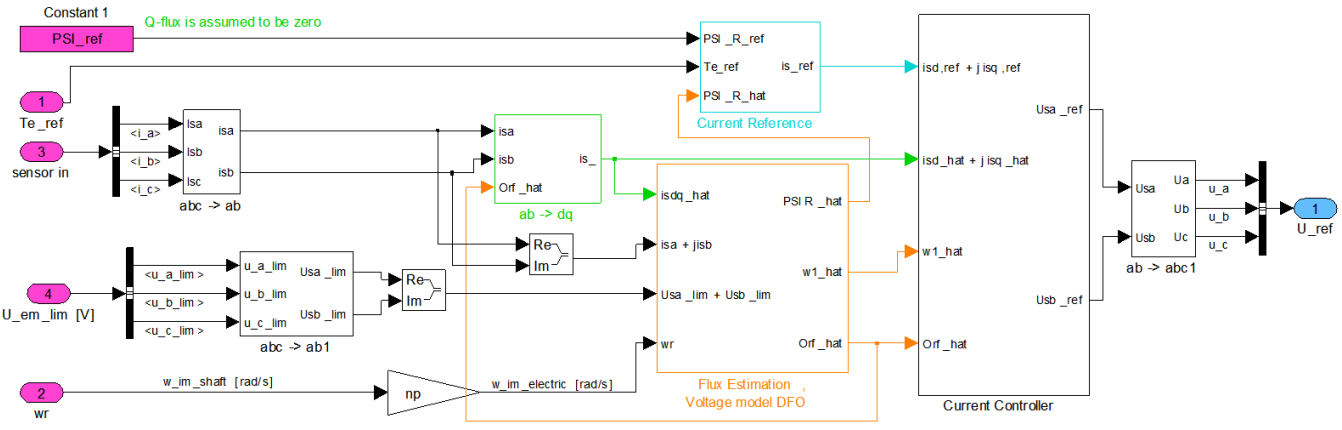

Figure 11.24

The controller block receives information about the torque reference, *Te_ref*, representing the positions of the gas and brake pedals. The induction machine's three phase currents and the desired three phase voltages of the induction machine are input signals from the induction motor and the inverter, respectively. The motor speed is also an input signal coming from the gear block.

The torque reference is sent to the Current Reference block, where a corresponding stator reference current is calculated and sent to the Current Controller block. The three phase currents are transformed to two phase currents in $\alpha\beta$-coordinates and then further transformed into dq-coordinates and sent to the Flux Estimation block. The three phase voltages are also transformed into their equivalent two-phase voltages in $\alpha\beta$-coordinates and sent to the Flux Estimation block. The motor speed is transformed into the corresponding electrical speed by multiplication of np and then sent to the Current Controller block.

Rotor flux estimation

The rotor flux estimation model, see Figure 11.25, is a voltage model with direct field orientation, DFO. The voltage model uses stator equations and DFO means that the rotor flux position is estimated from quantities in the $\alpha\beta$-system.

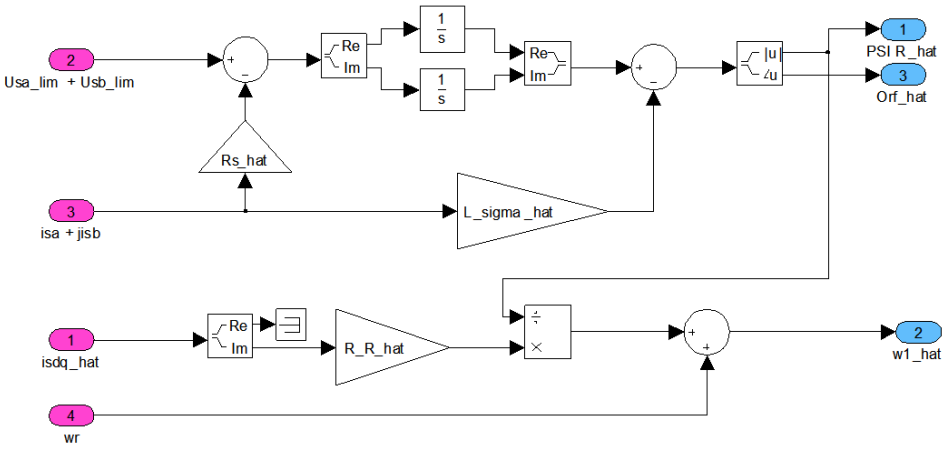

Figure 11.25: Flux estimation block. Voltage model, DFO.

The structure of the flux estimation block originates from the following equations:

$$\hat{\underline{\Psi}}_R^s = \int (\underline{u}_s^s - \hat{R}_s \underline{i}_s^s) dt - \hat{L}_\sigma \underline{i}_s^s \tag{11.9}$$

and

$$\hat{\omega}_1 = \omega_r + \frac{\hat{i}_{sq} \hat{R}_R}{\hat{\Psi}_R}, \tag{11.10}$$

where

$$\hat{R}_s = R_s \tag{11.11}$$

$$\hat{L}_\sigma = L_s - \frac{L_m^2}{L_r} \tag{11.12}$$

$$\hat{R}_R = (\frac{L_m}{L_r})^2 R_r \tag{11.13}$$

and

$\underline{\hat{\Psi}}^s_R$	:	estimated complex rotor flux (Vs)	L_s	:	stator inductance (H)
$\underline{u}^s_s$	:	complex stator voltage in stationary coord. (V)	L_r	:	rotor inductance (H)
$\underline{i}^s_s$	:	complex stator current in stationary coord. (A)	L_m	:	mutual inductance (H)
$\hat{\omega}_1$	:	estimated synchronous speed (rad/s)	R_r	:	rotor resistance (Ω)
R_s	:	stator resistance (Ω)			

Current controller

The current controller is needed in order to gain control of flux (i_d) and torque (i_q). Freescale's current controller is a PI controller with input and output signals in synchronous coordinates and therefore the current controller in the Simulink model is also made in synchronous coordinates. If the current controller is built in stator coordinates there can arise problems, during steady-state, for the actual current to follow the reference current. With synchronous coordinates the signals will be transformed to dc signals which the PI controller can handle much better.

Input signals to the current controller are the estimated and the reference stator currents in dq-coordinates, see Figure 11.26. From these signals an error signal is obtained which is sent to the PI-regulator. The output voltage from the PI-regulator is then compensated for the cross coupling term and the reference voltage is obtained and transformed into $\alpha\beta$-coordinates.

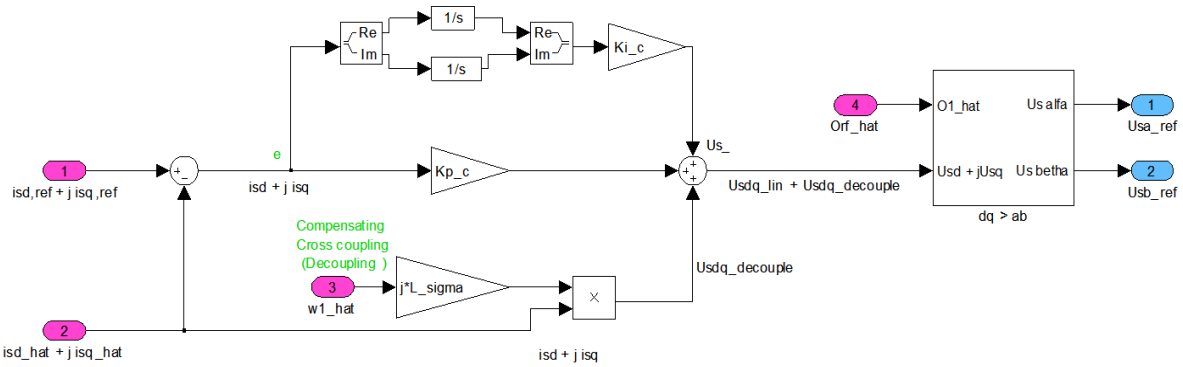

Figure 11.26: Block diagram model of the current controller.

Due to the fact that the stator voltages in dq-coordinates are dependent on both i_{sd} and i_{sq} a compensation term for the cross coupling is added to decouple the stator voltage equations, then it is possible to independently control i_{sd} (the rotor flux-producing component) and i_{sq} (the torque-producing component) which is desired.

Current reference

The current reference block, see Figure 11.27, calculates the reference currents in dq-coordinates.

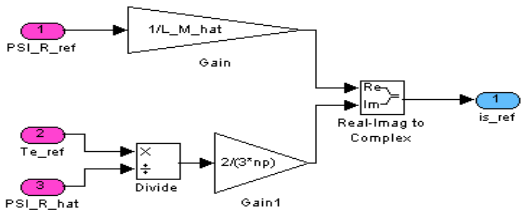

Figure 11.27: Block diagram model of the current reference.

The structure of the block originates from the following relations:

$$i_{sd,ref} = \frac{\Psi_{R,ref}}{\hat{L}_M} \tag{11.14}$$

$$i_{sq,ref} = \frac{2}{3n_p} \frac{T_{e,ref}}{\hat{\Psi}_R} \tag{11.15}$$

11.5.5 Permanent Magnetized Synchronous Machine

The Simulink model for the PMSM is shown in Figure 11.28.

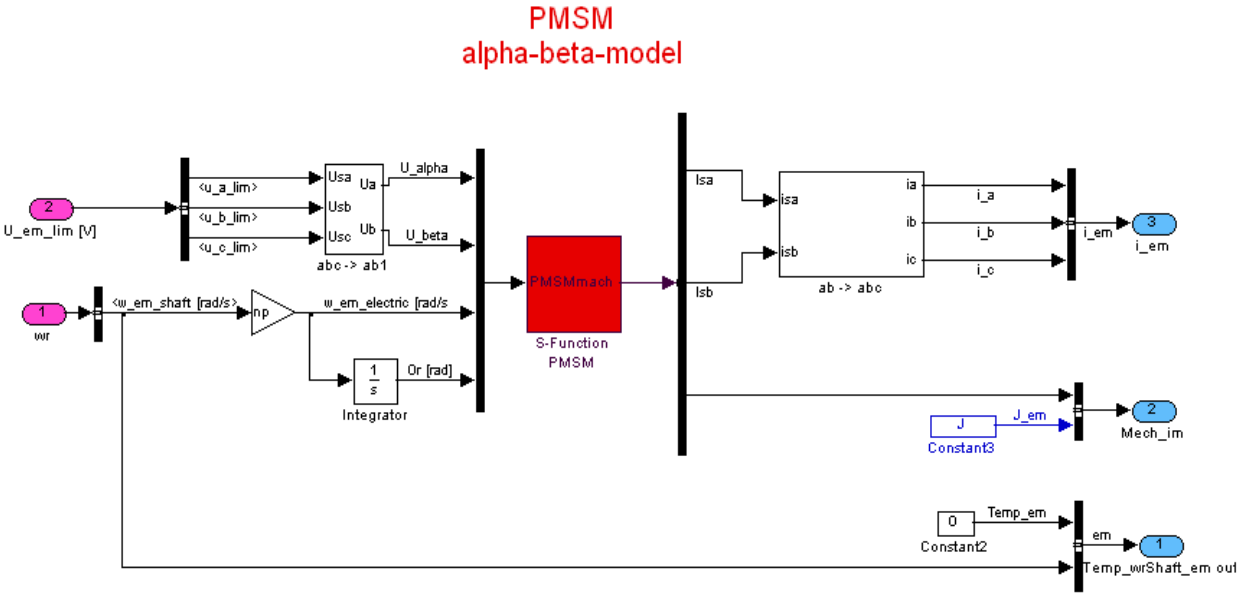

Figure 11.28: Block diagram model of the PMSM.

11.5.5.1 The S-function

The PMSM is also modeled as an S-function, which is derived from the state-space representation of the dynamic model of the PMSM.

$$\begin{bmatrix} \dot{i}_{sd} \\ \dot{i}_{sq} \end{bmatrix} = \underbrace{\begin{bmatrix} -\frac{R_s}{L_s} & \omega_r \\ -\omega_r & -\frac{R_s}{L_s} \end{bmatrix}}_{\text{Amat}} \begin{bmatrix} i_{sd} \\ i_{sq} \end{bmatrix} + \underbrace{\begin{bmatrix} \frac{1}{L_s} & 0 \\ 0 & \frac{1}{L_s} \end{bmatrix}}_{\text{Bmat}} \begin{bmatrix} u_{sd} \\ u_{sq} \end{bmatrix} - \begin{bmatrix} 0 \\ \frac{\omega_r \Psi_m}{L_s} \end{bmatrix} \tag{11.16}$$

11.5.6 Gear

Figure 11.29 shows the model of the gear between the motor and the wheels.

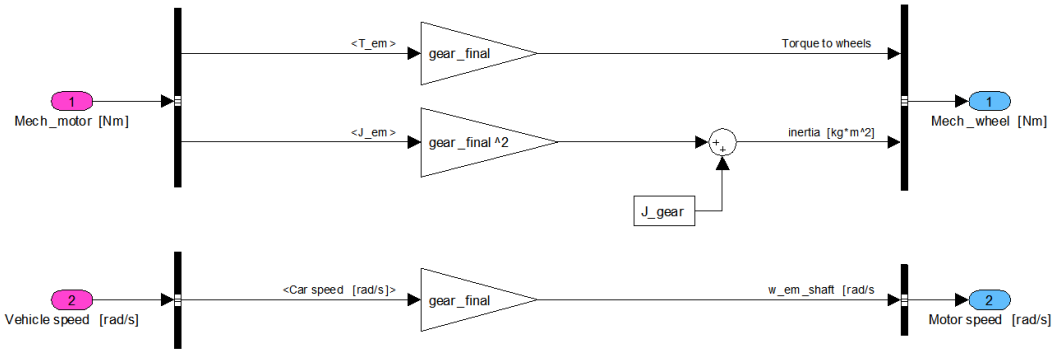

Figure 11.29: Block diagram model of the gear between the motor and the wheels.

The induction machine's torque and the go-kart's speed is multiplied by the gear ratio to obtain the corresponding driving/braking torque sent to the wheels and the rotational speed of the induction machine. The inertia of the induction machine is multiplied by the square of the gear ratio and added to the inertia of the gear itself.

The gear ratio was chosen to be one, in order to reach the higher values of speed that are desired in the speed vector, without utilizing field weakening of the electric motor. The maximum vehicle speed, $v_{max}\,(km/h)$, during nominal operation of the induction machine can be calculated as in

$$v_{max} = \frac{n_{rat}\frac{\pi}{30}}{gear} \cdot r_{wheel} \cdot 3.6 \tag{11.17}$$

where $n_{rat}\,(rpm)$ is the nominal speed of the induction machine, $gear$ is the gear ratio, $r_{wheel}\,(m)$ is the wheel radius, and 3.6 to give the result in km/h instead of m/s.

With a gear ratio of 55/23 or 2.39, the maximum go-kart speed would be $57\,km/h$, since the nominal speed of the induction machine is $2850\,rpm$. But with a gear ratio of one the maximum speed would be $136\,km/h$, which is more than enough.

11.5.7 Chassis

The block diagram model representing the chassis of the electric go-kart can be seen in Figure 11.30.

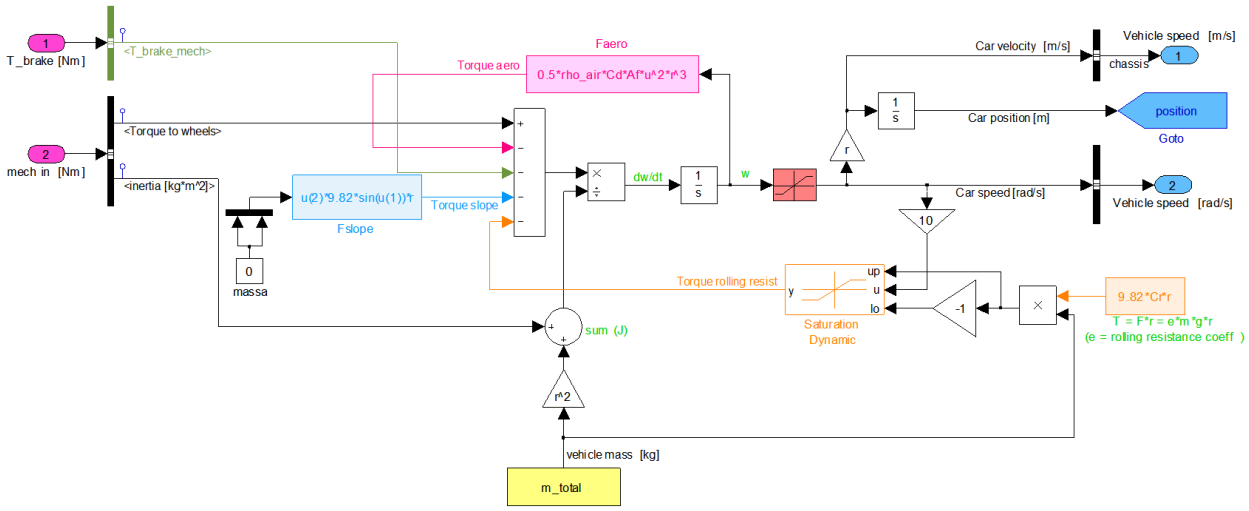

Figure 11.30: Block diagram model of the go-kart chassis.

The model of the go-kart chassis is basically the same as for Smarter, see the structure description of the chassis model of Smarter in Section 5.5.9. However, the two models differentiate in some aspects. No slope input signal since the simulation vector did not contain any information about possible slope, the torque acting on the wheels due to inclination is therefore set to zero. Moreover, the go-kart chassis model does not have the same number of output signals, only sending the vehicle speed to the controller block and to the gear block and the go-kart's position to the environment model.

Chapter 12

Examples of simulation results

Here follows some examples of what the simulator can be used for and what can be examined, e.g. how the junction temperature in the inverter increases and how much the battery is discharged during a race as well as component dimensioning in general. The simulations have been run with the use of the specific simulation vector described in the previous chapter.

Below follows some of the go-kart parameters which are used when running the simulations. Other parameters can be found in Appendix B

Table 12.1: Go-kart setup

Battery		**Chassis**	
SOCmin	0.1	C_r	0.007
SOCmax	0.9	C_d	0.6
SOCinit	0.8	A_f	0.5 m^2
Vmin	22 V	Tire radius	0.127 m
Vmax	200 V		
Gear - motor to wheel		**Miscellaneous**	
Gear ratio	1	Tot. go-kart weight	90.9 kg
Efficiency	100 %	Driver weight	30 kg
		Air temperature	25 °C

12.1 Battery performance

The battery cycle life or life expectancy is, as mentioned earlier, dependent on how deep the cycles are. One should avoid the terminal voltage of the battery to drop below the cut-off voltage. Through simulations one gets a rough estimate of how well the battery is dimensioned for the task.

With this simulator it is also possible to find out how much energy is recovered through regenerative braking, by integrating the battery power. According to simulations 24.25 % of the energy was regenerated during the simulated race of about 10 minutes and a half.

12.1.1 Battery voltage

The change in terminal voltage of the battery is shown in Figure 12.1. Thirteen laps was run in the simulation, which implies driving for about ten minutes.

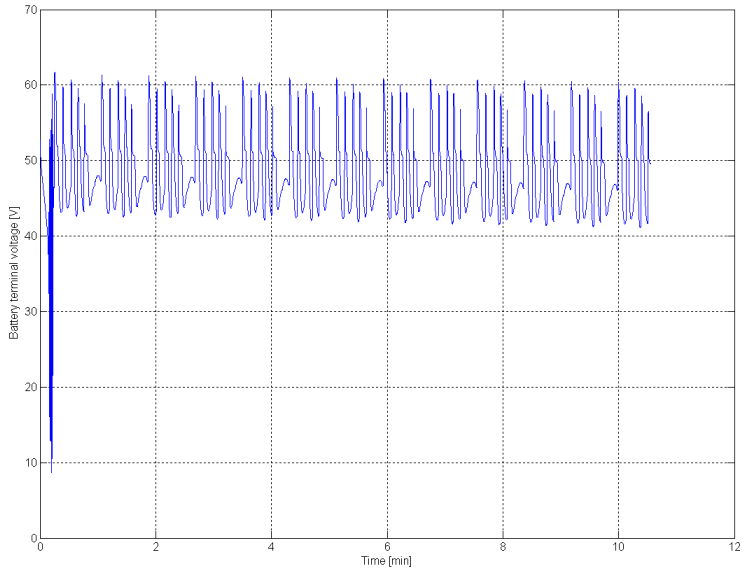

Figure 12.1: Battery terminal voltage during thirteen laps.

As can be seen in the graph above, there are relatively large changes in the terminal voltage during short time. The reason is that the current being sent to or from the battery, which is proportional to the demanded torque, affects the magnitude of the voltage drop across the battery's internal resistance. When instead looking at the open circuit voltage, see Figure 12.2, one can see that the OCV of the battery has only slightly dropped, about 1.4 V, during the thirteen laps.

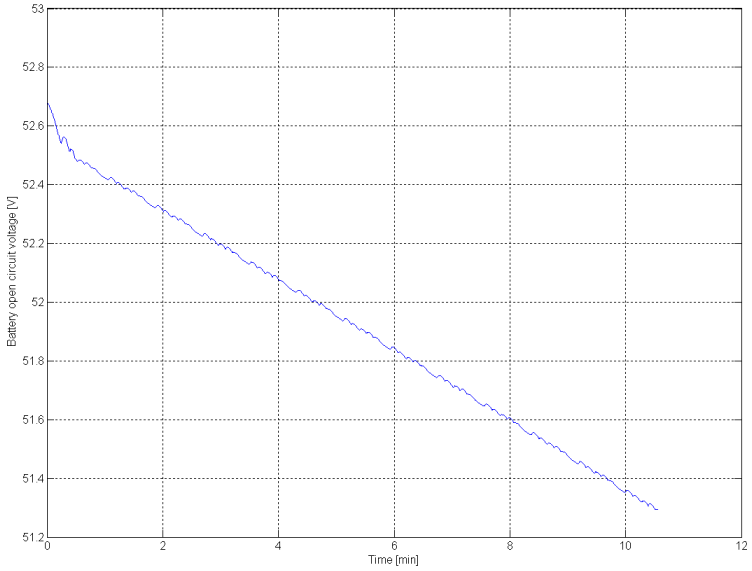

Figure 12.2: Battery open circuit voltage during thirteen laps.

12.1.2 SOC

Figure 12.3 shows how the battery's state of charge drops from 0.8 to about 0.45 during the race. From this one could conclude that the battery pack may be a bit over dimensioned for this particular race. One could be interested in removing some of the modules in the battery, making the battery pack lighter.

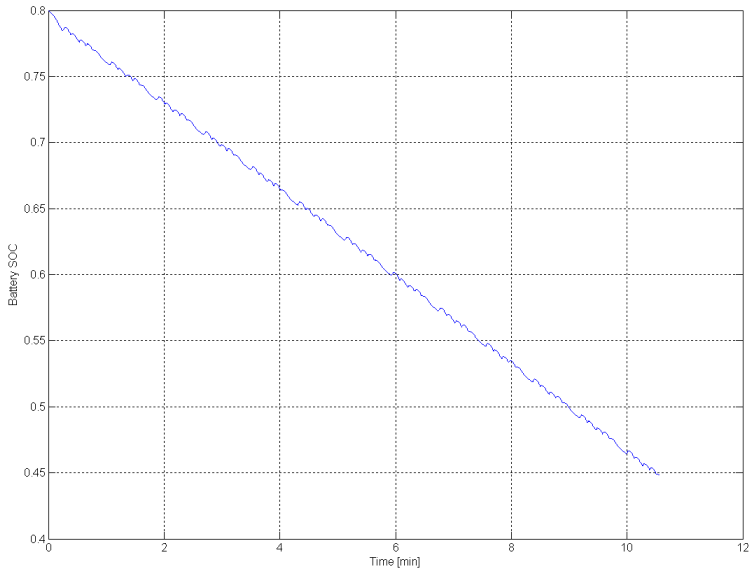

Figure 12.3: Battery state of charge during thirteen laps.

If six battery modules are used instead of eight, the SOC would drop from 0.8 to about 0.35 (still not crossing the recommendations given from the battery manufacturer mentioned in the previous chapter) during the race, see Figure **??**. This could be of interest during competition since a lighter go-kart results in the possibility to accelerate faster.

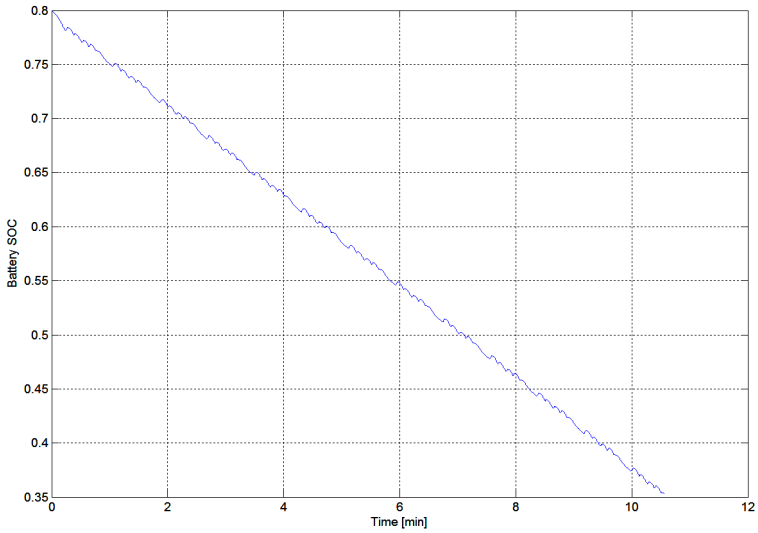

Figure 12.4: Battery state of charge during thirteen laps with six battery modules.

If, e.g., the driving force is 200 N and the battery pack contains six modules instead of eight, giving a go-kart weight which is 7.8 kg lighter, then the acceleration would be 1.77 m/s^2 instead of 1.65 m/s^2 according to

$$F = ma. \tag{12.1}$$

That would imply an acceleration from standstill to 90 km/h in 14.1 s instead of 15.2 s with a battery pack consisting of eight modules.

12.2 Inverter performance

In Figure 12.5, the change in junction and case temperatures during the thirteen laps is presented. The overall trend is a gradual increase in temperature, and since the motor currents varies so will the currents through the transistors and hence the power dissipation in the MOSFETs. It can also be seen that the junction temperature is much more sensitive to changes in the dissipated power than the case temperature, due to the smaller thermal capacity in the junction.

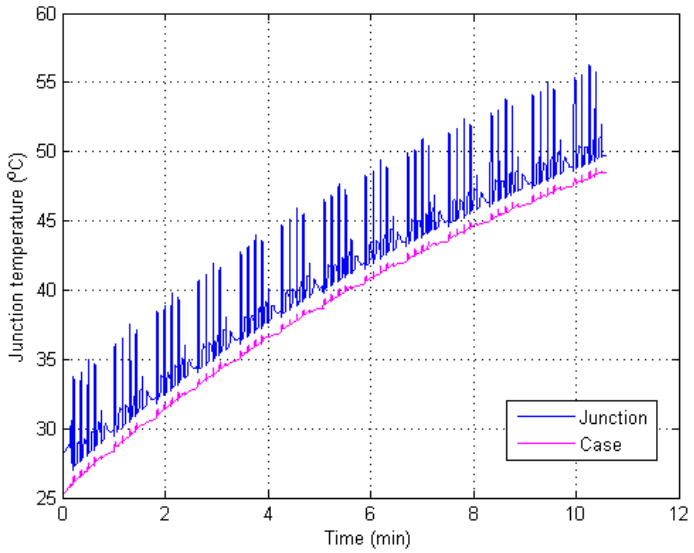

Figure 12.5: Junction and case temperatures in one of the five MOSFETs in the original inverter model.

The total inverter power dissipation is shown in Figure 12.6. The efficiency of the inverter is about $97 - 98\,\%$, according to the simulations.

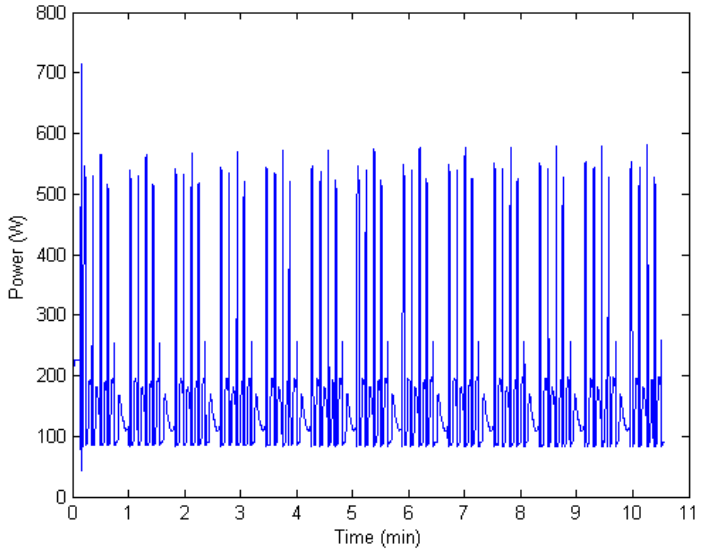

Figure 12.6: Total power dissipation in the original inverter model.

The junction temperature in the transistors does not even reach 60 ℃, which is far below the maximum operating junction temperature, 175 ℃ given in the datasheet of the MOSFET. Since the junction temperature is far below the maximum permissible it might not be necessary that every switch in the inverter consists of five parallel connected MOSFETs. The reasons for parallel connected transistors are to distribute the current between the transistors not to exceed the maximum allowable current and to prevent the junction temperature to become too high. Figure 12.7 shows the junction temperature in one of the MOSFETs when only having three parallel connected MOSFETs instead of five. As can be seen in Figure 12.7 the junction temperature is still far below the maximum permissible when considering this driving cycle.

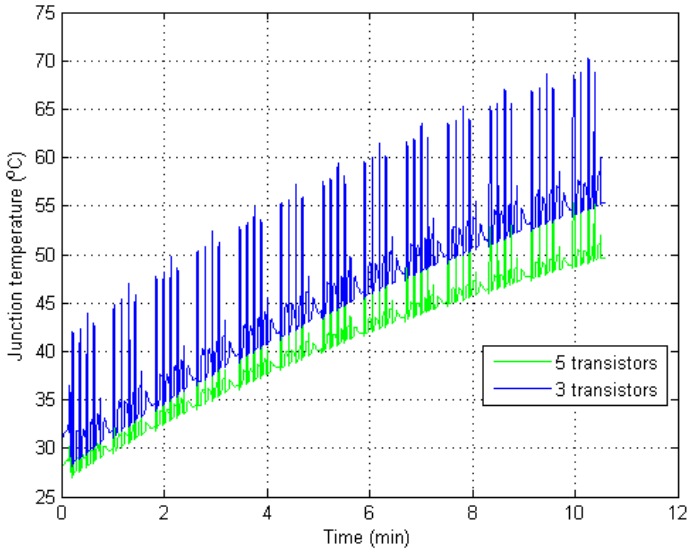

Figure 12.7: Junction temperature in one of the three MOSFETs in the modified inverter model.

Due to the shown temperature increase in the transistors, the on-state resistance of the transistors will increase and the time-trace pattern from the junction temperature can also be seen in the resistance, see Figure 12.8.

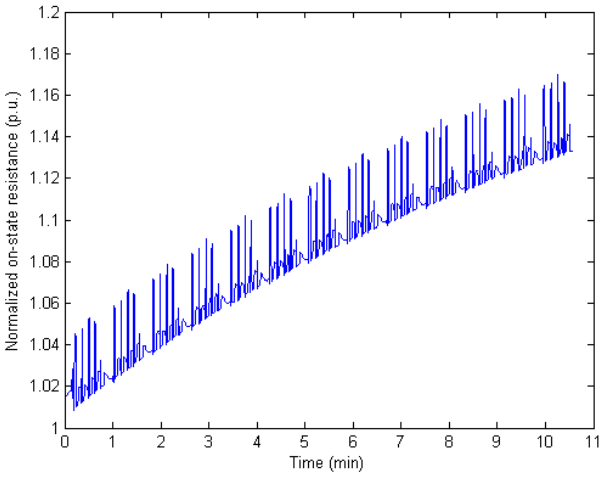

Figure 12.8: The development of the normalized transistor on-state resistance during the simulated race.

12.3 Torque and power demand of the induction machine

Figure 12.9 shows the demanded torque from the induction machine during one lap.

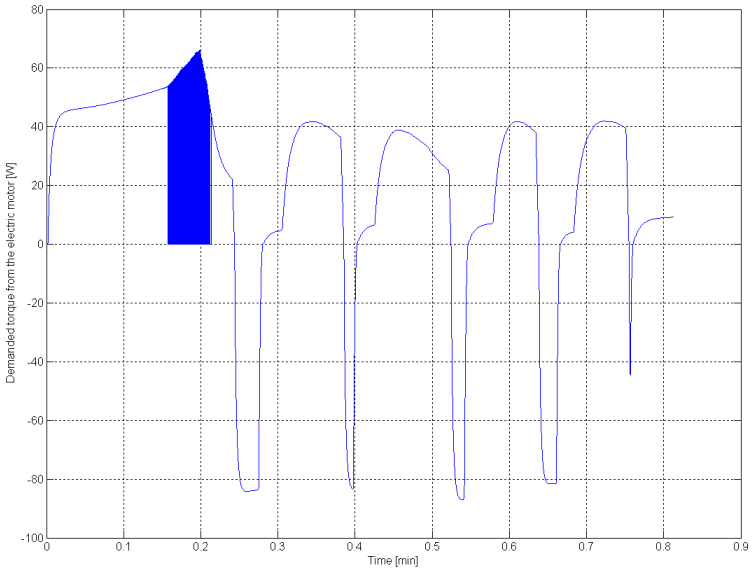

Figure 12.9: Demanded torque from the electric motor during one lap.

The maximum positive demanded torque is about 65 Nm and occurs at the end of the starting acceleration phase. The maximum negative torque is about 85 Nm. A negative torque occurs when the induction machine is operating as a generator, which happens when the driver slows the go-kart down.

Figure 12.10 shows the mechanical power delivered by the induction machine during one lap.

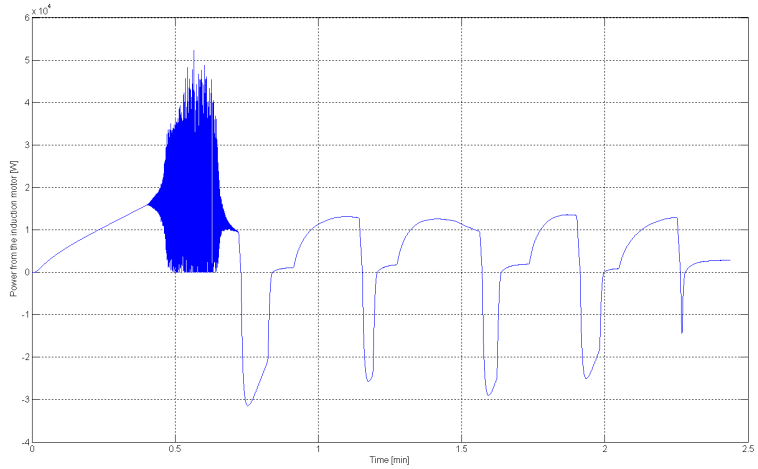

Figure 12.10: Power from the induction motor during one lap.

Due to the oscillations at the end of the accelerating phase it is difficult to tell how large the mechanical power delivered by the induction motor will be, perhaps 20 kW can be a reasonable assumption. The maximum mechanical power of the induction machine when it is operating as a generator is about -30 kW, which is about five times larger than the induction machine's rated power.

Chapter 13

Conclusions and future work proposals

The goal was to make a platform for modelling an electric go-kart, not necessarily to evaluate the go-kart's performance. By adjusting different parameters in the go-kart model, further performance investigations were also exemplified.

Here follows some conclusions on how well the goal of the thesis was fulfilled and what needs to be done still.

13.1 Modelling aspects

An electric go-kart has been modelled and its performance during a modelled race have been simulated. However no such go-kart has yet been assembled in reality and no testing or measurements have been conducted on the go-kart or its components to verify the accuracy of the model. That is the main weakness of the work that has been done.

Moreover some mechanical and electrical losses are not included such as; electrical motor mechanical losses, gear and wheel mechanical losses and electrical losses in wires.

The electrical parameters of the induction machine have been modelled to bo constant when in reality they vary. The rotor resistance for example, increases with increasing temperature and current frequency. Also the magnetization of the motor iron may become saturated, and this will reflect on the inductances as well.

When there is a physical go-kart that is desired to be investigated using this simulation tool, there are a few key parameters, apart from the driveline parameters, that need to be verified and possibly adjusted in order to attain a reliable result. Those are; the total mass of the go-kart including a driver, the cross sectional area, the air drag and rolling coefficient. In this model, these values are only rough estimates.

Also the regulator parameters, K_p and K_i, in the reference torque controller block are now only rough assumptions. First after the go-kart has been finalized can these figures be tuned to have the desired effect on the reference torque.

Regarding the SOC estimator in the controller block, it may be difficult to know the initial SOC-value without considering the whole charge and discharge history of the battery including temperature and pressure developments. A rough figure may be found by simply charging the battery fully, and then define it as an SOC of 100 %.

13.1.1 Future work proposals

The controller block can be edited or extended to include desired features. For example, it could be interesting to be able to limit the reference torque by an external input, from outside the go-kart, to the reference torque control unit. That could be, for example, if an accident occurs on the track the leader of the competition might want to force the drivers to slow down.

The current battery model is relatively simple. It could be enhanced by e.g.; making the internal resistance dependent on SOC and temperature instead of being modelled as a constant, modelling self discharge of the battery by adding a parallel resistance across the OCV and making the OCV not only dependent on SOC, but also on temperature and current. For more details regarding an enhanced battery model see section *Battery model* in chapter two.

The driver model could be enhanced, making in possible to send out both a non-zero gas pedal position and brake pedal position. The torque reference controller block should then also be developed to handle such a situation. If both a non-zero gas pedal position and brake pedal position is sent to the controller block then it has to be able to set the propelling torque to zero, only sending out a braking torque reference to the controller block of the electric machine.

There is no finalized control block for the PMSM, as a suggestion the control block should be based on Freescale's vector control of a PMSM.

When it comes to the simulated race vector, the initial acceleration part was set to last for $10\,s$. Perhaps it is more realistic for this acceleration to last for only $5\,s$. That would naturally need a larger torque from the motor and then this simulator could be used to find how the final go-kart would cope in the situation.

Even better still would be to find a speed-time-vector from a real race. This can be found placing a GPS on board a real go-kart during a race.

Part IV

Epilogue

Bibliography

[1] Robert Bosch GmbH, *Automotive Handbook, 5th edition*, Society of Automotive Engineers (SAE), Stuttgart 2000

[2] John B. Heywood, *Internal Combustion Engine Fundamentals*, McGraw-Hill, New York 1988

[3] Mehrdad Ehsani, *Modern Electric, Hybrid Electric, and Fuel Cell Vehicles - Fundamentals, Theory, and Design*, CRC Press LLC, Boca Raton c2005

[4] Mats Alaküla, *Hybrid Drive Systems for Vehicles, Part I*, Industrial Electrical Engineering and Automation, Lund University 2006, Last edited: 2006-11-06, Avaliable at: `http://www.iea.lth.se/hfs/Kompendium%2006/Hybridkompendium_1_2006.pdf`, 2009-02-01

[5] L. Guzzella and A. Sciarretta, *Vehicle Propulsion Systems - Introduction to Modeling and Optimization*, Springer, Zurich 2005

[6] Ned Mohan, Tore M. Undeland, William P. Robbins, *POWER ELECTRONICS, Converters, Applications and Design, 3rd edition*, John Wiley & Sons, Inc. Hoboken New Jersey, 2003

[7] Yunus A. Çengel, *Introduction to Thermodynamics and Heat Transfer, 2nd edition* McGraw-Hill, New York 2008

[8] Y.C. Gerstenmaier, W. Kiffe, G. Wachutka, *Combination of thermal subsystems by use of rapid circuit transformation and extended two-port theory* Microelectronics Journal, Volume 40, Issue 1, January 2009, Pages 26-34

[9] Filip Christiaens, Eric Beyne, *Transient thermal modeling and characterization of a hybrid component* Electronic Components and Technology Conference, 1996. Proceedings., 46th, 28-31 May 1996, Page(s):154 - 164

[10] Austin Hughes, *Electric Motors and Drives: Fundamentals, Types and Applications, 3rd edition*, Elsevier Ltd, 2006

[11] Michael H. Westbrook, *The Electric Car: Development and Future of Battery, Hybrid and Fuel-Cell Cars*, Institution of Engineering and Technology, 2001

[12] Lennart Harnefors, *Control of Variable-Speed Drives*, Applied Signal Processing and Control, Department of Electronics, Mälardalen University, Libris, Västerås 2002

[13] Peter Vas, *Sensorless Vector and Direct Torque Control*, Oxford University Press, 1998

[14] Andrzej M. Trzynadlowski, *The Field Orientation Principle in Control of Induction Motors*, Kluwer cop., Boston 1994

[15] ELFA, Electronics supplier of Northern Europe, *Factsheet*, Last edited; 2007-02-16, Avaliable at: https://www1.elfa.se/elfa~ex_en/b2b/start.do, 2009-07-31

[16] Maxwell Technologies, Inc., *BOOSTCAP® Product Guide*, Last edited; 2008-07-16, Avaliable at: http://www.maxwell.com/ultracapacitors/technical-support/manuals.asp, 2009-07-31

Webpages:

[17] www.eme.ee.kth.se/kurser/uploads/Vector%20Control%20of%20Induction%20Machines.ppt, 2009-05-12

[18] www.abb-drives.com/StdDrives/RestrictedPages/Marketing/Documentation/files/PRoducts/DTCTechGuide1.pdf, 2009-05-12

[19] https://www.freescale.com/webapp/sps/site/prod_summary.jsp?code=RDCFPMSMSVC"och"nodeId=016246844916882695632 4, 2009-06-08

[20] http://www.kilowattclassroom.com/Archive/SyncMotors.pdf, 2009-06-08

[21] http://www.alphatron.com/upload/pdf/mc_power_series_48-1.pdf, 2009-07-30

[22] http://www.jmenergy.co.jp/en/product.html, 2009-08-09

[23] http://www.batteryuniversity.com, 2009-07-31

[24] http://www.automotivedesignline.com/184417266;jsessionid=L1JOMOJJGTIBGQSNDLOSKHOCJUNN2JVN?pgno=2, 2009-07-31

[25] http://www.honda-engines.com/mini.htm, 2009-01-28

[26] http://www.raceit.nu/karting.html, 2009-08-11

[27] http://en.wikipedia.org/wiki/Kart_racing, 2009-08-11

[28] http://www.capsim.se/, 2009-08-11

[29] http://www.shell.com/home/content/eco-marathon-en/europe/2009/participants/dir_sem_participating_teams_2009.html, 2009-01-28

[30] http://en.wikipedia.org/wiki/PID_controller#Proportional_term, 2009-09-02

Pictures:

[31] https://www1.elfa.se/data1/wwwroot/webroot/Z_DATA/06488027.pdf, 2009-08-15

[32] http://lees.mit.edu/lees/posters/double_layer_capacitors_poster.ppt, 2009-08-15

[33] http://www.electronics-tutorials.ws/io/io31.gif, 2009-08-19

[34] http://books.google.com/books?id=ywiBVSnYm6IC&pg=PA104&lpg=PA104&dq=%2B%22four-quadrant%22+operation+%2Bdc+machine&source=bl&ots=H6qDGrcclM&sig=WHHbJTpYmda4UyJegZVC2ObCnQw&hl=en&ei=UX5pSuPKLprKnAPpuaXACQ&sa=X&oi=book_result&ct=result&resnum=10, 2009-08-24

[35] http://books.google.com/books?id=y3xN7jZTesUC&pg=PA14&lpg=PA14&dq=forces+acting+on+a+vehicle&source=bl&ots=gz_ZohtmwA&sig=WH4Q71NSnb168PS2cAJ8OMY0DQo&hl=en&ei=2Q1qSrC1II38_Aax0ez9Dg&sa=X&oi=book_result&ct=result&resnum=8, 2009-08-24

[36] "Course Material" course in Electrical Drives 2, Göteborg, 2009

[37] http://shop.maxonmotor.com/maxon/assets_external/Katalog_neu/Downloads/allgemeine_informationen/Technik_kurz_und_buendig/DC-Technik-kurz-und-buendig_08_EN_024-25.pdf, 2009-01-27

[38] http://shop.maxonmotor.com/maxon/assets_external/Katalog_neu/Downloads/Katalog_PDF/maxon_dc_motor/RE-programm/new/RE-65-353294_08_EN_085.pdf, 2009-01-27

[39] http://shop.maxonmotor.com/maxon/assets_external/Katalog_neu/Downloads/Katalog_PDF/maxon_dc_motor/wichgtiges_dc_ec_motoren_036-43_e.pdf, 2009-01-27

[40] http://shop.maxonmotor.com/maxon/assets_external/Katalog_neu/Downloads/Katalog_PDF/maxon_motor_control/4-Q-DC-Servoverstaerker/ADS/ADS_E_50-10/ADS_E-50-10_168049_08_277_e.pdf, 2009-01-27

[41] http://en.wikipedia.org/wiki/File:3-phase_inverter_cjc.png, 2009-06-18

Appendix A

Smarter m-files

Here follows the m-files for modelling and simulation of Smarter for Shell Eco-marathon.

A.1 The main m-file; *SMARTERsimrun.m*

```
%*************************************************************************
%
%  Modelling and simulation of Smarter, for Shell Eco-marathon
%
%  Developed by Emma Grunditz and Emma Jansson, in the spring of 2009,
%  for Chalmers University of Technology
%  at the Department of Energy and Environment
%  and the Division of Electric Power Engineering
%  as a part of the master thesis work:
%  "Modelling and Simulation of a Hybrid Electric Vehicle
%  for Shell Eco-marathon and an Electric Go-kart"
%
%*************************************************************************}

clear all;
clc;

%*************************************************************************
%*************************************************************************
%
% COMPONENT AND PARAMETER CHOICES
%
%*************************************************************************
%*************************************************************************

% ======================================
%  Fuel Tank
% ======================================

    %-Fuel volume [L]
    V_fuel = 0.35;              % Value from Philip in Lausitz
```

```
    %-Fuel density [kg/L]
    % = 0.74616 [kg/L], Assumed by Shell Eco-marathon
    % "Official rules 2009" p.20
    rho_fuel = 0.73;            % A rough estimation given by Emma Sjöblom
                                % at Shell Eco-marathon via mail 2009-03-16

    %-Initial fuel mass [kg]
    m_fuel_init = rho_fuel*V_fuel;

% ======================================
%  ICE - "Mapped" values
% ======================================
% choose between GX25 and GX35

%     % --- GX25 ----------------------
%     % Torque-speed & Fuel flow speed: Look-Up Table -
%     % Based on measurements with wide open throttle, no modifications
%     % by Magnus Andersson, Maskin 2008
%     % Engine speed [rad/s]
%      w_ice = [0,188.496,219.912,251.328,314.16,376.992,439.824,502.656,
%               565.488,628.32,691.152,753.984,816.816];
%     % Engine torque [Nm]
%     T_ice = [0,0.4,0.51,0.51,0.62,0.75,0.76,0.9,0.87,0.8,0.71,0.97,0.86];
%     % Fuel flow rate [kg/s]
%      FUEL_flow = [0,2.5E-05,2.5E-05,2.77778e-5,3.61111e-5,4.44444e-5,
%                   5.27778e-5,6.9444e-5,6.9444e-5,8.3333e-5,8.88889e-5,
%                   1.08333e-4,1.02778e-4];
%     % Mass of ICE [kg]
%       m_ICE = 2.90;               % Data sheet value
%     % Inertia of ICE [kg m^2]
%       J_ICE = 1.38e-4*10;          % A rough assumption based on
%                                   % J = 0.5*m*r*r compared to the
%                                   % electric machine
%     % Drive chain gearwheel ratio
%       DrCh_ratio = 0.8;           % = 0.8
%     % Drive chain efficiency
%       n_DrCh = 0.9;               % Assumed value, "A good chain drive
%                                   % = 0.95-0.99": Anders Lindskog
%       % --- Starting the ICE with the generator----
%     % Time for the ICE to start [s]
%       start_delay = 0.5;
%     % Assumed starting torque needed [Nm]
%       start_torque = -0.359;      % =-0.359 to get about 75J energy loss
%                                   % during 0.5s of ICE start
%     % \GX25-------------------------------

    % --- GX35 ----------------------
    % Torque-speed & Fuel flow speed: Look-Up Table -
    % Based on measurements with wide open throttle, no modifications
```

```
    % by Magnus Andersson, Maskin 2008
    % Engine speed [rad/s]
     w_ice = [0,251.328,314.16,376.992,439.824,502.656,565.488,628.32,
              691.152,753.984];
    % Engine torque [Nm]
     T_ice = [0,0.6,1.36,1.435,1.605,1.67,1.685,1.6,1.35,1.33];
    % Fuel flow rate [kg/s] -a mean value calculation from
    % two measurement series
     FUEL_flow = [0,4.16667e-5,5.138889e-5,6.59722e-5,7.36111e-5,
                  8.88889e-5,1.06944e-4,1.16667e-4,1.31944e-4,1.50000e-4];
    % Mass of ICE [kg]
     m_ICE = 3.46;                    % Data sheet value
    % Inertia of ICE [kg m^2]
     J_ICE = 1.38e-4*10;               % A rough assumption based on
                                      % J = 0.5*m*r*r compared to
                                      % the electric machine
    % Drive chain gearwheel ratio
     DrCh_ratio = 0.8;                % =0.8
    % Drive chain efficiency
     n_DrCh = 0.9;                    % = 0.9 Assumed value,
                                      % "A good chain drive = 0.95-0.99":
                                      % Anders Lindskog
    % --- Starting the ICE with the generator----
    % Time for the ICE to start [s]
     start_delay = 0.5;
    % Assumed starting torque needed [Nm]
     start_torque = -0.535;           % =0.-535 to get about 90J energy loss
                                      % during 0.5s of ICEstart
    % \GX35-----------------------------


% ======================================
%  Generator
% ======================================

    % Number of generators in parallel
     n_gen = 2;
    % Mass of generator [kg]
     m_gen = 2.48;                   % Data sheet value
    % Inertia of generator [kg m^2]
     J_gen = 1.38e-4*n_gen;          % Data sheet value
    % Armature resistance [ohm]
     Ra_gen = 0.173;                 % Data sheet value
    % Generator torque-current constant [Nm/A]
     Tc_gen = 89.1e-3;               % Data sheet value
    % Maximum generator current [A]
     I_max_gen = 208;                % Data sheet value = starting current
                                     % at nominal voltage 36 V
    % No load torque [Nm]
```

```
    T_noload_gen = n_gen * 0.407 * Tc_gen;  % 0.407 [A] = no load current

% ======================================
%  Buffer - Super Capacitor
% ======================================

    % Supercapacitor Cell capacity [F]
     %C_cap = 154.3845;             % Maxwell supercapacitor, BMOD0140-P048
                                    % Measured value: 154.3845 F
      C_cap = 168.9793;             % Homemade super capacitor,
                                    % Measured value: 168.9793 F

    % Mass of one cell
     %m_cap = 13.5;                 % Maxwell, Data sheet value: 13.5
      m_cap = 4.680;                % Homemade super capacitor

    % Cell internal resistance [ohm]
     %R_cap = 14.3357e-3;           % Maxwell, Measured value: 14.3357 mohm
      R_cap = 39.2296e-3;           % Homemade super capacitor,
                                    % Measured value: 39.2296e-3 mohm

    % Voltage limits for the super capacitor
     Vmax = 44;                     %= 44
     Vmin = 38;                     %= 38

    % Initial charge in supercapacitor [C]
     Qinit=Vmax*C_cap;

    % Resistance of Fuse on Supercapacitor [Ohm]
    R_fuse = 3.1e-3;                % Data sheet value

% ======================================
%  Electric Motor - Maxon DC PM motor
% ======================================

    %Number of electric motors in parallel
     n_motor = 1;

    % Mass of ONE DC motor [kg] - see total mass calculation
     m_motor = 2.48;                % Data sheet value

    % DC Motor inertia [kg m^2]
     J_motor = n_motor*1.38e-4;     % Data sheet value

    % DC Motor torque-current constant [Nm/A]
     Tc_motor = 89.1e-3;            % Data sheet value

    % Armature ("Terminal") resistance for ONE motor [ohm]
     Ra_motor = 0.173;              % Data sheet value
```

```
    % No load torque for *n_motor [Nm]
      T_noload = n_motor * 0.407 * Tc_motor; % Data sheet value - no load
                                            %current* motor torque constant

     %--- Thermal Parameters ---
    % Temperature coefficient of Resistance for Cu [ohm/K]
     alfa_cu = 3.9e-3;
    % Thermal time constant winding [s]
     tao_w = 127;                   % Data sheet value
    % Thermal time constant motor [s]
     tao_h = 991;                   % Data sheet value
    % Thermal resistance housing-ambient [K/W]
     R_wh = 1.85;                   % Data sheet value
    % Thermal resistance housing-ambient [K/W]
     R_ha = 1.3;                    % Data sheet value
    % Heat capacity of winding [J/k]
     C_w = tao_w/R_wh;              % Calculated value
    % Heat capacity of housing [J/K]
     C_h = tao_h/R_ha;              % Calculated value
     % Maximum permissable winding temperature [deg C]
     Temp_max_motor = 125;
     % --- "Foster" equivalent of transient thermal impedance---
     s=tf('s');                     % Introducing the Laplace variable 's'
     Z_h = 1 / ( (1/R_ha) + s*C_h );% Equivalent thermal impedance of
                                    % housing
     Z_w = 1 / ( (1/R_wh) + s*C_w );% Equivalent thermal impedance of
                                    % winding
     Z_tot_2 = Z_h + Z_w;           % Equivalent thermal impedance of whole
                                    % motor
     [num_Zth,den_Zth] = tfdata(Z_tot_2,'v');   % Transfer function of
                                                % motor thermal model

% --- Converter parameters ----
    % Maximum allowed DC/DC converter current [A]
%      I_max_DcDc = 16;             % Measured max current from Maxon
                                    % converter, data sheet value = 20 A
     I_max_DcDc = 200;              % Chalmers designed converter,
                                    % "should be able to handle 50kW
                                    % theoretically at about 50 V",
                                    % Peter&Henrik

    % Continuously allowed DC/DC converter current [A]
     I_contin_DcDc = 10;            % Maxon data sheet value

    % Mass of converter [kg]
%      m_DcDc = 0.4;                % Maxon data sheet value
     m_DcDc = 0.5;                  % Chalmers designed converter
```

```
    % Efficiency of converter
%       eff_DcDc = 0.85;            % Measured by Peter&Henrik = 0.82-0.92.
                                    % Maxon data sheet value = 95 %
     eff_DcDc = 0.99;               % Chalmers designed converter;
                                    % "about 99 %" Peter&Henrik,
                                    % however it does have a considerable
                                    % amount of ripple, which may give a
                                    %lower total converter-motor efficiency

% ======================================
%  Chassis
% ======================================

    % Mass of chassis [kg]
     m_chassis = 54.3845;            % Residual weight to get 74 kg for the
                                     % Lausitz setup

     % Weight of driver [kg]
     m_driver = 50;                  % At least 50 kg according to rules of
                                     % Eco-marathon, Emma = 55,

    % Initial velocity [rad/s]
     w_init = 0 ;

    % Tire specification "width"/ "height" R "rim", ex: 205/55R16
    % The following values was given from Sasan.
     tire_width = 95 ;              %("tire_width" = 205), Data sheet value
     tire_height = 80 ;             %("tire_height" = 55), Data sheet value
     tire_rim = 16;                 % ("tire_rim" = 16), Data sheet value
     % Tire radius calculation [m]
     r = 0.001*((tire_rim*25.4) + (2*tire_height/100*tire_width))/2;

    % Length of moment of inertia [m]; r = J/F

    % Rolling resistance coefficient (rear?)
     Cr = 0.007;                   % =0.007 From Sasan

    % Air resistance / drag coefficient
     Cd = 0.28 ;                    % From Sasan

    % Vehicle frontal area [m^2]
     Af = 1.4 ;                     % From Sasan

    % Air density calculation [kg/m^3]
%       rho_air = 1.225;            % Density for dry air at standard
                                    % atmospheric pressure at sea level
                                    % at 15 deg C
        P_air = 101325;             % Air pressure at sea level [Pa]
        R_air = 287.05;             %Gas constant for dry air [J/(kg*degK)]
```

```
% ======================================
%  Gearbox - Motor to wheel
% ======================================

    % Mass of gears [kg]
     m_gear = 0.5 ;                 % From Sasan

    % Final gear
     gear_final = (21/12)*(95/12);  % From Anders

    % Inertia of gear/s [kg m^2]
     J_gear = 0.06 ;                % From Sasan


% ======================================
%  Driver - Speed Controller
% ======================================

    % PI - Speed controller
     Kp = 0.5;                      % Trial and error = 0.5
     Ki = 0.02;                     % Trial and error = 0.02

% ======================================
%  Environment
% ======================================
% possibility to choose between type of simulation vector
    % vehicle speed(time)
    % vehicle speed(position)
    % position(time)

    % Ambient temperature [degC]
    T_amb_air = 20;                     % Temperature of air
    T_amb = 40;                         % Temperature in Smarter engine room

    % 1 = f(position)    0 = f(time)
    Trig_speed_position_on = 0;
    Trig_hillslope_position_on = 1;

% ======================================
%  Vehicle Total mass [kg]
% ======================================
m_Smarter = m_ICE + m_fuel_init + n_gen*m_gen + m_cap + n_motor*m_motor +
            m_DcDc + m_chassis + m_gear
m_total = m_Smarter + m_driver


%************************************************************************
%************************************************************************
%
```

```
% SIMULATION VECTOR
%
%************************************************************************
%************************************************************************

[time speed position hillslope L_position L_hillslope] =
%                       FUNsimvect(I_max_DcDc,gear_final,n_motor,T_amb_air);

%************************************************************************
%************************************************************************
%
% RACE-SIMULATION
%
%************************************************************************
%************************************************************************

Trig_speed_position_on = 0;
Trig_hillslope_position_on = 1;


%--------------------------------
% RACE simulation
%--------------------------------

% Stops the simulation if V_buffer reaches 100V
STOPsim_voltage = 100;
% The Race! 7 laps, 3 pit stops
sim('SMARTERsim');

    % Parameter collection
    %[s] : Race time
    time_Race_tot=tout(end);
    %[m] : Race distance
    dist_tot = car_pos(end);
    %[l] : Fuel at Start of PreRace
    fuel_start = Fuel_left(1);
    %[l] : Fuel at End of race
    fuel_left_race = Fuel_left(end);
    %[l] : Fuel consumed during PreRace and race
    fuel_consumed_race = fuel_start - fuel_left_race;

    %[V] : Voltage level before PreRace
    V_buffer_start = V_buffer(1);
    %[V] : Voltage level after Race
    V_buffer_end_race = V_buffer(end);
    %[V] : Voltage difference between PreRace and finish of the Race
    V_buffer_diff = V_buffer_end_race - V_buffer_start;

    %[l] : Fuel level vektor for the whole simulation
```

```
    Fuel_left_tot = Fuel_left;
    %[V] : Voltage-vector for the whole simulation
    V_buffer_tot = V_buffer;
    %[s] : Time-vektor for the whole simulation
    tout_tot = tout;
    % On/Off-vektor for the whole simulation
    OnOff_tot = OnOff;
    %[C] : Generator temperature after race
    temp_gen_end = temp_gen(end);


%[kg] : Fuel left after the Race
m_fuel_init = rho_fuel*Fuel_left(end);
%[C] : Charge level in Buffer after the Race
Qinit=V_buffer(end)*C_cap;

%% POST-Race-simulation

%************************************************************************
%************************************************************************
%
% LEVELING OUT THE BUFFER VOLTAGE
%
%************************************************************************
%************************************************************************

% Stops the simulation if V_buffer reaches Starting Voltage
STOPsim_voltage = V_buffer_start;

            if V_buffer_diff < 0

                time = [0:100];
                speed = zeros([1 length(time)]);
                position = [zeros([1 length(time)-1]) 1];
                hillslope = zeros([1 length(time)]);
                L_position = [zeros([1 length(time)-1]) 1];
                L_hillslope = zeros([1 length(time)]);


                % Run ICE to charge the buffer up to start level
                sim('SMARTERsim');

                %[l] : Fuel level vektor for the whole simulation
                Fuel_left_tot = [Fuel_left_tot;Fuel_left];
                %[V] : Voltage-vector for the whole simulation
                V_buffer_tot = [V_buffer_tot;V_buffer];
                %[s] : Time-vektor for the whole simulation
                tout_tot = [tout_tot;tout_tot(end)+tout];
                % On/Off-vektor for the whole simulation
```

```
                OnOff_tot = [OnOff_tot;OnOff];
                %[C] : Generator temp.-vektor for the whole simulation
                temp_gen_tot = [temp_gen_end;temp_gen(end)];


            end
%[l] : Fuel left after PostRace
fuel_left_POSTrace = Fuel_left(end);
%[l] : Fuel consumed during PostRace
fuel_consumed_POSTrace = fuel_left_race - fuel_left_POSTrace;

%************************************************************************
%************************************************************************
%
% POSTPROCESSING
%
%************************************************************************
%************************************************************************

% ---------------------
%    RACE RESULTS
% ---------------------
% Total time minus the PreRace-time = 5s.
disp('Total Race Time [min]')
time_Race_tot/60
disp(' km/liter fuel');
dist_tot/1e3/(fuel_consumed_race+fuel_consumed_POSTrace)
disp('mean speed [km/h]')
dist_tot/time_Race_tot*3.6

fuel_consumption= dist_tot/1e3/(fuel_consumed_race+fuel_consumed_POSTrace);

% ---------------------
%    PLOTS
% ---------------------

% --- Buffer Total voltage ---
figure(15)
subplot(211);
plot(tout_tot,V_buffer_tot,'LineWidth',2);
ylim([36 48]);
title('Supercapacitor voltgage [V]','FontSize',12);
ylabel('Capacitor voltage [V]','FontSize',12);
subplot(212)
plot(tout_tot,OnOff_tot,'g','LineWidth',2);
ylim([-0.1 1.1]);
xlabel('Time [s]','FontSize',12);
title('OnOff-signal to ICE; 1 = On, 0 = Off','FontSize',12);
ylabel('ICE on/off','FontSize',12);
```

A.2 Simulation vector; *FUNsimvect.m*

```
function [time speed position hillslope L_position L_hillslope] =
                        FUNsimvect(I_max_DcDc,gear_final,n_motor,T_amb_air)

%--------------------------------------------------------------------------
%   Track speed and position vector  - resolution [per second]
%--------------------------------------------------------------------------

% The following parametrizatin gives: time(end)=3173, position(end) = 22073

v_car = 25.6;          %[km/h] : Velocity at constant speed   = 25.6
v_constant = v_car/3.6;%[m/s]  : Velocity at constant speed
s_tot = 3173;          %[m]    : Total length of one lap
s_diff = 130;          %[m]    : Length difference between start and finish

%--- Initial conditions
v1_1(1) = 0;                  %[m/s]  : initial velocity
s1_1(1) = 0;                  %[m]    : starting position
s3_1(1) = 0;                  %[m]

% - Maxon converter

% t3=t1:  1 motor: v = 25.7 => time(end)= 3179.
%         2 motor: v = 25.73 => time(end)= 3180.
% ONLY FOR TESTING, since this is given in the m-file;
% I_max_DcDc = 16; gear_final = (21/12)*(95/12); n_motor = 2; T_amb_air = 25;
% [acc_max] = FUNaccmax(v_car,I_max_DcDc,gear_final,n_motor,T_amb_air);
% t1 = round(v_constant/acc_max);         %[s] : acceleration time
%\ Maxon

t0 = 5;                                  %[s] : preRace time
t1 = 10;                                 %[s] : acceleration time
t3 = t1;                                 %[s] : braking time
t4 = 10;                                 %[s] : stop time

a_acc = v_constant/t1;                   %[m/s] : acceleration
a_br = v_constant/t3;                    %[m/s] : retardation

% Calculating Acceleration distance
t_acc = [0:t1];
s_acc_t = 0.*t_acc + 0.5.*a_acc.*t_acc.^2;
s_acc = s_acc_t(end);
% Calculating Retardation distance
t_br = [0:t3];
s_br_t = v_constant.*t_br - 0.5.*a_br.*t_br.^2;
s_br = s_br_t(end);

%--------------------------------------------------------------------------
```

```
% Vector creations - per section
%--------------------------------------------------------------------------

% === Pre Race ===
        v_0 = zeros([1 t0]);
        s_0 = zeros([1 t0]);
        t_0 = length(v_0);

% === LAP 1 ===
    % Acceleration
    for i = 2:t1
        v1_1(i) = v1_1(i-1) + a_acc*1;
        s1_1(i) = v1_1(1)*i + 0.5*a_acc*i^2;
    end

    % Constant velocity
    t2_1 = round((s_tot-s_acc-s_br)/v_constant);
    for i = 1:t2_1
        v2_1(i) = v_constant;
        s2_1(i) = v2_1(i)*i;
    end

    % Retardation
    v3_1(1) = v2_1(t2_1); %[m/s]
    for i = 2:t3
        v3_1(i) = v3_1(i-1) - a_br*1;
        s3_1(i) = v3_1(1)*i - 0.5*a_br*i^2;
    end

    % Pit stop #1 - 10s
    for i = 1:t4
        v4_1(i) = 0;
        s4_1(i) = 0;
    end

    v_1 = [v1_1,v2_1,v3_1,v4_1];
    s_1 = [s1_1, s1_1(t1)+s2_1, s1_1(t1)+s2_1(t2_1)+s3_1, s1_1(t1)+
                                                s2_1(t2_1)+s3_1(t3)+s4_1];
    t_1 = t1+t2_1+t3+t4;
%\END Lap 1

% === LAP 2 & 3 ===
    % Acceleration
    v1_23 = v1_1;
    s1_23 = s1_1;

    % Constant velocity
    t2_23 = round((2*s_tot-s_acc-s_br)/v_constant);
    for i = 1:t2_23
```

```
        v2_23(i) = v_constant;
        s2_23(i) = v2_23(i)*i;
    end

    % Retardation
    v3_23(1) = v2_23(t2_23); %[m/s]
    for i = 2:t3
        v3_23(i) = v3_23(i-1) - a_br*1;
        s3_23(i) = v3_23(1)*i - 0.5*a_br*i^2;
    end

    % Pit stop #2 - 10s
    for i = 1:t4
        v4_23(i) = 0;
        s4_23(i) = 0;
    end
    v_23 = [v1_23,v2_23,v3_23,v4_23];
    s_23 = [s1_23, s1_23(t1)+s2_23, s1_23(t1)+s2_23(t2_23)+s3_23, s1_23(t1)
                                          +s2_23(t2_23)+s3_23(t3)+s4_23];
    t_23 = t1+t2_23+t3+t4;
%/END Lap 2&3

% === LAP 4 & 5 ===
    % Acceleration
    v1_45 = v1_1;
    s1_45 = s1_1;

    % Constant velocity
    t2_45 = round((2*s_tot-s_acc-s_br)/v_constant);
    for i = 1:t2_45
        v2_45(i) = v_constant;
        s2_45(i) = v2_45(i)*i;
    end

    % Retardation
    v3_45(1) = v2_45(t2_45); %[m/s]
    for i = 2:t3
        v3_45(i) = v3_45(i-1) - a_br*1;
        s3_45(i) = v3_45(1)*i - 0.5*a_br*i^2;
    end

    % Pit stop #3 - 10s
    for i = 1:t4
        v4_45(i) = 0;
        s4_45(i) = 0;
    end
    v_45 = [v1_45,v2_45,v3_45,v4_45];
    s_45 = [s1_45, s1_45(t1)+s2_45, s1_45(t1)+s2_45(t2_45)+s3_45, s1_45(t1)
                                          +s2_45(t2_45)+s3_45(t3)+s4_45];
```

```
    t_45 = t1+t2_45+t3+t4;
%/END Lap 4&5

% === LAP 6 & 7 ===
    % Acceleration
    v1_67 = v1_1;
    s1_67 = s1_1;

    % Constant velocity
    % No -s_br, since no need to stop at finish line
    t2_67 = round((2*s_tot-s_diff-s_acc)/v_constant);
    for i = 1:t2_67
        v2_67(i) = v_constant;
        s2_67(i) = v2_67(i)*i;
    end

    v_67 = [v1_67,v2_67];
    s_67 = [s1_67, s1_67(t1)+s2_67];
    t_67 = t1+t2_67;

%/ END RACE


%-------------------------------------------------------------------------
% RACE-vector sumations
%-------------------------------------------------------------------------
% Minus 1; to get the same length as for "speed" and "position"
time = [0:(t_0+t_1+t_23+t_45+t_67-1)];
speed = [v_0, v_1, v_23, v_45, v_67];
position = [s_0, s_0(end)+ s_1,s_0(end)+s_1(end)+s_23,s_0(end)+s_1(end)+
               s_23(end)+s_45,s_0(end)+s_1(end)+s_23(end)+s_45(end)+s_67];
hillslope = time;

%-------------------------------------------------------------------------
% The Lausitz hillslope vector - resolution [per meter]
%-------------------------------------------------------------------------
 load Lausitz_hillslope.mat %=> L_slope
 load Lausitz_position.mat  %=> L_pos

 L_position = [L_pos;L_pos(end)+L_pos;2.*L_pos(end)+L_pos;3.*L_pos(end)+
        L_pos;4.*L_pos(end)+L_pos;5.*L_pos(end)+L_pos;6.*L_pos(end)+L_pos];
 L_hillslope = [L_slope;L_slope;L_slope;L_slope;L_slope;L_slope;L_slope];
```

A.3 Maximum acceleration; *FUNaccmax.m*

```
function [a_max] = FUNaccmax(v,I_max_DcDc,gear_final,n_motor,T_amb)
% Calculation of Max acceleration of Smarter
```

```
r = 0.2754;                     % Radius of tyre
Tconst = 89.1e-3;               % Motor torque constant
Tmotor_loss = 0.0363*n_motor;   % Motor friction etc. torque
Gear =  gear_final;
P_air = 101325;                 % Air pressure at sea level [Pa]
R_air = 287.05;                 % Gas constant for dry air [J/(kg*degK)]
rho_air = P_air/(R_air*(T_amb+273.15));
Cd = 0.28;
Af = 1.4;
v_car = v./3.6;
Taero = 0.5*rho_air*Cd*Af*v_car^2*r;
Taero_mean = Taero/2;            % Mean value during the acceleration

if n_motor == 1;

    Jtot = 9.528;            % Total inertia
    Tresist = 2.3245;         % Assumed constant value over time, = Cr*m*g*r
    Tmax = I_max_DcDc * Tconst - Tmotor_loss;

    Tloss = Taero_mean + Tresist;
    Tmax_wheel = Tmax * Gear - Tloss;
    a_max = (Tmax_wheel / Jtot) * r;

elseif n_motor == 2;

    Jtot = 9.748;            % Total inertia
    Tresist = 2.3721;        % Assumed constant value over time, = Cr*m*g*r
    Tmax = I_max_DcDc * Tconst - Tmotor_loss;

    Tloss = Taero_mean + Tresist;
    Tmax_wheel = Tmax * Gear - Tloss;
    a_max = (Tmax_wheel / Jtot) * r;
end

end
```

A.4 Vehicle mass calculation; *Smarter_ weight.m*

```
% Smarter weight in Lausitz = 74 kg

m_fuel_init =0.2555;        % starting volume 0.35 liter
m_ICE = 3.46;               % GX35
m_gen = 2*2.48;             % 2 generators
m_cap = 4.680;              % Li-ion capacitor
m_motor = 2*2.48;           % 2 driving motors
m_DcDc = 2*0.4;             % Maxon DC/DC converter
m_gear = 0.5;               % Motor to wheels
% Rest of the vehicle weight (wheels = 4*3.5 = 14 kg)
m_chassis = 74-(m_ICE + m_fuel_init + m_gen + m_cap + m_motor + m_DcDc +
```

```
            m_gear)% = 54.3845
m_driver = 50;

m_Smarter = m_ICE + m_fuel_init + m_gen + m_cap + m_motor + m_DcDc +
            m_chassis + m_gear

m_tot = m_Smarter + m_driver
```

Appendix B

Go-kart m-files

Here follows the m-files for modelling and simulation of the Gokart.

B.1 The main m-file; *GoKart_param.m*

```
clear all;
clc;
%************************************************************************
%************************************************************************
%
% COMPONENT AND PARAMETER CHOICES
%
%************************************************************************
%************************************************************************

% ======================================
%  Battery - Data sheet values for Nilar 24V 9Ah NiMH
% ======================================

    % Number of battery units
     n_cell = 8;

    % Battery total charge content [Ah*3600 = C charge]
     Q_battery = 9*3600*n_cell/2;   % 36 Ah

    % Mass of battery [kg]
     m_battery = 3.9*n_cell;

    % Battery internal resistance [ohm]
     R_battery = 0.1/2;

    % Initial state of charge (1 = fully charged, 0 = fully drained)
     SOCinit = 0.8;

    % Look-up table data; Open source voltage [V] as a function of SOC [-]
     socvec = [0 0.0055 0.1160 0.2265 0.3370 0.4475 0.5580 0.6685 0.7790 0.8895 1];
     ocvolvec =2.*[20 20.6+0.045 24+0.045 24.8+0.045 25.2+0.045 25.6+0.045 25.8+
```

```
                0.045 26+0.045 26.2+0.045 26.7+0.045 28.6+0.045];

    % Maximum battery current [A]
     Ibattery_max_cont = 18;
     Ibattery_max_peak = 90;

    % Voltage limits for the battery [V]
      Vmin = 22;
      Vmax = 200; %57.29

     % SOC limits for the battery [-]
      SOCmin = 0.1;
      SOCmax = 0.9;

     % Maximum allowed battery temperature [deg C]
      Temp_battery_max = 45;

% ======================================
%  Electric Machine
% ======================================

    %---Asynchronous motor:----
     % Mass of asynchronous machine [kg]
      m_motor = 19.2;

     % Measured values
      Rs=6.4e-3;                          % Ohm, Stator resistance
      Rr=7.1e-3;                          % Ohm, Rotor resistance
      Lsl=22.371e-6;                      % H, Stator leakage inductance
      Lrl=22.371e-6;                      % H, Rotor leakage inductance
      Lm=0.43871e-3;                      % H, Magnetizing inductance
      Ls=Lsl+Lm;                          % H, Stator inductance
      Lr=Lrl+Lm;                          % H, Rotor inductance
      J=0.05;                             % Assumed motor inertia
      np=2;                               % Poole pair
     % Gamma model parameters
      L_M = Lm^2/Lr;
      L_sigma = Ls-L_M;
      R_R = (Lm/Lr)^2*Rr;

     % Estimated values, representing the gamma modelled motor
      R_R_hat=R_R;
      Rs_hat=Rs;
      L_sigma_hat=L_sigma;
      L_M_hat = L_M;

     % Current controller
      alfa_sigma = 1000;                   % rad/s, Current controller band width
      Ra = alfa_sigma*L_sigma_hat - (Rs_hat+R_R_hat);   % Active damping resistance
```

```
      Kp_c = alfa_sigma * L_sigma_hat;  % Current controller Proportional Parameter
      Ki_c = alfa_sigma * (Rs_hat + R_R_hat + Ra);% Cur. cont. Integrating parameter

      xi=[0;0;0;0]; %initial conditions.
      PSI_ref = sqrt(2)*0.0399*Lm/Lr; % Flux magnitude reference.
      % 0.0399 is the flux magnitude reference at motor nominal power and speed
    %-------------------------------------------------

%     %---PMSM----
%     % Motor parameters:
%     % 50 Hz, 1500 rpm, 4000 W,400 V
%
%     % "S-function parameters:" Rs,Ls,Ym,np,xi
%      Rs=1.33;                          % = Ohm, Stator resistance
%      Lsl=0.008;                        % = mH, Stator leakage inductance
%      Lm=40e-3;                         % = mH, Magnetizing inductance
%      Ls=Lsl+Lm;                        % = 48 mH, Stator inductance
%      Ym = 0.894;                       % = Wb, Flux magnitude reference.
%      np=2;                             % Number of pole pairs
%
%     % Current controller
%      alfa_sigma = 1000;                % rad/s, Current controller band width
%      Ra = alfa_sigma*Ls - Rs;          % Active damping resistance
%      Kp_c = alfa_sigma * Ls;           % Current controller Proportional Parameter
%      Ki_c = alfa_sigma * (Rs + Ra);    % Current controller Integrating parameter
%      xi=[0;0];                         % Initial values of the stator current
%     %-----------------------------------------------------


% ======================================
%  Inverter
% ======================================

    % MOSFET On-state resistance [ohm]
     % r_DS_on = 2.1e-3; % at 25 deg C
     % Look-up table depending on junction temperature [deg C]
     temp_junction = [-40 -20 0 20 40 60 80 100 120 140 160 175];
     R_ds_temp = 2.1e-3*[0.65 0.75 0.86 0.97 1.08 1.19 1.34 1.46 1.61 1.76 1.91 2.06];

    % Number of MOSFETs per switch
     n_MOSFET = 5;

    % MOSFET Switching frequency [Hz]
    f_sw = 20e3;

    % MOSFET turn ON time [s];
     tc_on = 2*80e-9;

    % MOSFET turn OFF time [s];
```

```
tc_off = 2*64e-9;

% Mass of inverter [kg]
 m_AcDc = 5;            % Assumed weight

% Maximum inverter temperature [deg C]
 Tconv_max = 85;

% Ambient temperature [deg C]
  T_amb = 25;

%--- Thermal model of inverter---
s=tf('s');                  % Laplace operator

% MOSFET
%One RC-circuit, find the time constant in data sheet for
%when Z_JC = 0.63 * R_JC --> tao = 7 ms.
R = 0.40216;                % The sum of R1-R4. Data sheet value = 0.4 ohm
tao = 7e-3;                 % The 63% value of R according to data sheet
C = tao/R;                  % Calculated, see report
C_MOSFET = C*2*n_MOSFET;    % Total equivalent thermal capacity
R_MOSFET = R/(2*n_MOSFET);  % Total equivalent thermal resistance

% Thermal Clad - Calculated values of R and C
R_Cu = 4.425611011e-5;      % Roughly measured and calculated
R_dielec = 2.131e-3;        % Calculated, see report
R_Al = 6.562e-4;            % Calculated, see report
C_Cu = 3.9655;              % Calculated, see report
C_Al = 95.1964;             % Calculated, see report

% Heat Sink -
R_hs = 0.7;                 % Found in data from ELFA
C_hs = 959.616;             % Calculated, see report

Z_hs = (1/(s*C_hs))*R_hs/(R_hs+(1/(s*C_hs)));

% --- TOTAL JUNCTION THERMAL IMPEDANCE CALCULATION
% - using series and parallel calculations of total equivalent impedance
% C_Al in parallel with (Z_hs in series with R_Al)
Z_C_Al_R_Al_dielec = (1/(s*C_Al))*(R_Al+Z_hs)/((R_Al+Z_hs)+(1/(s*C_Al)));
% C_Cu in parallell with (R_Cu + R_ThClad+Z_C_Al_R_Al_ThClad)
Z_C_Cu_Rcu_Rdielec_Z_ans = (1/(s*C_Cu))*(R_Cu+R_dielec+Z_C_Al_R_Al_dielec)/
                         ((R_Cu+R_dielec+Z_C_Al_R_Al_dielec)+(1/(s*C_Cu)));
% Total thermal impedance = C_MOSFET in parallel with
                            (R_MOSFET + Z_C_Cu_Rcu_Rdielec_Z_ans)
Z_tot = (1/(s*C_MOSFET))*(R_MOSFET + Z_C_Cu_Rcu_Rdielec_Z_ans)/
                   ((R_MOSFET + Z_C_Cu_Rcu_Rdielec_Z_ans)+(1/(s*C_MOSFET)));
[num_th,den_th] = tfdata(Z_tot,'v');
```

```
    % --- CASE IMPEDANCE ---
    % C_Al in parallel with (Z_hs in series with R_Al)
    Z_C_Al_R_Al_dielec = (1/(s*C_Al))*(R_Al+Z_hs)/((R_Al+Z_hs)+(1/(s*C_Al)));
    % C_Cu in parallell with (R_Cu + R_ThClad+Z_C_Al_R_Al_ThClad)
    Z_C_Cu_Rcu_Rdielec_Z_ans = (1/(s*C_Cu))*(R_Cu+R_dielec+Z_C_Al_R_Al_dielec)/
                            ((R_Cu+R_dielec+Z_C_Al_R_Al_dielec)+(1/(s*C_Cu)));
    % Total thermal impedance = Z_C_Cu_Rcu_Rdielec_Z_ans
    Z_tot_Case = Z_C_Cu_Rcu_Rdielec_Z_ans;
    [num_th_Case,den_th_Case] = tfdata(Z_tot_Case,'v');
    %/end ---------------------------------

% ======================================
%  Chassis
% ======================================

    % Mass of chassis [kg]
     m_chassis = 35;

    % Weight of driver [kg]
     m_driver = 30;

    % Tire radius [m]
     r = 0.001*(25.4*tire_height)/2;

    % Rolling resistance coefficient
     Cr = 0.007 ;

    % Airdrag coefficient
     Cd = 0.6 ;

    % Vehicle frontal area [m^2]
     Af = 0.5 ;

    % Air density [kg/m^3]
     rho_air = 1.225;

% ======================================
%  Gearbox - Motor to wheel
% ======================================

    % Mass of gears [kg]
     m_gear = 0.5;

    % Final gear
     gear_ratio = 1;

    % Inertia of gear [kg m^2]
     J_gear = 0;
```

```
% ======================================
%  Driver - Speed Controller
% ======================================

    % PI - Speed controller
     Kp = 0.3;
     Ki = 0.05;

% ======================================
%  Vehicle Total mass [kg]
% ======================================

m_total = m_battery + m_motor + m_AcDc + m_chassis + m_driver + m_gear

% ======================================
% ======================================
%  Controller GoKart
% ======================================
% ======================================

    %-------------------------------------
    % Brake pedal
    %-------------------------------------
    % Rate of brake pedal position for motor braking
     max_em_brake_pos = 0.25;

    %-------------------------------------
    % Battery
    %-------------------------------------
    % Battery Total capacity [Ah*3600 = Q]=[C]
     Q_battery = 9*3600*n_cell/2; % 36 Ah

    % Initial state of charge (1 = fully charged, 0 = fully drained)
     SOCinit = 0.8;

    % SOC limits for the battery
      SOCmin = 0.1;
      SOCmax = 0.9;

    % Maximum battery current [A]
      Ibattery_max_cont = 18;
      Ibattery_max_peak = 90;

    % Voltage limits for the battery
      Vmin = 22;
      Vmax = 200;

    % Maximum allowed battery temperature [deg C]
      Temp_battery_max = 45;    %Data sheet
```

```
    % Temp regulator parameters
      Kp_Temp_battery = 1;
      Ki_Temp_battery = 1;

    %-------------------------------------
    % Inverter
    %-------------------------------------
    % Maximum inverter CASE temperature [deg C]
     Temp_conv_max = 90;

    % Temp regulator parameters
     Kp_Temp_conv = 1;
     Ki_Temp_conv = 1;

    %-------------------------------------
    % Electric Motor
    %-------------------------------------
    % Maximum temperature [deg C]
    Temp_em_max = 140;  % Value given from motor data sheet

    % Temp regulator parameters
     Kp_T_em = 1;
     Ki_T_em = 1;

    % Base speed for the electric machine [rad/s]
     w_base = 3000*2*pi/60;

    % Maximum electric motor torque production or "pull out torque" [Nm]
     Tem_max = 90;

    % Maximum mechanical power intended to be used during field weakening [W]
     Pem_mech_max = w_base * Tem_max;

    % Power regulator parameters
     Kp_motor_power = 1;
     Ki_motor_power = 1;

    % Maximum motor speed [rad/s]
     w_em_max = 12000*pi/30;

    % Speed regulator parameters
     Kp_em_speed = 1;
     Ki_em_speed = 1;

%************************************************************************
%************************************************************************
%
% SIMULATION VECTOR
```

```
%
%*************************************************************************
%*************************************************************************

%------Modified FlapTrack_Mini---
load('Mod_FlapTrack_Mini.mat');

%Lap #1
time = simvect(:,1);                                % 48.7780 s
speed = simvect(:,2);
position = simvect(:,3);                            % 969.4239 m

%Lap #2
meas = load ('FlapTrack_Mini.txt');
time = [time;time(end) + meas(:,2)];                % 97.5560 s
speed = [speed; meas(:,3)./3.6];
position = [position; position(end) + meas(:,4)];   % 1938.8478 m

%Lap #3
time = [time;time(end) + meas(:,2)];                % 146.334 s
speed = [speed; meas(:,3)./3.6];
position = [position; position(end) + meas(:,4)];   % 2908.2717 m

%Lap #4
time = [time;time(end) + meas(:,2)];                % 195.112 s
speed = [speed; meas(:,3)./3.6];
position = [position; position(end) + meas(:,4)];   % 3877.6956 m

%Lap #5
time = [time;time(end) + meas(:,2)];                % 243.89 s
speed = [speed; meas(:,3)./3.6];
position = [position; position(end) + meas(:,4)];   % 4847.1195 m

%Lap #6
time = [time;time(end) + meas(:,2)];                %292.668 s
speed = [speed; meas(:,3)./3.6];
position = [position; position(end) + meas(:,4)];   % 5816.5434 m

%Lap #7
time = [time;time(end) + meas(:,2)];                % 341.446 s
speed = [speed; meas(:,3)./3.6];
position = [position; position(end) + meas(:,4)];   % 6785.9673 m

%Lap #8
time = [time;time(end) + meas(:,2)];                % 390.224 s
speed = [speed; meas(:,3)./3.6];
position = [position; position(end) + meas(:,4)];   % 7755.3912 m

%Lap #9
```

```
time = [time;time(end) + meas(:,2)];                % 439.0002 s
speed = [speed; meas(:,3)./3.6];
position = [position; position(end) + meas(:,4)];   % 8724.8151 m

%Lap #10
time = [time;time(end) + meas(:,2)];                % 487.78 s
speed = [speed; meas(:,3)./3.6];
position = [position; position(end) + meas(:,4)];   % 9694.239 m

%Lap #11
time = [time;time(end) + meas(:,2)];                % 536.558 s
speed = [speed; meas(:,3)./3.6];
position = [position; position(end) + meas(:,4)];   % 10663.6629 m

%Lap #12
time = [time;time(end) + meas(:,2)];                % 585.336 s
speed = [speed; meas(:,3)./3.6];
position = [position; position(end) + meas(:,4)];   % 11633.0868 m

%Lap #13
time = [time;time(end) + meas(:,2)];                % 634.114 s
speed = [speed; meas(:,3)./3.6];
position = [position; position(end) + meas(:,4)];   % 12602.5107 m


% Initial velocity [rad/s] (used in integrator in chassis)
     w_init = speed(1)*30/pi;
```

B.2 S-function; *IMmach.m*

```
function [sys,x0,str,ts] = IMmach(t,x,u,flag,Rs,Rr,Ls,Lr,Lm,np,xi)
%CSFUNC An example M-file S-function for defining a continuous system.
%   Example M-file S-function implementing continuous equations:
%      x' = Ax + Bu
%      y  = Cx + Du
%
%   See sfuntmpl.m for a general S-function template.
%
%   See also SFUNTMPL.
%   Copyright (c) 1990-97 by The MathWorks, Inc.
%   $Revision: 1.4 $

switch flag,

  %%%%%%%%%%%%%%%%%
  % Initialization %
  %%%%%%%%%%%%%%%%%
  case 0,
    [sys,x0,str,ts]=mdlInitializeSizes(t,x,u,flag,Rs,Rr,Ls,Lr,Lm,np,xi);
```

```
  %%%%%%%%%%%%%%
  % Derivatives %
  %%%%%%%%%%%%%%
  case 1,
    sys=mdlDerivatives(t,x,u,flag,Rs,Rr,Ls,Lr,Lm,np,xi);

  %%%%%%%%%%
  % Outputs %
  %%%%%%%%%%
  case 3,
    sys=mdlOutputs(t,x,u,flag,Rs,Rr,Ls,Lr,Lm,np,xi);

  %%%%%%%%%%%%%%%%%%
  % Unhandled flags %
  %%%%%%%%%%%%%%%%%%
  case { 2, 4, 9 },
    sys = [];

  %%%%%%%%%%%%%%%%%%%%
  % Unexpected flags %
  %%%%%%%%%%%%%%%%%%%%
  otherwise
    error(['Unhandled flag = ',num2str(flag)]);
end
% end csfunc
%
%=============================================================================
% mdlInitializeSizes
% Return the sizes, initial conditions, and sample times for the S-function.
%=============================================================================
%
function [sys,x0,str,ts]=mdlInitializeSizes(t,x,u,flag,Rs,Rr,Ls,Lr,Lm,np,xi)

sizes = simsizes;
sizes.NumContStates  = 4;
sizes.NumDiscStates  = 0;
sizes.NumOutputs     = 4; % [t,isA,isb,Te]
sizes.NumInputs      = 4; % Usa, Usb, wr, Or
sizes.DirFeedthrough = 0;
sizes.NumSampleTimes = 1;

sys = simsizes(sizes);
x0  = xi;
str = [];
ts  = [0 0];
% end mdlInitializeSizes
%
%=============================================================================
```

```
% mdlDerivatives
% Return the derivatives for the continuous states.
%=============================================================================
%
function sys=mdlDerivatives(t,x,u,flag,Rs,Rr,Ls,Lr,Lm,np,xi)

% 4 state variables:
% x(1)=isa, x(2)=isb,x(3)=ira,x(4)=irb
isA=x(1);
isb=x(2);
ira=x(3);
irb=x(4);

% 3 input signals from m-file
% u(1)=usa, u(2)=usb, wr=u(3)
usa=u(1);
usb=u(2);
wr=u(3);

% Defining the resistance element matrix
Rmat=[  Rs     0     0      0      ;
        0      Rs    0      0      ;
        0    wr*Lm   Rr    wr*Lr   ;
      -wr*Lm   0   -wr*Lr   Rr    ];
% Defining the reactance element matrix
Lmat=[ Ls  0   Lm  0   ;
       0   Ls  0   Lm  ;
       Lm  0   Lr  0   ;
       0   Lm  0   Lr ];
% Forming the state space matrices
Bmat=inv(Lmat);
Amat=-Bmat*Rmat;
% Fomation of the 6 state spaces , xDot = Ax + Bu,  sys=xDot,
sys(1:4) = Amat*x(1:4) + Bmat*[usa;usb;0;0];
% Forming the electrodynamical tourque
Te = (3/2)*np*((Ls*isA+Lm*ira)*isb-(Ls*isb+Lm*irb)*isA);
% end mdlDerivatives
%
%=============================================================================
% mdlOutputs
% Return the block outputs.
%=============================================================================
%
function sys=mdlOutputs(t,x,u,flag,Rs,Rr,Ls,Lr,Lm,np,xi)

% the time t is already available in all function in the s-function
%Is, Ir, Te
isA=x(1);
isb=x(2);
```

```
ira=x(3);
irb=x(4);

Te = (3/2)*np*((Ls*x(1)+Lm*x(3))*x(2)-(Ls*x(2)+Lm*x(4))*x(1));

sys = [t,isA,isb,Te,];
%  end mdlOutputs
```

B.3 S-function; *PMSMmach.m*

```
 function [sys,x0,str,ts] = PMSMmach(t,x,u,flag,Rs,Ls,Ym,np,xi)
%CSFUNC An example M-file S-function for defining a continuous system.
%   Example M-file S-function implementing continuous equations:
%      x' = Ax + Bu
%      y  = Cx + Du
%
%   See sfuntmpl.m for a general S-function template.
%
%   See also SFUNTMPL.
%   Copyright (c) 1990-97 by The MathWorks, Inc.
%   $Revision: 1.4 $

switch flag,

  %%%%%%%%%%%%%%%%%%
  % Initialization %
  %%%%%%%%%%%%%%%%%%
  case 0,
    [sys,x0,str,ts]=mdlInitializeSizes(t,x,u,flag,Rs,Ls,Ym,np,xi);

  %%%%%%%%%%%%%%%
  % Derivatives %
  %%%%%%%%%%%%%%%
  case 1,
    sys=mdlDerivatives(t,x,u,flag,Rs,Ls,Ym,np,xi);

  %%%%%%%%%%
  % Outputs %
  %%%%%%%%%%
  case 3,
    sys=mdlOutputs(t,x,u,flag,Rs,Ls,Ym,np,xi);

  %%%%%%%%%%%%%%%%%%%
  % Unhandled flags %
  %%%%%%%%%%%%%%%%%%%
  case { 2, 4, 9 },
    sys = [];

  %%%%%%%%%%%%%%%%%%%%
```

```
  % Unexpected flags %
  %%%%%%%%%%%%%%%%%%%
  otherwise
    error(['Unhandled flag = ',num2str(flag)]);
end
% end csfunc
%
%=============================================================================
% mdlInitializeSizes
% Return the sizes, initial conditions, and sample times for the S-function.
%=============================================================================
%
function [sys,x0,str,ts]=mdlInitializeSizes(t,x,u,flag,Rs,Ls,Ym,np,xi)

sizes = simsizes;
sizes.NumContStates  = 2;
sizes.NumDiscStates  = 0;
sizes.NumOutputs     = 4; % [t,isA,isb,Te]
sizes.NumInputs      = 4; % Usa, Usb, wr, Or
sizes.DirFeedthrough = 0;
sizes.NumSampleTimes = 1;

sys = simsizes(sizes);
x0  = xi;
str = [];
ts  = [0 0];
% end mdlInitializeSizes
%
%=============================================================================
% mdlDerivatives
% Return the derivatives for the continuous states.
%=============================================================================
%
function sys=mdlDerivatives(t,x,u,flag,Rs,Ls,Ym,np,xi)

% 4 state variables:
% x(1)=isa, x(2)=isb
isA=x(1);
isb=x(2);

% 4 input signals from m-file
% u(1)=usa, u(2)=usb, u(3)=wr, u(4)=Or;
usa=u(1);
usb=u(2);
wr=u(3);
Or=u(4);

% Defining the resistance element matrix
Rmat=[  Rs     0     ;
```

```
        0      Rs    ];

% Defining the reactance element matrix
Lmat=[ Ls  0   ;
       0   Ls  ];

% Forming the state space matrices
Bmat=inv(Lmat);
Amat=-Bmat*Rmat;
% Fomation of the 6 state spaces , xDot = Ax + Bu,  sys=xDot,
sys(1:2) = Amat*x(1:4) + Bmat*[usa+wr*Ym*sin(Or); usb-wr*Ym*cos(Or)];
% Forming the electrodynamical tourque
Te = (3/2)*np*Ym*(isb*cos(Or)-isA*sin(Or));
% end mdlDerivatives
%
%=============================================================================
% mdlOutputs
% Return the block outputs.
%=============================================================================
%
function sys=mdlOutputs(t,x,u,flag,Rs,Ls,Ym,np,xi)

% the time t is already available in all function in the s-function
%Is, Ir, wr, Or, Te
isA=x(1);
isb=x(2);
wr=u(3);
Or=u(4);

Te = (3/2)*np*Ym*(isb*cos(Or)-isA*sin(Or));

sys = [t,isA,isb,Te];
% end mdlOutputs
```